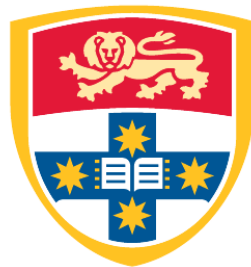


# Grainsize dynamics of granular flows

BENJAMIN MARKS

B.Sc (Adv), B.Eng (Hons)



THE UNIVERSITY OF  
SYDNEY

Supervisor: Professor Itai Einav  
Associate Supervisor: Dr Pierre Rognon  
Associate Supervisor: Dr Yixiang Gan

A thesis submitted in fulfilment of  
the requirements for the degree of  
Doctor of Philosophy

Particles and Grains Laboratory  
School of Civil Engineering  
Faculty of Engineering  
The University of Sydney  
Australia

29 August 2013

## **Abstract**

This dissertation deals with the description of a granular material as a continuum with an internal coordinate that represents the grainsize distribution. The inclusion of this internal coordinate allows us to describe polydispersity in a natural and simple manner.

The bulk of this dissertation is built on four published papers. Each paper is prefaced by an introductory section, where the motivation for the paper is presented. In the first paper, I show how the fundamental mechanism of granular segregation can be represented in a cellular automaton. An equivalent continuum model is derived from the rules of the cellular automaton, similar to previous theories.

The second paper extends this mechanism to include arbitrary grainsize distributions in a continuum framework. This continuum description predicts not only the evolution of the grainsize distribution in space and time, but also the kinematics of the flow. I also show an extension of the theory in Chapter 5 so that it can be included in a conventional numerical continuum solver. This is then used to describe steady state grainsize distributions in Chapter 6, where they are shown to be a function of only the stress gradient and diffusivity.

This new continuum theory predicts that segregation will create a lubrication effect that accelerates the flow. In the third paper, I show experimentally how this lubrication effect creates additional forces when a granular avalanche impacts a rigid obstacle. At experimental scale, a 20% increase in force is measured, as compared to a monodisperse avalanche.

In the final paper, comminution is added to the grainsize framework in a new cellular automaton, allowing me to model crushable flows. I show how the grainsize distributions measured in confined comminution can be predicted from this model. Additionally, when segregation is introduced log-normal grainsize distributions develop as in avalanche flow. The transition from power law to log-normal grainsize distributions is explained as an interaction between comminution, segregation, and to a lesser extent mixing.

All of these effects are treated as a direct result of the introduction of the grainsize distribution. This is a paradigm shift for modelling large deformation granular problems.

## **Acknowledgements**

Firstly, I would like to thank my supervisors, Professor Itai Einav, Dr Pierre Rognon and Dr Yixiang Gan, without whom I would not have had the constant friendship, guidance, support and expert knowledge which allowed me to accomplish this work. Secondly, I would like to thank all four of my parents for providing such essentials as food, education, genes, money, help, advice, friendship and understanding as I have repeatedly fled the country. Also, I would to thank my sister Leah for never failing to remind me that I am meant to be working, not just checking facebook.

At ETH Zürich I would like to thank Professor Sasha Puzrin for his indulgence in allowing me to visit and conduct experiments, when we both knew that I had no idea what I was doing. Also many thanks to Aurelio Valaulta for his tireless efforts in sieving, lifting, cleaning and measuring, which got such great results from the experiment at ETH. At University College London, I would like to thank everyone in the geomechanics group for their support, friendship, and free office space. Lastly, I would like to thank everyone in the Eagle's Nest Research Centre for the constant supply of coffee, beer and support, even after I abandoned you all. Twice.

## Publications and awards

The following publications have been produced as a result of this PhD:

- (1) B. Marks and I. Einav. A cellular automaton for segregation during granular avalanches. *Granular Matter*, 13(3):211-214, 2011.
- (2) B. Marks, I. Einav, and P. Rognon. Polydisperse segregation down inclines: Towards degradation models of granular avalanches. In *Advances in Bifurcation and Degradation in Geomaterials*, pages 145-151. Springer, 2011.
- (3) B. Marks, P. Rognon, and I. Einav. Grainsize dynamics of polydisperse granular segregation down inclined planes. *Journal of Fluid Mechanics*, 690:499-511, 2012.
- (4) B. Marks, A. Valaulta, A. Puzrin, and I. Einav. Design of protection structures: the role of the grainsize distribution. In *Powders and Grains 2013: Proceedings of the 7th International Conference on Micromechanics of Granular Media*. American Institute of Physics Conference Series, 2013.
- (5) B. Marks and I. Einav. The interactions between comminution, segregation and remixing in granular flows, [arXiv:1304.4468](https://arxiv.org/abs/1304.4468), 2013.

The following awards have been received during the course of this thesis:

- (1) The Annie B Wilson Prize for Research in Civil Engineering, School of Civil Engineering, The University of Sydney, 2011
- (2) Certificate of Research Excellence, Faculty of Engineering, The University of Sydney, 2012

## Contents

<b>Abstract</b>	<b>ii</b>
<b>Acknowledgements</b>	<b>iv</b>
<b>Publications and awards</b>	<b>v</b>
<b>Contents</b>	<b>v</b>
<b>List of Figures</b>	<b>ix</b>
<b>Chapter 1 Introduction</b>	<b>1</b>
<b>Chapter 2 Literature review</b>	<b>4</b>
2.1 Granular materials .....	4
2.1.1 Three phases in one .....	5
2.1.2 The microscopic world .....	6
2.2 Grainsize .....	7
2.2.1 Grain size .....	8
2.2.2 Polydispersity .....	10
2.2.3 Grainsize dynamics .....	11
2.3 Granular flows .....	12
2.3.1 Granular avalanches .....	15
2.3.2 Constitutive models .....	16
2.3.3 Modelling full scale avalanches .....	19
2.3.4 Historical note .....	20
2.4 Segregation .....	22
2.4.1 The brazil nut effect .....	23
2.4.2 Rotating tumblers .....	24

2.4.3	Heap formation.....	25
2.5	Kinetic sieving.....	25
2.5.1	Statistical mechanics.....	27
2.5.2	Continuum models.....	28
2.6	Mixing.....	31
2.7	Crushing.....	32
2.7.1	Confined comminution.....	33
2.7.2	Crushable flows.....	36
2.8	Numerical methods.....	36
2.8.1	Cellular automata.....	37
2.8.2	Finite volume methods.....	38
2.8.3	Discrete element method.....	39
2.9	Summary.....	40
<b>Chapter 3 Motivation</b>		<b>41</b>
3.1	A dominant mechanism.....	42
3.2	Contribution towards paper.....	43
<b>Paper 1 A cellular automaton for segregation during granular avalanches</b>		<b>43</b>
<b>Chapter 4 Population balance models</b>		<b>48</b>
4.1	Cellular automaton.....	48
4.2	Continuum description.....	48
4.3	Contribution towards paper.....	49
4.4	Post processing.....	50
<b>Paper 2 Grainsize dynamics of polydisperse granular segregation down inclined planes</b>		<b>50</b>
<b>Chapter 5 Bulk, mean and grainsize dynamics</b>		<b>64</b>
5.1	Conservation of mass.....	66
5.2	Conservation of momentum.....	67
5.3	Summary of governing equations.....	68

5.4	Towards numerical implementation of grainsize dynamics .....	69
<b>Chapter 6</b>	<b>Steady State Solutions</b>	<b>71</b>
6.1	Continuum description .....	72
<b>Chapter 7</b>	<b>Chute experiment</b>	<b>75</b>
7.1	Lubrication effect.....	75
7.2	Contribution towards paper .....	77
<b>Paper 3</b>	<b>Design of protection structures: the role of the grainsize distribution</b>	<b>77</b>
<b>Chapter 8</b>	<b>Comminution during flow</b>	<b>82</b>
8.1	Contribution towards paper .....	82
<b>Paper 4</b>	<b>The interactions between comminution, segregation and remixing in granular flows</b>	<b>82</b>
<b>Chapter 9</b>	<b>Conclusion</b>	<b>95</b>
9.1	Future outlook.....	98
<b>Bibliography</b>		<b>100</b>
<b>Appendix A</b>	<b>Post processing</b>	<b>113</b>
A1	Volumetric analysis .....	113
A2	Homogenisation.....	114
A2.1	Solid fraction .....	115
A2.2	Average size .....	116
A2.3	Standard deviation of size .....	116



## List of Figures

1.1	Grainsize dynamics.	2
2.1	A sand dune.	5
2.2	Stress patterns in a single grain.	6
2.3	Common sizes.	8
2.4	Polydispersity of granular materials.	10
2.5	Grading curves.	11
2.6	Barchan sand dunes.	13
2.7	Six common flow geometries.	14
2.8	A granular avalanche.	15
2.9	Rheological models.	16
2.10	The brazil nut effect.	23
2.11	Segregation and heap formation.	25
2.12	ABS ® avalanche airbag.	26
2.13	Segregation profiles.	27
2.14	Steady state solutions.	29
2.15	Single grain crushing.	33
2.16	Particle redistribution after crushing.	34
2.17	Gosper's glider gun.	37
3.1	Comparison of two theories.	41
3.2	Motivation for a cellular automata.	42
5.1	Dynamics hierarchy.	65
5.2	Numerical implementation.	69
6.1	Steady state solution for bidisperse problems.	73
7.1	Factor of safety due to lubrication.	76

## CHAPTER 1

### **Introduction**

---

Granular materials are ubiquitous in our everyday lives, and in our surroundings. These materials can exist over many orders of magnitude of sizes, from molecules interacting via electromagnetic forces, to sand and gravel via mechanical interaction and to asteroids, planets and stars which are governed by gravitational attraction.

The unification of such disparate systems into a single model is obviously a daunting task. In fact, the key purpose of this dissertation is to describe how such a range of sizes can be described mathematically, and to model such systems in a unified manner.

Modelling over many orders of magnitude has its limitations. What is considered ‘continuous’ when viewed at the metre scale can appear very different when viewed at the micron scale. As a first step towards such a grand goal, let us focus our attention on sands and gravels. This material is chosen because it is a convenient size for experimentation, of the order of millimetres. Large representative volumes of such particles can be assembled in laboratories, and they can be treated as a continuum.

Granular materials exhibit all three phases of matter: solid, liquid and gas. When flowing as a liquid, particles segregate by size. Once this fluid stops flowing, evidence of the patterns created by the segregation are trapped in the solid phase.

Granular flows are present in mainly geophysical and industrial problems, however many of their properties are poorly understood. This work aims to increase our understanding of how the grainsize distribution affects such flows, and to unify the description of size-related problems in a continuum framework, where the grainsize is treated as an internal coordinate, as shown in Figure 1.1.

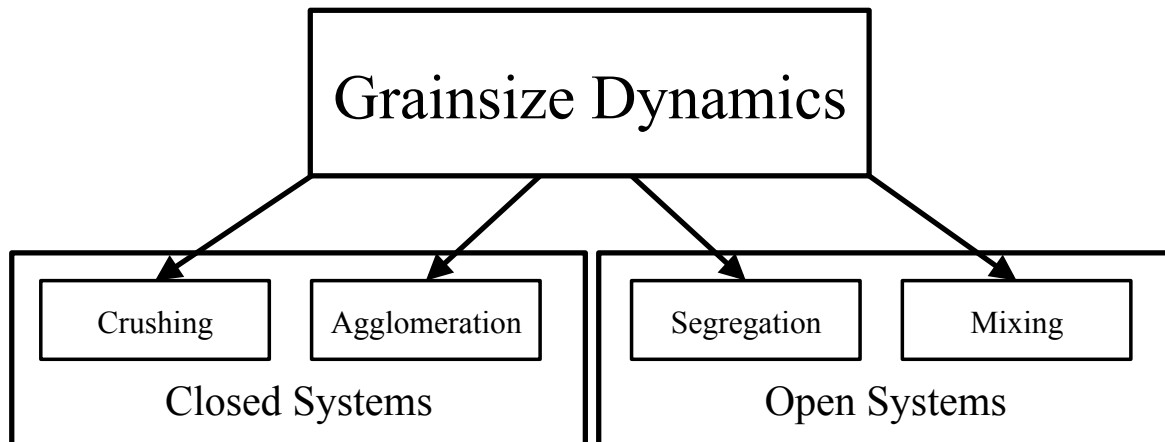


FIGURE 1.1: Grainsize dynamics. This involves changes in the grainsize distribution for both open and closed systems. In this dissertation I will discuss mixing, segregation and comminution only.

One of the most readily observed effects of grainsize variation in a granular material is its tendency to segregate during flow. Granular materials segregate for many reasons and under many conditions. Small differences in size, density, or even surface roughness, can cause the particles to segregate while flowing. While generally granular materials can be described as a continuum, and hence as fluids, there is no analogous segregative term in fluid flow.

Traditionally, instances of segregation are analysed separately for different boundary value problems. No theory has explained segregation quantitatively in multiple geometries, or for different sized particles. Additionally, the physical size of the particles is generally neglected in a segregation analysis.

The bulk of the research into segregation is phenomenological in nature, being derived solely from experimental and numerical investigation. No universal scaling has been found to explain multiple instances of segregation across the literature.

Another process that often occurs during granular flows is grain crushing. It is well known that significant grain crushing occurs in a variety of flow situations, such as avalanches, landslides, debris flows and milling operations. In each of these cases, the grainsize distribution evolves in space and time as a result of the crushing, altering the constitutive behaviour of the material.

There are as yet no models to explain how the constitutive parameters and grainsize distribution are linked in open systems where particles can advect in space. Additionally, there are no models to track the grainsize distribution in space and time whilst segregation and crushing occur.

This project aims at solving the second problem, where one wishes to track the evolution of the grainsize distribution within a flowing material from a variety of processes, such as segregation, crushing and mixing. In this work, cellular automata are created, which then inspire continuum models that can represent this behaviour.

This thesis begins with a simple numerical model of granular segregation, explaining the important physical processes relevant to the phenomenon. Once the physics is well understood, a rigorous continuum model is developed that describes segregation in terms of changes in the local grainsize distribution of the material. Experimental evidence of this phenomenon is then shown, and further refinements to the theory are given. Finally, segregation is coupled with comminution in another simple numerical model to explain the grainsize distribution evolution for natural avalanches, landslides and debris flows.

## CHAPTER 2

### Literature review

---

And every one that heareth these sayings of mine, and doeth them not, shall be likened unto a foolish man, which built his house upon the sand.

— The King James Bible, Matthew 7:26

Around 2000 years ago, when the Bible was first canonized, very little was understood about granular materials such as sand, and construction was difficult. Fortunately, many advances have occurred in the field since then. This Chapter gives a summary of the history and state of the art of granular materials research, in particular focused on segregation during flows on inclined planes. It also briefly describes some important points concerning mixing, comminution processing, cellular automata, finite differencing and the discrete element method.

## 2.1 Granular materials

Granular materials have a loose definition in the literature. According to some, they are considered to be systems composed of a large number of particles with a diameter greater than 1 micron (Gennes 1999). For others, this size constraint is too limiting, and granular materials exist over all sizes, in essence only limited by the Planck length<sup>1</sup>. Also, the notion of energy loss through interactions between particles seems to be a defining characteristic (Duran 2000).

---

<sup>1</sup>Personal communication with Professor Einav.



FIGURE 2.1: A sand dune. The dune is approximately 500 m across, whereas an individual sand grain is about 500 microns. At this scale, we can treat the dune as being a continuous medium. (© wikimedia.org)

In the absence of cohesive forces between particles, the shape of the material at rest will be determined by that of the container in which it is resting. Even though this is a property commonly attributed to fluids, these materials exhibit a large number of behaviours and phenomena which are not present in continuous media.

The prototypical example of a granular material is sand. It is composed of a large number of small grains that interact to give macroscopic properties, such as in Figure 2.1. In a conventional fluid, such as water, a single water molecule is approximately  $2.75 \times 10^{-10}$  m long. A droplet of water, the smallest common unit in day to day life, is approximately 500 microns wide, which is roughly 2,000,000 molecules across, or  $10^{21}$  molecules per droplet. This is a big number — approximately the number of sand grains on earth ( $10^{20}$  to  $10^{24}$ ). When we have small numbers of particles in a system, the discrete nature of the material becomes more evident.

### 2.1.1 Three phases in one

The most obvious property which distinguishes a granular material from a solid or fluid becomes evident when one attempts to pour sand into a container. As mentioned previously, the material will flow into and fill the container. An astute observer will, however, notice a critical distinction between what one expects of water and what actually occurs. Once the material has settled down, the top of the sand will not form a flat surface, as a liquid would,

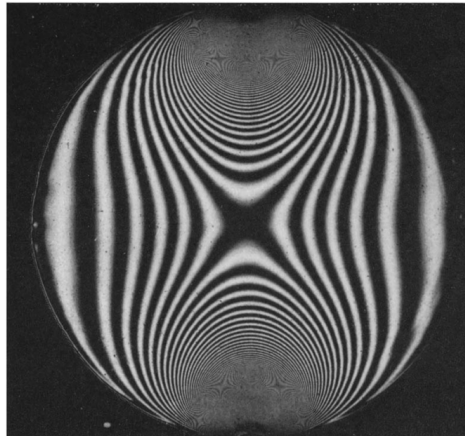


FIGURE 2.2: Stress pattern within a single spherical grain loaded diametrically. (Hiramatsu and Oka 1966)

but will rather form a peak. The angle of the slope forming this peak is called the angle of repose (Coulomb 1773).

The material has flowed into the container, just like a liquid, but has now frozen in a shape that is non-trivial. This transition from fluid-like to solid-like behaviour is referred to as the jamming transition (Liu and Nagel 2001; Majmudar et al. 2007), and is generally associated with grains interlocking at high density. This is a well known concept in geotechnical engineering, being a function of the relative density of the soil.

A curious person might attempt to find a third phase in the material by shaking the container and forming a gas by agitating the particles. Another way to make a gas would be to blow air upwards through the base of the container. We call this a fluidised bed, and it is widely used in the industrial processing of granular materials (Menon and Durian 1997).

### 2.1.2 The microscopic world

When talking about granular material so far, we have imagined an outside observer who is much larger than a single grain. Now, let us peer in closely at a pair of sand grains undergoing some deformation. What becomes immediately clear is that the grains interact at specific points, known as contacts, where electrostatic repulsion prevents them from overlapping (Hertz 1882).

There are a few ways in which these two particles can collide: it is possible for them to slide past one another, roll over each other, or hit head on. They could of course also undergo any combination of those collisions. Collision can cause small fragments (asperities) to break off each other, and degrade the contact points. This can change the local surface conditions and potentially widen cracks within the grains. These mechanisms are dissipative — the particles lose energy.

But what happens inside a grain? At each collision, stresses propagate through the grain (Hiramatsu and Oka 1966). Waves of elastic energy pass through the particle, placing some areas in compression and other areas in tension, as shown in Figure 2.2. In areas of tension, cracks are pulled open, weakening the individual grain. If the crack becomes large enough, the grain can fracture into a collection of small fragments.

Zooming out a little to consider the neighbourhood around the grain, we can observe contact networks, where loads are transmitted long distances through force chains which branch and interconnect (Drescher and De Josselin de Jong 1972). Each particle could be in contact with many other particles – we call this value the coordination number,  $Z$  (Smith et al. 1929). If a grain were to fracture, it would cause nearby particles to rearrange (Russell and Einav 2013), and change the stress state in the neighbourhood.

## 2.2 Grainsize

The linear scale, since it was first cut on the wall of an Egyptian temple, has come to be accepted by man almost as if it were the one unique scale with which Nature works and builds. Whereas it is nothing of the sort. Its sole value lies in giving due prominence to the differences and sums of quantities, when these are what we want to display. But Nature, if she has any preference, probably takes more interest in the ratios between quantities; she is rarely concerned with size for the sake of size.

— Ralph A. Bagnold



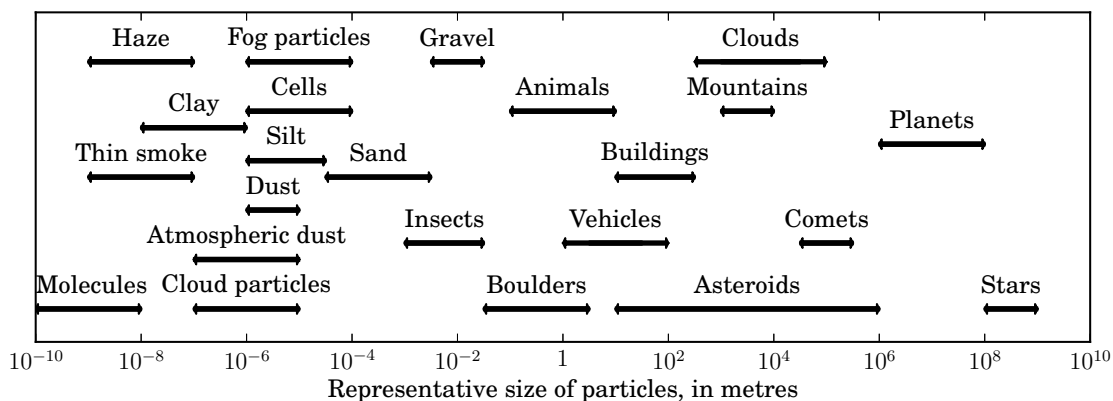


FIGURE 2.3: Common sizes of particles. Adapted from Bagnold (1941).

### 2.2.1 Grain size

When dealing with particulate matter, we often require a measure of the size of each grain in the system, or some representative measure of the distribution of sizes. A range of common sizes are shown in Figure 2.3. There is an inimitable relationship between sizes and scaling laws. Once we have a definition of a representative size for a particular instance of a class of bodies, we can then begin to unify our description of that class based on its size, as done famously in biology in Haldane (1926).

There exist, however, many representative sizes of a particular particle. For a sphere, the diameter is proportional to the volume cubed. The diameter is also the same as the diameter of the smallest circular hole through which the particle will pass. If we were to measure the drag force on the particle falling through a liquid or gas, it would also be directly related to the diameter. For any other shape, however, all of these quantities may be different. The size that we measure should be relevant to the physical property which we wish it to describe.

One of the first rigorous characterisation of grain size was done using sieves (Udden 1898). Depending on the construction of the sieve, a sieve measures either the smallest sphere or square that a particle can fall through. This size will vary with the sphericity of the particles, even if the volume remains the same.

A sieve analysis is usually coupled with a hydrometer, in which particles fall through a liquid, and the time to fall is compared against analytic solutions for spheres. In this way, the aerodynamic size of the particle is measured, since streamlined particles fall faster than others. Particle size can also be measured when falling through air (Bagnold 1954). A comprehensive review of grain size characterisation techniques is given in Syvitski (2007).

Another classical technique is the measurement of individual grains by hand with calipers, to find quantities such as the maximum, minimum and mean particle diameter (Savage and Lun 1988). This method, however, is sensitive to the operator, and the number of measurements taken. In fact, repeated handling of materials in this way can often lead to changes in the surface properties.

A more modern approach to measuring such morphology is to use optical techniques. In this case, particles can be laid down on a slide and imaged with a microscope, identifying cross sections of the particles, and properties such as elongation, circularity, aspect ratio and convexity can be measured rapidly and with a minimal amount of operator error.

Unfortunately, this technique requires the particles to be placed on a slide, which generally causes them to fall into a stable state such that their principal axis is parallel to the slide. This can give distorted views of the particles, as they can appear more flat and broad than is truly representative. To compensate for this, another method was developed in which particles are allowed to fall past a camera, and images of each grain can be taken of fairly random faces of the particles (note that particles will preferentially align to reduce wind load, however tumbling motion does reduce this effect (Goossens 2008)).

A further common method of particle size analysis is to use laser diffraction methods, where scattered light is analysed to back calculate particle properties (Boer et al. 1987). This method gives average properties of the medium, rather than individual particle data.

A recent development involves using three dimensional tomography to image the full volume of each grain (Andò et al. 2012). Using this method, there is no bias from the direction of imaging. Also, each particle's surface can be imaged in full. The drawbacks of this method are the complexity, expense and time that must be taken to image a large number of particles.



FIGURE 2.4: Polydispersity of granular materials. *Left*: A pile of well sieved gravel. This has a grainsize distribution that is composed of a small range of sizes, of the order of centimetres. *Right*: Detritus deposited after a debris flow. The grainsize distribution features every size of particle from clay to boulders, spanning over at least 6 orders of magnitude. (© United States Geological Survey)

After we measure the size of each grain in a sample, there are many ways to convert this data into a distribution (Folk 1966). Each method gives a particular skew or kurtosis to the data, especially for small data sets.

### 2.2.2 Polydispersity

Granular materials are inevitably polydisperse — they are made up of particles of a variety of sizes. It is difficult to create a sample, even in a laboratory, that has uniform size and sphericity. Most of the granular materials which we commonly use in our homes, such as flour, sugar, salt and pepper all have some variety in the size and shape of the constituent grains, even after careful preparation and manufacturing processes. Naturally occurring granular materials, such as soils and snow have much larger distributions of sizes, see for example Figure 2.4.

Polydispersity is one of the greatest elephants in the room of geotechnical engineering. Almost any geotechnical site investigation begins with a sieve and hydrometer analysis that measures a grading curve (Bolton 2000), such as shown in Figure 2.5. We take this grading curve, and use it to define what type of soil we must deal with, typically using the Unified Soil Classification System (D2487 2011) or some other equivalent model. But then we generally discard the grading curve for the rest of any analysis, even though we know it to be an important property

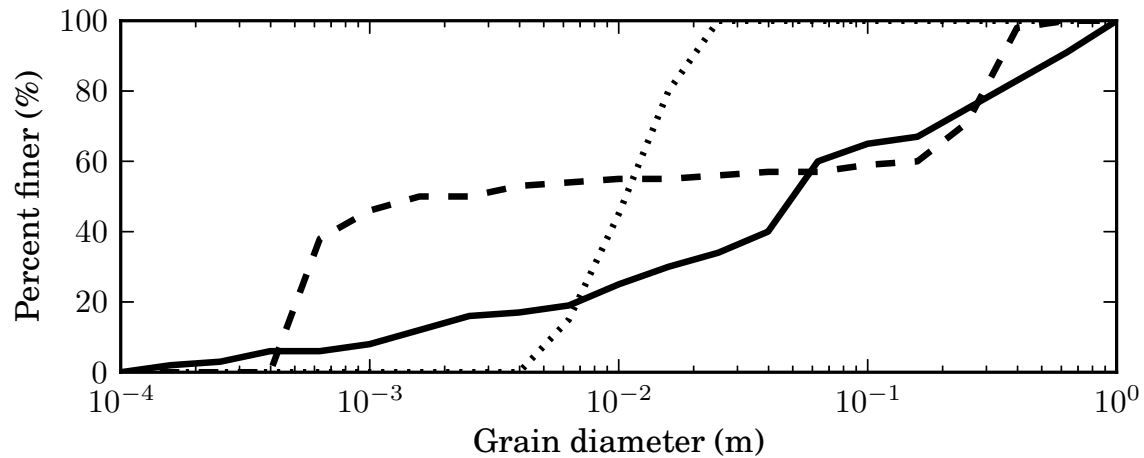


FIGURE 2.5: Examples of grading curves. Each line represents the grain size distribution of a particular soil sample. The solid line represents a well graded sample, which is composed of a wide range of particle sizes. The dashed line represents a gap-graded, or bidisperse sample, that is mostly composed of just two sizes (or at the least missing some sizes in the middle). The dotted line represents a uniformly graded, or monodisperse sample, which is composed of grains of a small range of sizes.

of the soil (Zhao et al. 2012; Zhao and Zhang 2013). A vast minority of constitutive models include as parameters spot measurements from the grading curve, such as taking  $d_{50}$ , the mean diameter (Pouliquen 1999). There is a singular case of a family of models for tracking changes in the grainsize distribution to model constitutive behaviour (Einav 2007a; Einav 2007b). Two situations where the grading curve is used to good advantage is in the prediction of permeability (Hazen 1911; Kozeny 1927; Carman 1937; Masch and Denny 1966) and pore size distribution (Arya and Paris 1981).

### 2.2.3 Grainsize dynamics

But it is time that we pass to some of the advantages of size.

— JBS Haldane

Generally, we account for the spatial variability of the grain size distribution by applying different constitutive models in each applicable area. While this is fine for material which does not advect in space, we often encounter problems where things move, such as in Figure 2.4. For situations where we observe polydisperse materials advecting, we need to account for

the evolution of the grainsize distribution at every point in space. Note that we now change to grainsize, rather than grain size, to indicate a reference to an internal coordinate which describes the grain size distribution at every point in space within the material (Marks et al. 2012).

There are many advantages to including a grainsize coordinate in an analysis. Firstly, poly-disperse materials can be described naturally. Secondly, processes where the grain size distribution changes, such as milling operations, can be described simply. Thirdly, processes where the grainsize distribution varies in space, such as segregation, can also be described, in the same straightforward manner.

Since the analysis uses conventional continuum mechanics, but with an additional coordinate, we retain all of the advantages of a continuum theory. Motion can be described in terms of conservation of mass, momentum and energy. Material behaviour can be described using traditional constitutive models. Scaling laws can be used to simplify the grainsize dynamics.

The possibilities for describing polydisperse granular material using a grainsize coordinate are wide, varied and exciting. By including a grainsize coordinate in an analysis, the energy associated with changes in the grainsize distribution can be attributed directly. Once this energy is known, the dynamics of the grainsize distribution can be described. Then forces, stresses, displacements and strains can be described in terms of their effect on the grainsize distribution.

## **2.3 Granular flows**

Flowing granular materials have been studied systematically since 1885 (Reynolds 1885), however it was only during the second world war that the quantitative study of flowing sand truly began (Bagnold 1941). Much of this research focused on the interaction of wind and individual sand grains, and aeolian transport processes, such as in the formation of barchan dunes, as in Figure 2.6. When particulate matter flows, we say that it is in a liquid state, as



FIGURE 2.6: Barchan sand dunes. *Left:* A barchan on Earth. *Right:* Barchan dunes on Mars's Hellespontus region as seen by HiRISE on the Mars Reconnaissance Orbiter. (© wikimedia.org)

opposed to being a solid or gas. This flowing behaviour can occur in many geometries, both in natural flows and during the industrial processing of granular materials.

We categorise these flows generally by the amount of fluid contained within the pore spaces. Dry flows are common in industrial manufacturing, rock avalanches, snow (only if it is very cold — snow melts when sheared (Turnbull 2011)), sand dunes, heap formation, and hopper filling and discharge.

In nature, things are normally at least a little bit wet. Flows under these conditions are termed unsaturated. This is a misleading term and should be avoided — try to use partially saturated if possible. Examples of these flows are landslides, debris flows and snow avalanches at moderate temperatures, where significant amounts of liquid water exist within the ice matrix. For these flows, the water is most definitely not distributed uniformly throughout, but is expelled from the front of the avalanche, which is fairly dry, and accumulates in the tail. The mechanisms behind this are still unclear (McArdell et al. 2007).

Finally, there are fully saturated, or submerged flows, which occur wholly under water (or another liquid). An example of these is a submarine landslide, which can devastate sea bed pipelines and other offshore infrastructure.

The description of granular materials using computational and analytic models is still an open area of research. This is especially true for flowing granular materials (Iverson 2003). In the literature there are no well developed constitutive models which represent a broad variety of behaviours. There is also little consensus as to what experimental or numerical

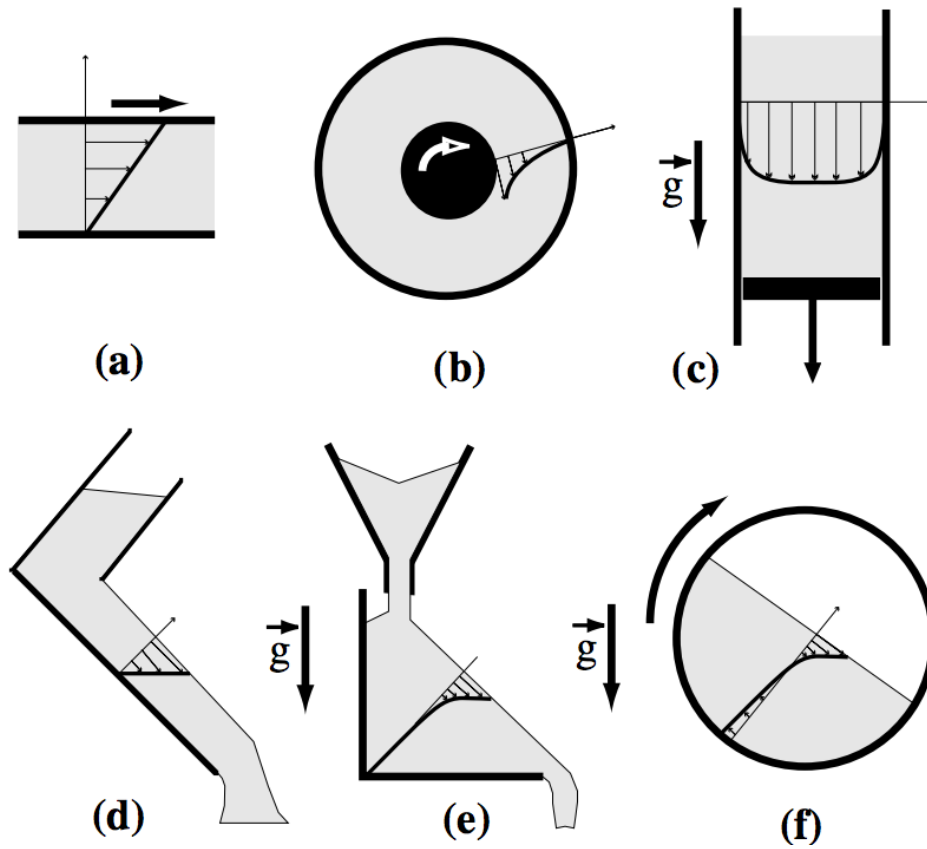


FIGURE 2.7: Six common flow geometries: (a) plane shear, (b) annular shear, (c) vertical chute, (d) inclined plane, (e) heap flow and (f) a rotating drum. (MiDi 2004)

data can be used to compare against such models (Hutter et al. 2005). Most of the data we do have comes from discrete element simulations (see 2.8.3) where the assumptions of low particle stiffness and small numbers of particles are hard to validate experimentally (Cleary et al. 1998; Bertrand et al. 2005). A seminal paper is MiDi (2004), in which a collection of experimental and numerical results are published that agree on many aspects of flows in a variety of geometries (shown in Figure 2.7) for spheres and discs.

We generally treat these flows as being monodisperse — i.e. they are constituted of particles of similar size. This is done to remove unnecessary complication, and ‘unwanted’ effects, such as segregation and mixing, that complicate the material behaviour. This is an open challenge, which will be investigated in Chapter 7.



FIGURE 2.8: The head of an avalanche of gravel passing down an inclined chute. The flow is from left to right. At the head, particles saltate above the free surface, while behind in the body of the avalanche a dense flowing layer dominates.

### 2.3.1 Granular avalanches

Granular avalanches, for example as shown in Figure 2.8, occur frequently on many different scales (Davies and McSaveney 1999). They are characterised by a dense layer of particles flowing down an inclined slope under the influence of gravity, with a free surface above. They may be channelised or free to spread laterally. At large scales, examples are snow avalanches (Bartelt and McArdell 2009), pyroclastic flows (Branney and Kokelaar 1992), rock avalanches (Davies and McSaveney 1999), debris flows (Naylor 1980) and submarine (Hampton et al. 1996) or terrestrial landslides (Savage and Hutter 1989). At smaller scales they occur in hopper filling and discharge (Shinohara et al. 1972), chute flows (Pouliquen 1999) and heap formation (Khakhar et al. 2001).

At slope inclinations just above the angle of repose of the material, the avalanche may progress at relatively constant velocity. During flow, gravitational potential energy is dissipated as heat, sound, friction and plastic deformation of the constituent particles. At high normal stress or shear strain rate, this can result in particle crushing or ablation. At higher slope angles, these losses cannot overcome the addition of energy due to gravity, and the avalanche can accelerate rapidly. At lower angles, the avalanche loses energy and comes to rest.

In natural avalanches, measurements are normally taken of the vertical fall and horizontal distances travelled, as well as an estimate of the total mass that moved. In large scale avalanches, an important mechanism that fuels avalanche propagation is erosion, where a moving avalanche can scour material from beneath it, adding to the mass of the avalanche,



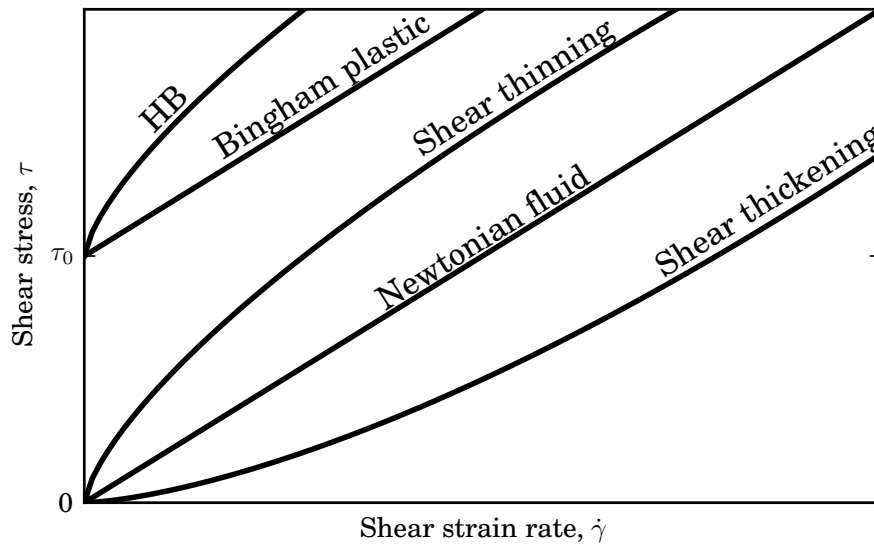


FIGURE 2.9: Common rheological models for viscous fluids.

and increasing its runout distance. This is coupled with deposition, as material is left behind the trailing edge of the avalanche.

Physical modelling of dry granular avalanches usually occurs in the simplest possible geometry — an inclined chute. This set up involves an inclined plane, usually roughened, and two glass side walls through which the flow is imaged (Savage and Hutter 1989; Moriguchi et al. 2009). Characterisation of the internal properties of the flow are still in progress (Sanvitale and Bowman 2012; Hill et al. 2010). Because of this, boundary measurements of the flow properties are all that are commonly available. Relations between the boundary measurements have been found, especially for cases where the flow interacts with obstacles (Faug et al. 2009; Chanut et al. 2010; Moro et al. 2010). For the case of grains submerged in an index matched fluid, tracer particles can be used to image the internal velocity field in 3D (Wiederseiner et al. 2011b).

### 2.3.2 Constitutive models

Granular materials are frictional in nature. The response of the material is dependent on both the particulate nature of the material, and the properties of each individual grain. A first order

description of the material is that proposed by Coulomb, and formalised in the Mohr-Coulomb model, where the shear stress required to move the material,  $\tau$ , increases with normal stress,  $\sigma$ , (Coulomb 1773), as

$$\tau = c + \sigma \tan \phi,$$

where  $\phi$  is the friction angle of the material, and  $c$  is the apparent cohesion. For a cohesionless material, if we imagine a block resting on an inclined plane, with slope  $\theta$ , the block would begin to slide when the angle of the plane was  $\theta = \phi$ . This can be expressed as

$$\frac{\tau}{\sigma} = \mu_c,$$

where  $\mu_c = \tan \phi$  is the critical slope at which sliding begins. Unfortunately, this model ignores effects that occur as the material begins to speed up — a rate dependency. For traditional flow problems, the simplest model that addresses this case is that of a Newtonian fluid

$$\tau = k\dot{\gamma},$$

where  $k$  is the shear viscosity of the fluid. A variety of constitutive models for fluids are shown in Figure 2.9. For a Newtonian fluid, the viscosity is independent of the applied normal stress, and is directly proportional to it. If the material gets more viscous the faster it is stirred, it is called shear thickening. The most common example of such a fluid is oobleck (a cornstarch and water mixture). If you walk slowly over a pool of oobleck, you will sink into it, but if you move quickly, you can stay afloat. The opposite condition is if a fluid gets easier to stir as the stirring speed increases — a shear thinning material, such as blood, ketchup or syrup. If the material does not flow below a certain shear stress,  $\tau_0$ , it may be a Bingham plastic — also known as a yield stress fluid (Bingham 1917),

$$\tau = \tau_0 + k\dot{\gamma}.$$

A good example of a Bingham plastic is toothpaste. You need to squeeze the bottle to build up a shear stress of  $\tau_0$  before the toothpaste will start to flow out. If the viscosity also changes with the shear strain rate, such that it is either shear thickening or shear thinning, it may be described as a Herschel-Bulkley (HB) fluid (Herschel and Bulkley 1926) where

$$\tau = \tau_0 + k\dot{\gamma}^n,$$

and  $n$  is a free parameter. By also accounting for the granular nature of the material, and including the Mohr-Coulomb criterion, we recover a simple description of a granular flow

$$\frac{\tau}{\sigma} = \mu_c + (K\dot{\gamma})^n, \quad (2.1)$$

where  $K$  is some time scale. This is a moderately robust fluid model of granular material, known to work for steady flows far from boundaries (Rognon et al. 2007). From observations of experimental flows of dry granular material, (Bagnold 1954), and validation with discrete element simulations (Silbert et al. 2001; Lo et al. 2010), it has been shown that material flowing over a rough base follows the following scaling

$$\dot{\gamma}(z) \propto \sqrt{1-z}.$$

This can be derived by considering a lithostatic stress distribution, and an HB fluid model, as will be shown in Chapter 4. A more sophisticated constitutive model for monodisperse spheres of diameter  $d$  was developed in Pouliquen (1999); Pouliquen and Forterre (2002). Here the material is controlled by the inertial number  $I$  as

$$\begin{aligned}\frac{\tau}{\sigma} &= \mu(I), \\ I &= \dot{\gamma}d\sqrt{\frac{\sigma}{\rho}}, \\ \mu(I) &= \mu_c + \frac{\mu_2 - \mu_c}{I_0/I + 1},\end{aligned}$$

where  $\mu(I)$  is the friction coefficient,  $\mu_2$  is the viscosity at high  $I$  and  $I_0$  is a constant. This model informs us about the nature of the parameter  $K$  from (2.1), and has been shown to successfully represent monodisperse flow (MiDi 2004). In Weinhart et al. (2012b), the model was extended to account for variations in slope angle, bed roughness and flow depth. It has also been extended into three dimensions to model wall effects in an inclined chute geometry (Jop et al. 2006).

Because of the complexity of granular flows, model materials with known rheology are often used instead in experiments, to replicate granular flows (Ghemmour et al. 2008). There are many challenges that lie ahead to create rheological models which represent full scale avalanches, where the avalanche body can have variable saturation, pore pressure, grainsize distribution and turbulence.

### 2.3.3 Modelling full scale avalanches

Current computational modelling of large scale granular avalanches is generally done using a finite volume solver for the depth-averaged shallow water equations (Christen et al. 2010). This is an extension to those initially proposed in Savage and Hutter (1989) for granular avalanche flow.

Because these are depth-averaged equations, they cannot replicate many behaviours that are intrinsic to avalanches, such as vertically varying shear strain rates or segregation (Armanini 2013). In addition, the model assumes that the terrain has only small curvatures, and so is not applicable to model impact on structures, or even steep changes in gradients, such as found on many hillsides (Hutter et al. 2005).

This type of model generally uses either the Voellmy-Salm (Salm 1993) or the Norwegian NIS (Norem et al. 1988) constitutive model. These models are designed to reliably predict the runout distance of snow avalanches, rather than to mimic the internal dynamics of an avalanche. These are engineering approximations of a constitutive model, rather than attempts to describe the stress-strain behaviour of small representative volumes of the material.

There are many effects which cannot be captured in this class of model (Iverson 2003), such as steep coarse surge fronts, fine grained tails and lateral levees. These phenomena are largely due to segregation-induced non-uniformities in the solid components of the avalanche. By taking a depth-averaged approach, the ability to track these internal flows within the material is lost.

To tackle this problem directly, and describe the important processes controlling the avalanche dynamics, the change in grainsize distribution spatially within the avalanche has to be accounted for. A five-dimensional model, describing space, time, and an internal coordinate describing the grainsize, are unfortunately all required to model the physical system reliably. The simplicity gained by depth averaging, and describing the system in just two spatial dimensions and time, means that we have neglected important physical processes. This is why current models of granular avalanches largely do not reproduce physical behaviour (Iverson 2003).

#### **2.3.4 Historical note**

Snow avalanches are a serious threat, but to ignore the achievements made in our science between 1960 and 1990 is unfair. During the last catastrophic avalanche winter in Switzerland (1999), 97% of all hazard maps functioned as designed. The failure of the remaining 3% was not due to calculation error (Gruber and Margreth 2001). This is a remarkable achievement and credit should be given to these earlier researchers. More importantly, this feat was accomplished without numerical models, without GIS systems, without considering snow entrainment and without an accurate constitutive

model describing the internal deformation of the flow. Most hazard maps were prepared with simple avalanche dynamics models based on steady state flow. No effort was made to track the motion of the avalanche from initiation to runout. Lateral spreading was accounted for in an easy way. Maps and historical records were consulted. The question of why this system worked so well is perhaps the more honest and intriguing scientific query than blindly stating new differential equations.

— Bruno Salm 2004

There are various reasons why the work contained within this dissertation is vital for predicting avalanche runout, and I will here attempt to set out some of those reasons in terms of the effects observed in granular avalanches.

While many aspects of granular avalanches are at this stage only understood phenomenologically, the bulk of the work in saving lives from avalanches has already been done (Gruber and Margreth 2001). Such previous methods rely extensively on historical data to find areas that are subject to avalanches. Unfortunately, it seems that the frequency and location of avalanches, landslides and debris flows are changing rapidly (Petley 2012), in part because of anthropogenic climate change, and in part due to changing land usage patterns.

To appreciate fully what is still to be done in terms of increasing safety for people and property, a distinction needs to be made between predicting the initiation of an avalanche, and predicting the runout characteristics. We require models of both these phenomena to be able to give accurate information about safety from avalanches.

This work makes no advances in our understanding of avalanche initiation. With respect to the runout of an avalanche, however, I will argue that an understanding of the processes that are involved within an avalanche are highly important. Since we have no way of predicting accurately the runout distance of any given snow slab movement over arbitrary terrain, we have no way of gauging the factors of safety embodied in current hazard maps.

By creating models to represent flow behaviours of snow avalanches accurately, we can begin to reduce the overdesign inherent in existing hazard maps, enhance the abilities of protection structures, and provide safer, cheaper and more reliable design practices to those of the past.

In Armanini (2013) there is a call to better understand the migration of boulders internally within debris flows, as these boulders affect dynamic impact of avalanches with structures. A first step towards understanding this effect is presented in Chapter 7.

It should be borne in mind that this work is in no way limited to snow avalanche modelling. With regards to the industrial processing of granular materials, efficiency is far from good (Lowrison 1974). Current models consider the processing of granular materials as an initial value problem. Given an initial grainsize distribution and a particular grinder or mill, there are models to produce expected output grainsize distributions. The geometry of the mill, as well as the physical processes involved in the crushing, are obfuscated by this level of abstraction. To increase efficiency, we need better models to account for particle crushing as a boundary value problem.

According to a 2005 NASA technical report, (Wilkinson et al. 2005), there are many aspects of granular materials research that will need to be advanced significantly to facilitate extraterrestrial human survival. We do not have models with sufficiently deep understanding to be able to design mineral transport and processing techniques in variable gravity.

## **2.4 Segregation**

When we have such a mixture of grains that are of different sizes, they have a tendency to separate when moved. In a packet of cereal, the crumbs are always at the bottom of the box. In a jar of mixed nuts, the brazil nuts rise to the top (Mobius et al. 2001). In some situations, this is a useful tool for separating constituents in a mixture (Kelly and Spottiswood 1982), but it often causes unwanted demixing, leading to poor quality control (Johanson 1978) and safety (Muzzio et al. 2002).

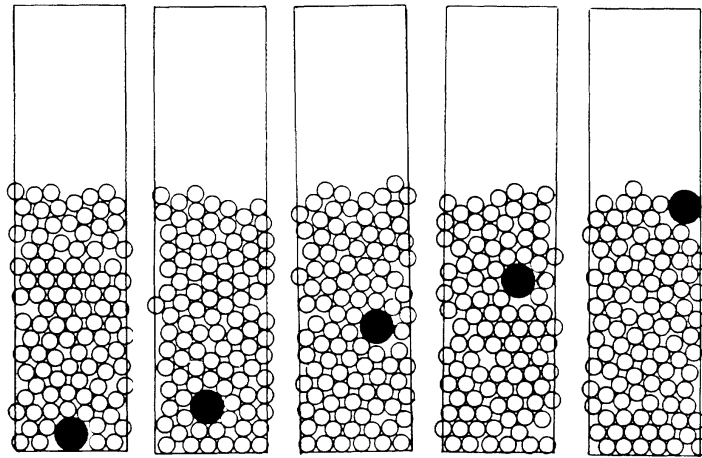


FIGURE 2.10: The brazil nut effect. After many periods of shaking the system, the particle rises to the top of the material. *Left to right*: The simulations snapshots are taken after 0, 10, 30, 40 and 60 shakes. (Rosato et al. 1987)

The phenomenon of segregation has largely been posed historically as an issue affecting the quality of mineral processing (Williams 1968; Drahn and Bridgwater 1983). Additionally, the soil formed from flows which have undergone segregation are also commonly observed in geological deposits as ‘reverse grading’, where material is deposited with large particles vertically above smaller ones (Bagnold 1954).

Many mechanisms have been found which could lead to segregation, including kinetic sieving, trajectory segregation, convection and fluidization (McCarthy 2009). These will now be investigated in more detail for a variety of well known cases of segregation.

### 2.4.1 The brazil nut effect

For the case of a jar of nuts, as mentioned before, we notice that large particles rise to the top of the container after being shaken, as shown in Figure 2.10. There have been a variety of investigations into how this segregation occurs, and a large number of potential mechanisms have been proposed. It has been shown that the size (Rosato et al. 1987), density (Hong et al. 2001) and even the background air pressure (Mobius et al. 2001) all contribute to the segregation dynamics. The segregation has also been shown to be dependent on the convection cells which form in a cylindrical container (Knight et al. 1993) due to the shaking motion.



This form of segregation has been studied at low gravity, as it is believed to be responsible for the surface conditions of asteroids (Güttler et al. 2013). As a result, we know that this segregation velocity is proportional to gravity.

### **2.4.2 Rotating tumblers**

A common industrial operation involves placing a granular material into a rotating tumbler, such as a front loading tumble dryer. At low rotational speeds, intermittent or continuous avalanches form at the surface of the granular bed. Magnetic resonance imaging has revealed that the free surface flow has a linear velocity profile with a maximum at the free surface, and stops within the bulk (Nakagawa et al. 1993). During flow, there is a tendency to segregate material by size (Donald and Roseman 1962) or density (Ristow 1994) in the radial direction, such that one species accumulates near the axis of the drum, and the other species collects at the circumference. This phenomenon has been studied for a range of cylinder geometries experimentally (Khakhar et al. 2003) analytically (Prigozhin and Kalman 1998) and numerically (Khakhar et al. 1997), but laws for predicting the rate of segregation are still phenomenological. At varying fill levels, different patterns of segregation are visible (Hill et al. 2004), varying from star-shaped to disc-shaped.

Another form of segregation that may occur in rotating tumblers is axial segregation. After significant rotation of the cylinder, alternating axial bands can form at the surface due to size or density differences in particles. This is believed to be a result of the difference in angles of repose of the mediums, which causes them to flow at different rates in the axial direction (Donald and Roseman 1962). Yanagita (Yanagita 1999) used a three dimensional cellular automaton to model this phenomenon and was the first to explain the transition from radial to axial segregation.

MRI imaging has been conducted to validate this work, and view into the bulk of the material, not merely at the surface (Hill et al. 2010). The work has noted that some axially segregated regions exist in the bulk without extending to the surface. This implies that axial segregation may not in fact be driven exclusively by a surface phenomenon.

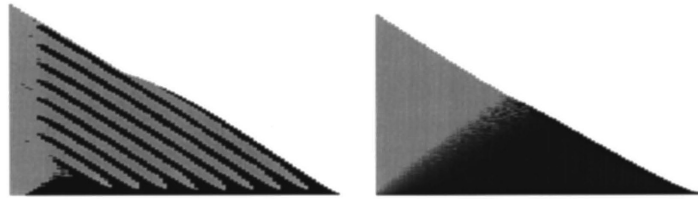


FIGURE 2.11: Steady state solutions of Makse's heap theory showing two different modes of segregation. The grey particles are larger than the black particles. *Left*: Intermittent avalanches create layers of segregation. *Right*: Continuous avalanching allows small particles to migrate towards the base of the flow. (Makse 1997)

### 2.4.3 Heap formation

When a granular material is poured onto a flat plane, it does not spread infinitely far from the point of pouring (as a traditional fluid would), but rather forms a heap, with a characteristic slope angle over most of the heap, and a logarithmic tail near the plane (Alonso and Herrmann 1996). As the heap forms, progressive avalanches occur at the free surface, disturbing the top few layers of the pile as they pass. As this intermittent avalanching occurs, two types of segregation by size, shape or density are commonly observed, as shown in Figure 2.11.

Drahn and Bridgwater (Drahn and Bridgwater 1983) poured a bidisperse mixture into a two dimensional heap, and watched how avalanches created alternating striations of the different particles, which was termed stratification. This was further investigated quantitatively by Koeppel (Koeppel et al. 1998) and explained in detail by Makse (Makse 1997) as a combination of 'spontaneous stratification' and 'spontaneous segregation'. The stratification was explained as a result of the difference in the angle of repose of the mixture components. Because of this difference, one component preferentially avalanches, creating layers of mono-disperse deposition. The segregation is a bulk movement of the large grains to the bottom of the pile.

## 2.5 Kinetic sieving

Stay on top to stay alive.



FIGURE 2.12: ABS ® avalanche airbag. Deploying this airbag during an avalanche causes you to increase in volume, and rise above the flow, potentially saving your life. (ABS-Lawinenairbags 2013)

Many of the above examples of segregation are a result of granular avalanches. While all of them have been explained either phenomenologically or analytically, there is still no unified theory to describe all of the size effects as a boundary value problem. This Section deals with a mechanism of segregation, kinetic sieving, rather than an example of where it is produced in nature and/or industry.

When a granular material flows, many collisions between particles will occur. After each collision, the incident particles separate, creating a void space. Over a short time span, this void grows, until it is filled by another particle. As the void is growing over time, it is more likely that a small particle will fit into this void than a larger one. Also, there is a preference for the void to be filled from the direction of the principal stress gradient (generally this is due to gravity). Because of this void filling effect, there is a net percolation of small particles in the direction of the principal stress gradient (normally downwards — in the direction of gravity).

The flow, however, maintains a fairly uniform solid fraction spatially, and so the large particles are forced in the opposite direction (upwards), balancing the mass flux of small particles

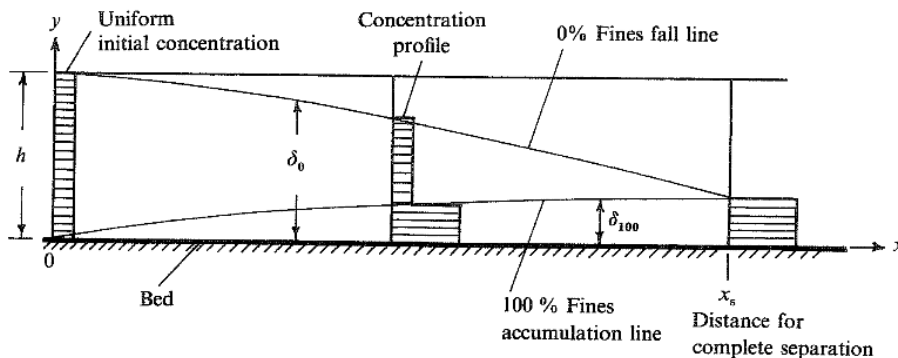


FIGURE 2.13: Concentration profiles of small particles as a function of distance down slope. The concentration profiles are averaged over one third of the flow using splitter plates. 0% and 100% fines lines indicate areas above/below which there are no/only fine particles respectively. (Savage and Lun 1988)

(downwards). This mechanism of small particles filling voids is termed kinetic sieving, and is believed to be responsible for many types of segregation.

In a snow avalanche, this mechanism is leveraged to save lives by outfitting skiers with airbags which deploy when submerged in an avalanche, as shown in Figure 2.12. The large volume of the person/airbag unit (the airbag is generally around 170 L, a human 66 L) causes the person to rise rapidly through the flow, giving a 91% reduction in mortality rate if used correctly (Brugger et al. 2007).

### 2.5.1 Statistical mechanics

In Savage and Lun (1988) two mechanisms are proposed, which, when coupled together, predict segregation in good agreement with experiments conducted on bidisperse material flowing down an inclined chute. The first is the ‘random fluctuating sieve’, which is a gravity-induced flow of particles into the voids below. By arranging the flow into layers, particles which are above a vacant hole can pass down into it by free falling under gravity. The second is ‘squeeze expulsion’ whereby particles can become dynamically unequilibriumed and be ‘squeezed’ out from their current layer in a random direction. Squeeze expulsion was used as a mechanism to satisfy overall mass conservation, so the authors deemed its exact physical nature to be unimportant.

By using a maximum entropy argument to find percolation velocities, Savage and Lun derive a continuum theory for particle size segregation in inclined chute flow. Their analytic results are then compared to experimental work done with polystyrene beads over a 1.1 m chute. Two angles of inclination were tested,  $26^\circ$  and  $28^\circ$ , and for two concentrations of fines, 10% and 15%. These results were found to agree well with the results of the analytic work, although the experimental results were quite coarse. Instead of tracking individual particles through the flow (which was impossible at the time), particles were collected in three bins, giving information on the vertical particle size distribution averaged over one third of the height of the flow.

The analytic work predicts a 100% fall line (a line above which no small particles are present) and a finite time for the flow to segregate fully, as well as the segregation pattern, as shown in Figure 2.13. This is in keeping with the experimental work, but due to the micromechanical origins of the analysis, extension to other geometries and grainsize distributions is prohibitively complicated.

### 2.5.2 Continuum models

The second dominant theory explaining kinetic sieving is that proposed in Dolgunin and Ukolov (1995) and expanded further in Gray and Thornton (2005). In their paper, a binary mixture theory is used to formulate a model for kinetic sieving. The model is based on the idea that each component of the mixture carries a different amount of the overburden stress. The scaling of this stress between the two species, however, is not explained, but assumed.

Because little is known about the stress scaling between the two components, percolation velocities are assumed to be constant through the bulk material. They are taken to be  $q_{GT} = \pm Bg \cos \theta$ , where  $\theta$  is the inclination of the slope,  $c$  is some inter-particle friction, and  $B$  is a dimensionless parameter that is intended to account for varying particle size, roughness and shape. However, it does not account for the interaction between particles causing segregation, which is governed by the shear strain rate.

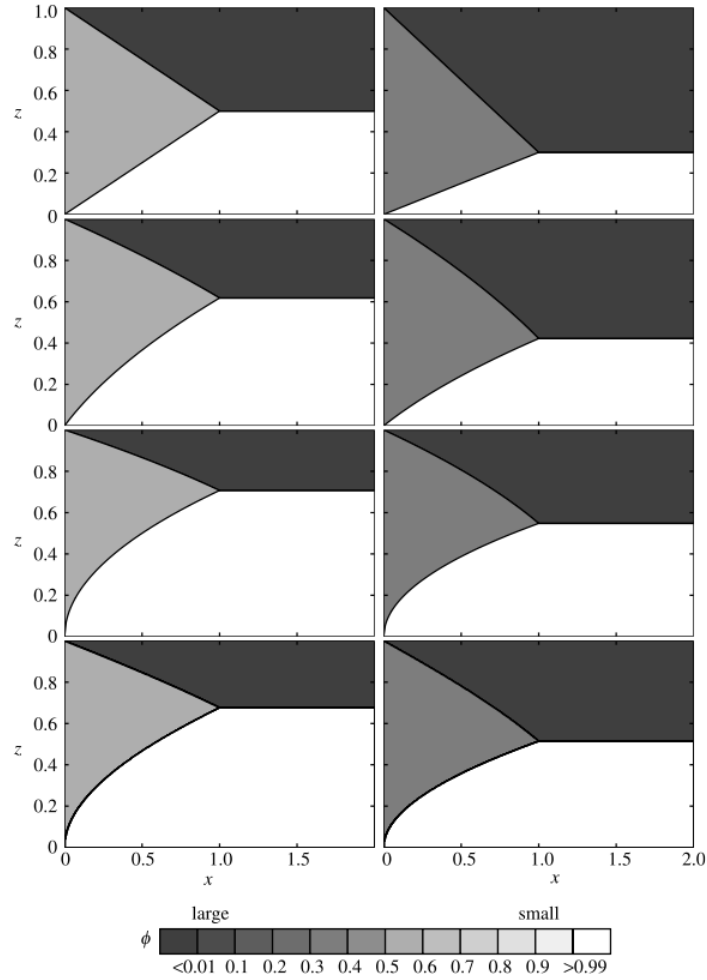


FIGURE 2.14: Gray and Thornton's steady state solutions for four different velocity profiles and two different initial concentrations. Left:  $\phi_0 = 50\%$ . Right:  $\phi_0 = 30\%$ . *Top row*: plug flow,  $u = 1$ . *Second row*: basal slip,  $u = 0.5 + z$ . *Third row*: simple shear  $u = z$ . *Bottom row*: Bagnold velocity profile  $u = 3(1 - (1 - z)^2)$ .  $S_r = 1$  for all cases,  $S_r = 1$ , i.e. all solutions fully segregate at  $x = 1$ . (Gray and Thornton 2005)

Gray and Thornton define  $\phi_s$  and  $\phi_l$  as the small and large particle concentrations at any point in space such that  $\phi_s + \phi_l = 1$ . For the case of spatially homogeneous initial conditions, they use  $\phi_0$  to indicate the small particle concentration.

A non-dimensional segregation equation is ultimately found in terms of the small particle concentration  $\phi$ , the assumed downslope velocity profile  $u(z)$ , the height  $z$ , the time  $t$  and the segregation number  $S_r$ , as

$$\frac{\partial}{\partial t}(\phi u) = S_r \frac{\partial}{\partial z}(\phi(1 - \phi)),$$

where  $S_r$  is a non dimensional fitting parameter that determines the time for complete segregation to occur. This equation is then solved for varying initial concentration  $\phi_0$ , varying velocity field  $u(z)$  and segregation number  $S_r$ . The theory is used to predict both the time evolution of the flow and the steady state segregation patterns, as shown in Figure 2.14. The solution of Gray and Thornton's advection equation presents three discontinuities in  $\phi$  for all shear cases, in the form of shocks. Two of these occur at the top and bottom of the flow, and propagate towards each other through the medium. Where they meet, the third discontinuity forms, at the triple point of the flow.

From this point, two separate flows exist, that of exclusively large particles at the top, and small particles at the bottom. Further research has investigated a dependence of the percolation velocity on the shear strain rate (May et al. 2010). Also, the competing theory of Savage and Lun proposes that the percolation velocity is a function of the shear rate,  $du/dz$ . Because of this assumption, Gray and Thornton predict that segregation occurs in plug flow, as shown in Figure 2.14. Plug flow is a case where the downslope velocity is constant along the height of the flow, such as in rigid body motion. In this case there is no change in the orientation of particles with respect to one another, and so no segregation should or can occur.

Figure 2.14 shows how the theory predicts different segregation patterns depending on the assumed flow velocity and mixture concentrations. Other solutions have been shown for inhomogeneous initial conditions, and even temporally varying input concentrations. The model has been extended several times to include a passive liquid phase (Thornton et al. 2006), diffusive remixing (Gray and Chugunov 2006), avalanche fronts (Thornton and Gray 2008; Gray and Kokelaar 2010) and larger numbers of mixture components, which implicitly represent sizes (Gray and Ancey 2011).

These continuum models have been validated experimentally in Wiederseiner et al. (2011a) and values for the fitting parameters have been found from numerical tests (Thornton et al. 2012). The stability of such hyperbolic equations has also been studied (Shearer et al. 2008).

These continuum theories are dissociated from the bulk behaviour of the material, describing only the segregation patterns observed during flow. To describe the segregation that occurs during non-steady flows, the segregation pattern needs to be coupled to the kinematics. In addition, these continuum models neglect the physical size of the grains in the analysis, and so have no way of capturing size effects.

The major holes existing in such continuum theories that I wish to address are:

- (1) using the physical size of the constituent particles,
- (2) inclusion of a constitutive model,
- (3) the effect of size contrast on the time for segregation and
- (4) modelling arbitrary grainsize distributions.

## 2.6 Mixing

Another important mechanism in granular flows is mixing. As material flows, random fluctuations in particle motion occur due to repeated collisions giving rise to mixing. As with traditional fluids (Fick 1855), we can measure the diffusive flux of some variable  $T$  in a system as

$$J = -D\nabla T,$$

with diffusion coefficient  $D$ , which has units  $\text{length}^2$  per unit time. This is known as Fick's first law, and is analogous to Darcy's law for hydraulics. It is well known that a material made up of particles undergoing a random walk, or Brownian motion, will reproduce this behaviour (Einstein 1905).

There are several quantities which are generally represented as diffusive; mass, momentum and energy. In contaminant transport in gases, mass diffuses through a system without external forcing. On the other hand, in the mixing presented in this dissertation, momentum diffuses through the material. In the heat equation, thermal energy diffuses through a medium.



For a granular material, it has been shown in experiments that the diffusion of momentum in fact varies linearly with shear strain rate (Campbell 1997; Utter and Behringer 2004). This has ramifications for the flow of granular material down a slope, as shown in Buser and Bartelt (2009), where the random kinetic energy, associated with the diffusivity, affects the prediction of velocity profiles in snow avalanches.

The interaction between segregation and mixing has been investigated for the case of inclined plane flow (Gray and Chugunov 2006). Mixing causes the otherwise perfect segregation to become diffuse, matching experiments more closely (Wiederseiner et al. 2011a).

## 2.7 Crushing

A final important process in granular mechanics is that of crushing. When particles are loaded, they have some finite probability of fragmenting. When this occurs, the mean grainsize decreases, as a large particle is converted into several fragments. This could occur from erosion, where the surface is merely ablated, or from industrial comminution processing at high confining stress which crush the particle.

During any of these events, the specific surface of the material increases, which requires an input of energy. During industrial comminution, where a target grainsize distribution is to be produced, there are huge energy demands for the crushing of brittle materials (roughly 3% of global electricity - (Schoenert 1986)). In this situation, it is known that we operate at exceedingly low efficiency, roughly 0.1% - 1% (Lowrison 1974).

As identified by the larger community, we require methods to model comminution that describe the evolution of the full grainsize distribution related to the specific boundary value problem (King 1993; Powell and Morrison 2007). Inadequate models are one of the main limiting factors in increasing efficiency for one of the world's most energy hungry industries.

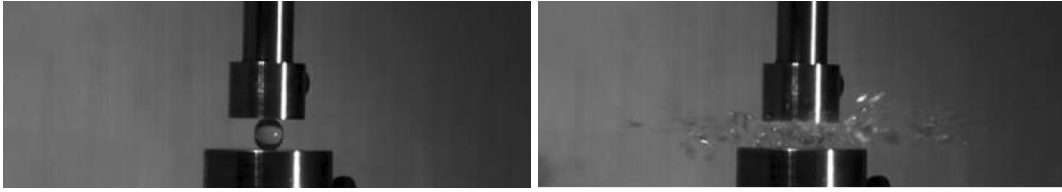


FIGURE 2.15: A single grain being crushed. The glass bead is loaded diametrically until it fragments explosively. A large range of fragment sizes are created as a result of the process. (Cataldo 2012)

### 2.7.1 Confined comminution

Comminution modelling is generally described in three ‘laws’ attributed to Rittinger, (Rittinger 1867), Kick (Kick 1885) and Bond (Bond 1952). These ‘laws’, or more accurately ‘rules of thumb’ describe the energy required to facilitate comminution. They inform us that the useful energy consumed in comminution (the part doing the crushing) is proportional to the newly generated surface area. Secondly, the energy can be related to the change in particle sizes from input to output. Lastly, the total useful work in breakage is inversely proportional to the square root of the diameter of the fragment particles.

#### 2.7.1.1 A single grain

A more enlightening viewpoint can be gained by looking at what happens to individual grains when crushed, as shown in Figure 2.15. The fracture behaviour of many materials and shapes have been investigated (Yashima et al. 1987; Perfect 1997). We learn from these experimental studies that there are common fragment size distributions that occur for a given loading condition and material type. Also, there is a typical crushing stress at which a particle will crush, which is related to its material, shape and size.

The variability of particle crushing stress was first described using a weakest link analogy from Weibull et al. (1951). In this case, we must imagine that a pile of grains has been carved out of a homogeneous material, with homogeneous crack distribution. Larger particles will have on average more cracks in them, and so will crush at a lower stress. Small particles will have low probability of containing a large crack, and so will have a higher crushing stress.

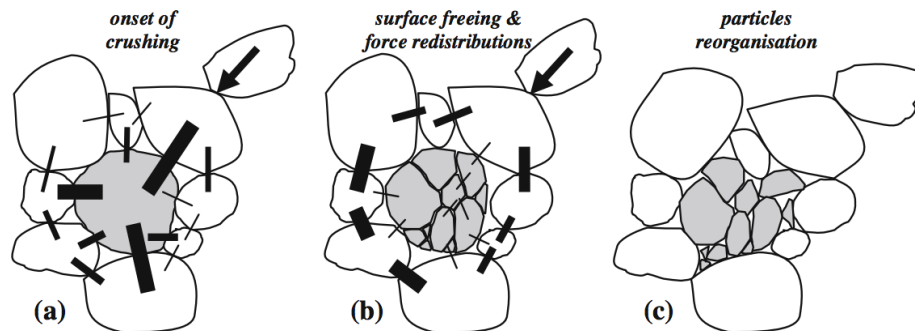


FIGURE 2.16: Energy loss from a crushing event. (a) A particle is about to be crushed. Contact forces are proportional to the line thickness. (b) Some energy is converted into new surface area. Other energy is lost due to force rearrangement as new particles must carry the load. (c) Particle rearrangement is a further mode of energy dissipation, causing plastic volumetric dissipation from friction. (Einav and Nguyen 2009; Russell and Einav 2013)

The other component of single particle crushing is the fragment size distribution. In general, this distribution depends on the loading state of the particle, and the material which is being crushed. If the material is loaded diametrically, as in a Brazillian test, explosive fragmentation can be observed and a broad fragment size distribution is measured. If, however, the grain is merely repeatedly sheared lightly, as in an erosion process, the fragment size distribution will include many new fragments, orders of magnitude smaller than the initial particle, as well as a single particle almost as large as the initial particle.

### 2.7.1.2 Collections of grains

To understand the effect of particle crushing on the system behaviour, we must now consider an assembly of particles. We can imagine that these particles are loaded in such a way that one or more of the particles is likely to break. The system chooses certain particles to break, and these will be particles with large tensile stresses developing within them, causing cracks to open. A simple model to represent which particles will break was presented using a cellular automaton in Steacy and Sammis (1991). In this model, particles with neighbours of a similar size are those that will break.

Particles much larger than their neighbours will be surrounded by many contact points, and will be subject to fairly isotropic loading. These are unlikely candidates to crush. Similarly,

small particles will be free to move around the pore spaces, and will not carry significant load. These are also unlikely to crush. Only those particles surrounded by neighbours of a similar size will be likely to crush. This nearest neighbour model explains much of the nature of breakage processes, when coupled with the material behaviour predicted from the weakest link analogy mentioned above.

We find that in the limit of incredibly high confining stress, the system reaches a stable grainsize distribution, which is power law in nature (Turcotte 1986; Ben-Zion and Sammis 2003; Crosta et al. 2007). The power law distribution is a signature of a system with no characteristic size, as any size that was preferentially favoured by the system would then have a higher likelihood of being crushed.

These power law distributions have in fact been shown to also be fractal in nature using discrete element method simulations (Ben-Nun et al. 2010) and cellular automata (Stacey and Sammis 1991; McDowell et al. 1996). The characterisation of the behaviour of the system into just an evolution towards a fractal state is, however, a simplistic view of the system. When a single particle crushes, it causes rearrangements not only of the nearby particles, but also of the force network, as shown in Figure 2.16 and described in Einav and Nguyen (2009); Russell and Einav (2013).

### **2.7.1.3 A continuum process**

There exists a family of constitutive models for granular materials based on degradation of the grainsize distribution due to breakage (Einav 2007a; Einav 2007b). These breakage mechanics models use a scalar parameter to describe changes in the grainsize distribution due to crushing, from its initial grading to an assumed fractal grading, as first proposed in Hardin (1985). As the grainsize distribution changes, the constitutive behaviour of the material changes, capturing the mechanism of isotropic hardening directly.

Another means of modelling the evolution of the grainsize distribution is by harnessing population balance models (Randolph and Ranjan 1977; Peterson et al. 1985; McGrady and Ziff 1987; Williams 1990). These models describe the evolution of the full grainsize

distribution over time using an internal coordinate. The models require the knowledge of two terms: the specific breakage rate of each size, and the fragment size distribution from a crushing event.

The fragment size distribution has been measured in single particle crushing tests under different loading conditions (Ryu and Saito 1991; Cheong et al. 2004; Cataldo 2012). The specific breakage rate, however, is generally assumed to be a power law, which obfuscates the physical processes involved in these models. Because these models require a priori ultimate grainsize distributions, they do not give us any guidance as to how crushing will behave in open systems, such as when the material is flowing.

### **2.7.2 Crushable flows**

When grading curves are measured in the field inside avalanche and landslide runout, log-normal grainsize distributions are often measured, rather than the power law distributions measured in static tests. These have been measured in the field (Bartelt and McArdeell 2009; Rastello et al. 2011), in experiment (Imre et al. 2010) but have not been predicted in theory.

How the system reaches a log-normal grading is still unknown. Furthermore, how the grainsize distribution transitions from a power law, with no typical sizes, to a log-normal one, with a well defined local size, is also unknown. These challenges will be discussed, and a possible explanation will be provided, in Chapter 8.

## **2.8 Numerical methods**

This dissertation uses three distinct numerical methods. Firstly, cellular automata are described to explain pattern forming behaviour. Secondly, continuum conservation equations are solved numerically using the finite volume method. Thirdly, the discrete element method is used to validate the continuum theory. A brief description of the rationale for the choice of each method is outlined below.

FIGURE 2.17: Gosper's glider gun in Conway's Game of Life. This set up creates a constant stream of gliders that propagate down and right. These features move themselves through the grid. By interacting these gliders with each other, universal computation can be achieved. (Conway 1970) ©

### 2.8.1 Cellular automata

Fermi often expressed a belief that future fundamental theories in physics may involve nonlinear operators and equations, and that it would be useful to attempt practice in the mathematics needed for the understanding of nonlinear systems. The plan was then to start with the possibly simplest such physical model and to study the results of the calculation of its long-time behavior.

— Stanislaw Ulam

Cellular automata are the progenitors of modern computational methods for modelling physical systems (Wolfram 1986), beginning with Stanislaw Ulam in 1952, who began investigating discrete cellular automata to study nonlinear waves and solitons with Enrico Fermi (Ulam 1952; Fermi et al. 1955). Cellular automata generally consist of a regular cartesian grid of cells which contain binary information in each cell. A simple rule, or set of rules, is implemented such that the value in each cell evolves due to the values in each neighbouring cell. A famous example of a cellular automata is Conway's Game of Life (Conway 1970), which exhibits a vast array of behaviours. A famous structure, known as

Gosper's glider gun, is shown in Figure 2.17. This structure creates gliders, or spaceships, which are self-propelling patterns.

Many cellular automata have been proposed which model phenomena from all branches of science (Wolfram 2002). Due to the wide applicability of cellular automata to model physical processes, there is an open field of research aiming to answer the question of whether or not the real world is in fact merely a cellular automaton (Ilachinski 2001). Efforts are also underway to model reality using cellular automata (Fredkin 1991), where the universe is fully discrete. Additionally, some one dimensional cellular automata have been shown to be Turing complete (Cook 2004) – i.e. they are capable of universal computing.

There are an exceptionally large number of models using cellular automata that are available in the literature. They have been used extensively in numerous applications in stochastic problems, neural networks, pattern recognition, HIV drug therapy, reaction-diffusion systems (Chopard and Droz 1998), fluid dynamics (Margolus et al. 1986) and biology (Ermentrout, Edelstein-Keshet et al. 1993). For physical modelling, there are also many examples of using cellular automata to replace partial differential equations, (Chopard and Droz 1998; Bagnoli 1941; Schweitzer and Zimmermann 2001; Deutsch et al. 2005).

## **2.8.2 Finite volume methods**

In the finite volume method (FVM), the governing equations are integrated piecewise over a mesh of representative volumes. Using these integrals, fluxes can be balanced across the boundaries of control volumes (LeVeque 2002).

The FVM is generally used exclusively for solving conservation equations, such as those presented in Chapter 4. This method is widely popular in computational fluid dynamics software. FVM is especially powerful on coarse nonuniform grids and in calculations where the mesh moves to track interfaces or shocks.

There are three main ways of handling discontinuities in a solution using FVM (E Ewing and Wang 2001). The first is to use an algorithm that tracks the discontinuity, and either

refines the mesh locally around it, or somehow forces the solution to remain stable. This is often problematic because the number and location of discontinuities are often unknown and variable.

A more refined method is to use Riemann solvers, where a decomposition of the solution space resolves shocks as characteristic solutions (Godunov 1959). Any solution can then be treated as a superposition of discontinuities, and stable, accurate solutions can be found. This method is very good at capturing discontinuities and shocks in a wide variety of computational fluid dynamics, magnetohydrodynamics and relativistic problems. Unfortunately, the method is also complex to solve, and numerically highly intensive.

The method I have chosen to use for this dissertation is a third type. In this method, flux limiters are used to locally switch between two solution schemes (Van Leer 1979). One solution scheme is highly accurate, and non-dissipative. This is used when small fluxes pass between control volumes. The other solution scheme is still accurate, but strongly dissipative, and is only used when large fluxes pass between control volumes. This gives accurate and stable solutions, that are simple to implement numerically (Kurganov and Tadmor 2000).

### **2.8.3 Discrete element method**

In the study of granular materials, a common method for simulating the particulate behaviour of the system is the discrete element method (also known as the distinct element method, discrete particle method or molecular dynamics simulation). In this type of simulation, a large number of individual grains are modelled, generally as spheres, that interact with one another. The method itself is not limited to spherical grains, but computational efficiency generally requires this. There are many implementations of ellipsoids, prisms or any other shape (Alonso-Marroquin and Wang 2009).

Particles can either be modelled as perfectly rigid, or soft (Luding 2004). For rigid particles, event driven algorithms are implemented where the system is numerically time stepped from collision to collision, with some rule governing the interaction at the instant where the particles touch.



Soft particles are allowed to overlap, and a force is applied counter to the overlap such that the particles are gradually forced away from one another (Cundall and Strack 1979). The normal force is modelled either as a linear spring, or using a Hertzian contact (Hertz 1882). In addition, tangential, sliding and rotational forces can be calculated to satisfy the needs of a given model. For this dissertation, I have used a soft body model, called SoftDynamics, written by Dr Pierre Rognon (Rognon and Gay 2008).

## 2.9 Summary

As I have outlined, there are many compelling reasons for modelling the evolution of the grainsize distribution. This can be observed in a number of geometries, and for a number of physical processes. These include:

- segregation models of granular flows with arbitrary grainsize distributions,
- population balance models for crushing that predict final grading curves,
- constitutive models for granular avalanches with varying grainsize distribution,
- general models for flows of material with arbitrary grainsize distributions in three dimensional space, and
- coupled comminution, segregation and mixing models of granular flows with coupled constitutive models.

Once these models have been created, we will begin to understand more completely the role of the grainsize distribution in facilitating physical phenomena that are at the moment only poorly understood. This is a necessary step towards building useful design tools that treat granular flows as boundary value problems of governing equations with wide applicability.

## Motivation

---

When an avalanche occurs, we observe a rapidly flowing region of particles near the free surface. Due to the chaotic and turbulent nature of the flow, there is a large degree of mixing and redistribution of particles. Because of this, we do not expect the particle size distribution to change as the avalanche moves downslope.

In a slightly less energetic flow, such as inclined chute flow at moderate angles (i.e. those near the friction angle of the material), we see what could be termed ‘laminar’ flow of particulate matter. In these conditions, many interesting phenomena arise. The one studied in this Chapter is that of particle size segregation via kinetic sieving.

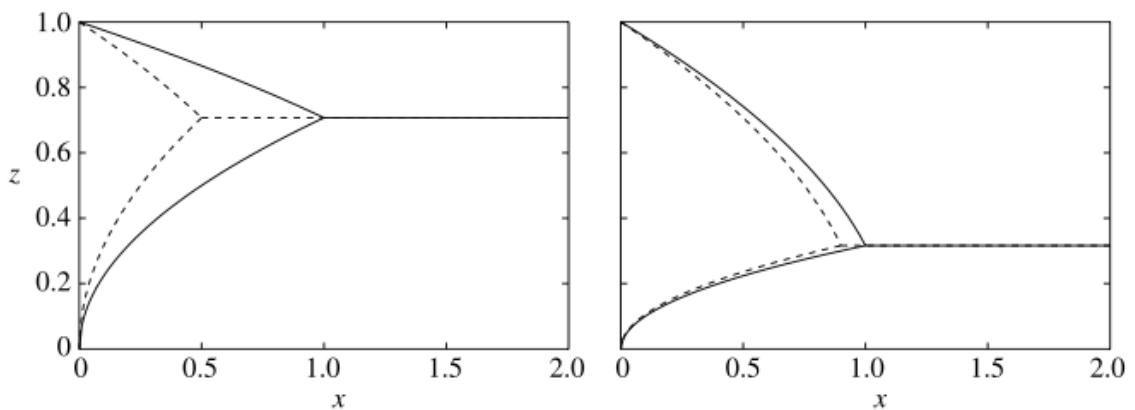


FIGURE 3.1: Comparison of two theories. Position of concentration shocks for homogeneous initial conditions and two different initial concentrations of large particles. *Left*:  $\phi_0 = 50\%$ . *Right*:  $\phi_0 = 10\%$ . Dashed lines are from Savage and Lun (1988), solid lines are from Gray and Thornton (2005). (Gray and Thornton 2005)

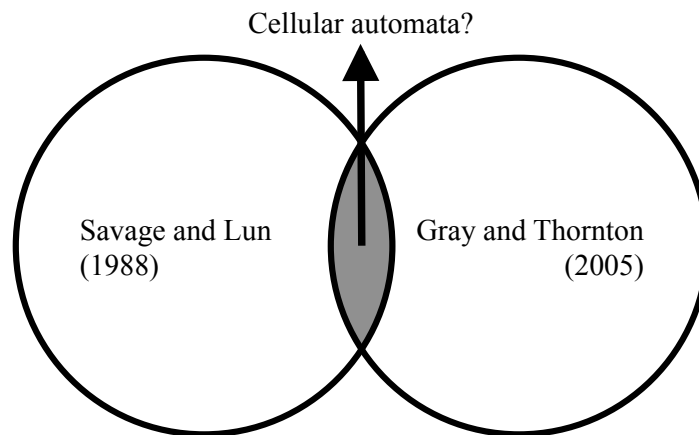


FIGURE 3.2: Motivation for a cellular automata. We wish to explain the fundamental behaviour common to two different theories.

### 3.1 A dominant mechanism

In the field of kinetic sieving, two main theories are those described by Gray and Thornton (2005) and Savage and Lun (1988). They both describe thin, rapidly flowing avalanches of bi-disperse mixtures down an inclined chute. Gray and Thornton use a binary mixture theory to find concentration shocks which define their solutions. Savage and Lun use a maximum entropy argument to arrive at a method-of-characteristics approach which describes a concentration profile.

Both of these theories place significant effort into developing complex mechanisms to predict the time evolution of the patterns formed by segregation. Solutions to these theories, however, produce similar results, as shown in Figure 3.1.

Because these two theories have different forms and produce similar results, we are interested to find the common physics that exists in these models. The subset of physics which exists in both models should allow us to infer the true behaviour of the system, as shown in Figure 3.2.

In both cases, the mechanism responsible for the segregation predicts that a mixture will de-mix into two areas of uniform particle size. Additionally, the evolution of the system towards this fully segregated state should be controlled by the kinematics. We wish to find the simplest model to explain these two phenomena.

The work contained within this Chapter aims to describe the phenomenon in its simplest terms, as a cellular automaton. Finally, I recover a continuum description of the system from the rule of the cellular automata, which closely matches existing theory.

## **3.2 Contribution towards paper**

In the following paper, published in *Granular Matter* during my PhD, I was the primary researcher and author, being supervised by Professor Itai Einav.

# A cellular automaton for segregation during granular avalanches

Benjy Marks · Itai Einav

Received: 5 August 2010 / Published online: 30 January 2011  
© Springer-Verlag 2011

**Abstract** Segregation is a complex and poorly understood phenomenon that is prevalent in many industrial and natural granular flows. When grains flow down a slope [1–5], are spun in a rotating drum [6–8] or shaken in a box [9], we observe those grains organising into intriguing patterns. Kinetic sieving is the dominant mode of segregation in granular avalanches, where separation of particles occurs according to size. Using a cellular automaton we have modelled kinetic sieving as the swapping of particles in a one-dimensional system. From the cellular automaton we have deduced a continuum model to describe the segregation.

**Keywords** Granular flow · Cellular automata · Kinetic sieving · segregation

## 1 Motivation

The authors would like to begin by mentioning that this work was the result of inspiring discussions with Prof. Vardoulakis, with whom we were initially aiming at establishing a new mathematical theory of segregation. Before too long, we found in the literature two distinctively comprehensive and successful theories essentially predicting similar patterns [1,2]. Our interest was then to step back and search for the simplest explanation to this problem. This is the aim of this paper.

Many theories have been developed to explain segregation in granular avalanches, in particular those involving kinetic

sieving mechanisms [1,2]. Cellular automata have been used to model a variety of granular systems [10,11], including segregative systems [12–14].

Kinetic sieving is a result of local fluctuations in the porosity of a granular avalanche [2]. These cause internal voids to be produced, which are in turn filled with particles under the influence of gravity. Since it is more likely that a small particle will fit in any given void, there is a net movement of small particles downwards through the bulk, and a corresponding net movement of large particles upwards (Fig. 1a). We ignore the mechanism by which very small particles spontaneously fall through the pore throats, with almost no help from external perturbations.

In the field of kinetic sieving, two main theories are those described by Gray and Thornton [1] and Savage and Lun [2]. They both describe thin, rapidly flowing avalanches of bi-disperse mixtures down an inclined chute. Gray and Thornton use a binary mixture theory to find concentration shocks which define their solutions. Savage and Lun use a maximum entropy argument and a statistical approach to describe their steady state concentration profiles.

## 2 Approach

We define a cellular automaton that works in a regular one-dimensional lattice, where the diameter of each particle,  $d_i$ , is a Boolean variable attached to each discrete position  $i$  of the lattice. We then define a rule which specifies the time evolution of the diameter at each site.

In Fig. 1b, either of the two particles indicated could fall into the available space. It has been observed [2] that the smaller particle is more likely to fall into the pore, and so this has a greater probability of occurring. This is expressed in simplest terms as two particles swapping places. With some frequency  $f$ :

---

IE acknowledges grant DP0986876 from the ARC.

---

B. Marks · I. Einav (✉)  
Particles and Grains Laboratory, School of Civil Engineering,  
University of Sydney, Sydney, NSW, Australia  
e-mail: itai.einav@sydney.edu.au

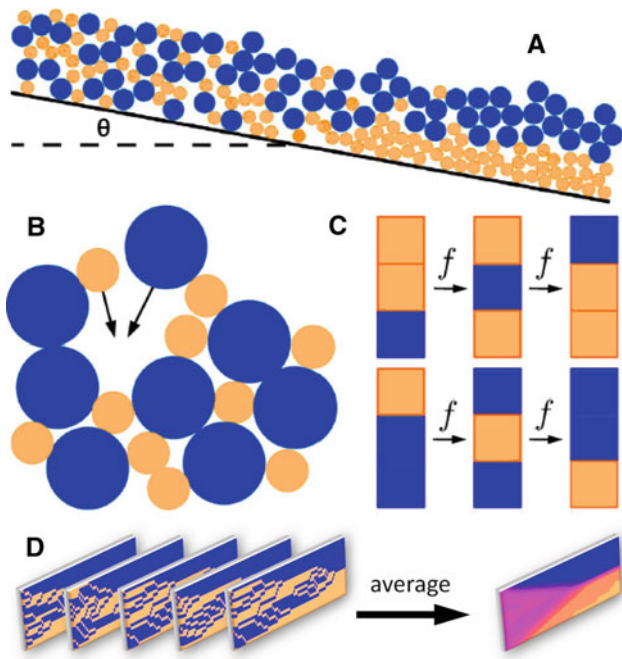


**Fig. 1** Schematics of segregation and corresponding cellular automaton rule. *Orange* are small particles, *Blue* are large particles. **a** Effect of kinetic sieving on particles flowing down an inclined slope. **b** Two particles attempting to fall into an available space. **c** The automaton mechanism, where large and small particles swap places with frequency  $f$ . **d** Individual simulations are averaged to produce mean model behaviour

$$d_i \Leftrightarrow d_{i-1} \quad \text{if } d_i < d_{i-1}.$$

Here the double arrow indicates that the variables representing the diameters have swapped positions at cells  $i$  and  $i - 1$ . Figure 1c illustrates two iterations of the rule on a three particle system. In both cases, the small particles swap with the large particles, creating segregation. We consider a purely non-diffusive system, in which large particles cannot move down and small particles cannot move up. We run our simulation simultaneously in many instances, and average the particle diameter at each point across these simulations (Fig. 1d).

We generalise our model with the inclusion of a swapping frequency,  $f$ , which defines the rate of segregation as a function of the shear strain rate [15] that drives the kinetic sieving process,  $\dot{\gamma}$ . We can then describe the tendency for our mechanism to occur as a function of the height  $z$  such that  $f \propto \dot{\gamma}$ .

The simplest case of flow is that of plug flow, where the down slope velocity is constant along the depth. For this case,  $\dot{\gamma} = 0$  and we expect no segregation. A more complicated case is that of simple shear. Here we use a linear velocity profile, giving us a constant shear rate, and  $f_1 = k$  where  $k$  is a non-dimensional frequency of swapping.

For a more accurate representation of shallow particle flow down an inclined plane, we assume that the shear rate

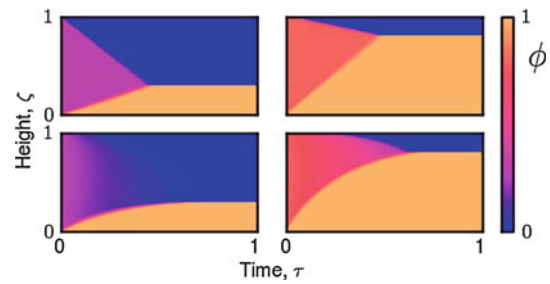


**Fig. 2** Time evolution for two different shear flows. The *top* row assumes simple shear, i.e.  $f_1 = k$ , while the *bottom* row assumes Bagnold shear, i.e.  $f_2 = k\sqrt{1-\zeta}$ . The system is initially filled with a mixture of 30 and 80% (left to right) small concentration. Colour bar represents small particle concentration  $\phi$

is approximated by Bagnold shear [16–18], where  $f_2 = k\sqrt{1-\zeta}$ ,  $\zeta = \frac{z}{H}$  and  $H$  is the avalanche depth.

In our model,  $\zeta = \frac{i}{N}$ , where  $N$  is the total number of cells in the vertical direction. We define a non-dimensional time  $\tau = j \frac{k}{N} = t \frac{kU}{H}$ . The first equality refers to the cellular automaton, where  $j$  is the time step. The second equality refers to the physical time  $t$ , where  $U$  is the average bulk velocity across the depth.

The cellular automaton outputs the time evolution of the flow for any applied shear regime and initial mixture. The flow is described by  $\phi$ , the small particle concentration. We find  $\phi$  by summing the number of small particles at a given height across all of the simulations, and dividing by the total number of simulations.

For a homogeneous initial condition, we start the system as a randomly generated sample with given concentration of small particles,  $\phi_0$ . As in [12] we begin at the bottom of the system, working our way up, checking if each particle has on average smaller particles above it. If it does, it swaps at frequency  $f$  with the above particle. For stability, we work in half time steps, checking only for particles in odd or even rows. This stops particle from moving many times in a single time step. The top row is never explicitly checked, but has small particles taken out of it by the row below.

### 3 Results

The top of Fig. 2 shows the behaviour of a system undergoing simple shear flow. This is described by  $f_1 = k$ , i.e. the frequency is constant over the height. Three sharp concentration shocks develop during the time evolution, marking the boundaries between the two fully segregated states and the mixed state. The shocks are linear, and move towards a discrete triple point. The height of this point depends on the initial concentration of the particles  $\phi$ .

The bottom of Fig. 2 outlines the case of Bagnold shear, i.e.  $f_2 = k\sqrt{1-\zeta}$ . Because of the large swapping frequen-

cies at the base of the flow, a concentration shock develops. At the top of the flow, however, the swapping frequency is uniquely zero, and a second concentration shock does not develop. In this case, there is no robust definition of complete segregation. In a flow of infinite width relative to the grain size, segregation would never fully occur.

We do not expect a concentration shock at the top of the flow. This is in contrast to suggestion by both Gray and Thornton and Savage and Lun. Experimental tests [2, 19] generally involve a small number of particles (flows typically 10–20 particles deep and with minimal width) and full segregation may occur because the problem becomes stochastic in nature with insufficient realisations of the segregation statistics.

When looking at the Bagnold shear case it is evident that the small particles saturate the bottom before the large particles saturate the top. Is one faster than the other?

To answer this, we look at a case of heterogeneous initial conditions. We define two regions of mono-disperse particles such that the large particles are below the small particles. The insets of Fig. 3 picture large particles moving upwards through the bulk (3D), and small particles moving downwards (3B). These two cases correspond to distinctly different aspect ratios between the upper and lower regions, 9:1 and 1:9.

We place a ‘gate’ at some height  $\delta$ , and time until 90% of the contaminating particles have passed beyond this gate. The curves at the right of Fig. 3 plot this time,  $\tau_{90}$ , for a range of values of  $\delta$  for both simulations. The idea is to present a competition between the two particles—a race to pass a gate at a similar distance from their initial point.

We see that for any distance moved by the particles, the small particles (yellow line) take longer to reach the gate. It should be noted at this stage that we only consider small size differences between the two species, and do not account for filtration of very small particles through the bulk. Also, the time for one particle to go from the top to the bottom, or the bottom to the top will be the same. The reason the times vary in intermediate lengths is due to the asymmetry of the shear strain rate. For example, if the asymmetry was inverted, it would be the smaller particles that trickle faster than the large particles float. Using this understanding, it may be possible to tailor industrial processes to obtain faster separation times.

### 4 Continuum model

By averaging over a sufficiently large number of simulations, cellular automaton can be used to represent continuum flow equations [20] by looking at the flux of volume fraction  $\phi$  between adjacent cells over time. Over one time step, the flux that moves downwards out of a point  $(\zeta, \tau)$  is the product of the swapping frequency at that height  $f(\zeta)$ , the amount of that size present at that height  $\phi(\zeta, \tau)$  and the available space to move into. A small particle will only move if it is larger than the average particle below it and so the available space can be expressed as  $1 - \phi(\zeta - \Delta\zeta, \tau)$ . Taking conservation of mass over a single time step we get:

$$\begin{aligned} \phi(\zeta, \tau)\Delta\zeta + f(\zeta + \Delta\zeta)\phi(\zeta + \Delta\zeta, \tau)(1 - \phi(\zeta, \tau))\Delta\tau \\ = \phi(\zeta, \tau + \Delta\tau)\Delta\zeta + f(\zeta)\phi(\zeta, \tau)(1 - \phi(\zeta - \Delta\zeta, \tau))\Delta\tau \end{aligned}$$

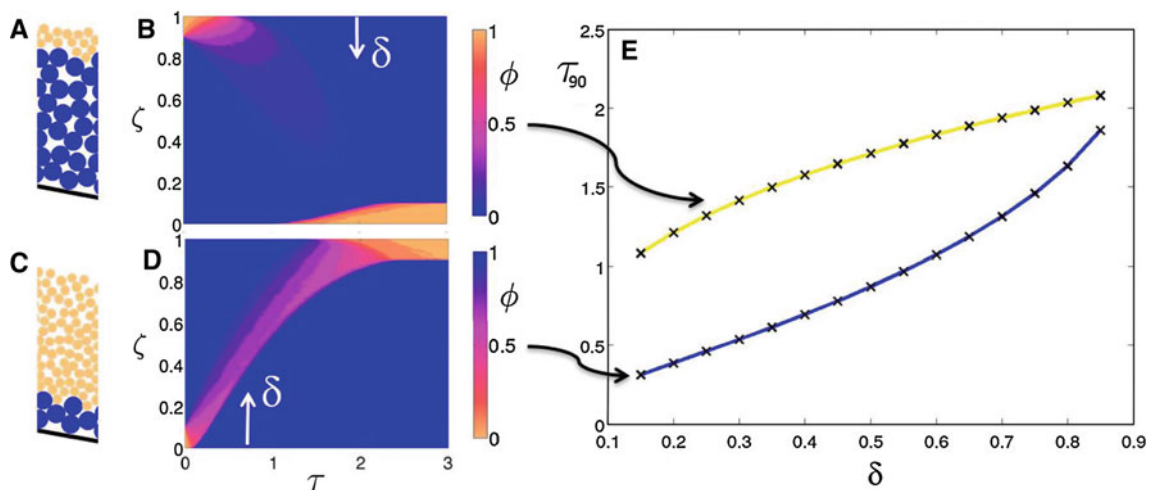


**Fig. 3** a An initial configuration of small particles sitting above large particles. b These small particles sinking to the bottom of the flow, under Bagnold shear. c An initial configuration of large particles sitting below small particles. d These large particles rising to the top of the

flow, under Bagnold shear. e The time for 90% segregation,  $\tau_{90}$  at a particular height  $\delta$ . The blue line is large particles moving upwards, and the yellow line is small particles moving downwards

Taking  $f(\zeta) = k\dot{\gamma}$ , we represent the segregation mechanism in terms of the variation of shear strain with height. In continuum terms this can be expressed as:

$$\frac{\partial \phi}{\partial \tau} = k \frac{\partial(\dot{\gamma}\phi(1-\phi))}{\partial \zeta}$$

This continuum formula differs from that described by Gray and Thornton [1], as it replaces a constant segregation co-efficient  $S_r$  with a contribution due to shear strain rate  $\dot{\gamma}$ . Gray and Thornton's continuum formulation in one spatial dimension is:

$$\frac{\partial \phi}{\partial \tau} = S_r \frac{\partial(\phi(1-\phi))}{\partial \zeta}$$

Our model predicts that in a physical flow, such as that approximated by Bagnold shear, a concentration shock develops at the bottom of the flow only. The appearance of a shock at the top of the flow is a result of the small number of particles being observed. Flow near the free surface in Bagnold shear can be approximated by plug flow, corresponding to a situation with extremely slow segregation.

This paper could be viewed in a different light by seeing the cellular automaton as an effective numerical tool to solve partial differential equations. These problems are known to be extremely challenging to solve [21] and such a simple approximate solution, which handles shocks and rarefactions without qualms, is of great help.

**Acknowledgments** We would like to thank the members of the Particles, Grains and Complex Fluids Group at the University of Sydney, in particular Dr. Pierre Rognon and Dr. Bjornar Sandnes for useful discussions.

## References

- Gray, J., Thornton, A.: A theory for particle size segregation in shallow granular free-surface flows. *Proc. R. Soc. A Math. Phys. Eng. Sci.* **461**(2057), 1447–1473 (2005)
- Savage, S., Lun, C.: Particle size segregation in inclined chute flow of dry cohesionless granular solids. *J. Fluid Mech.* **189**, 311–335 (1988)
- Gray, J., Hutter, K.: Pattern formation in granular avalanches. *Continuum Mech. Thermodyn.* **9**(6), 341–345 (1997)
- Naylor, M.: The origin of inverse grading in muddy debris flow deposits: a review. *J. Sediment. Res.* **50**(4), 1111–1116 (1980)
- Makse, H., Havlin, S., King, P., Stanley, H.: Spontaneous stratification in granular mixtures. *Nature* **386**(6623), 379–382 (1997)
- Nityanand, N., Manley, B., Henein, H.: An analysis of radial segregation for different sized spherical solids in rotary cylinders. *Metallurg Trans B* **17B**, 257 (1986)
- Khakhar, D., McCarthy, J., Ottino, J.: Radial segregation of granular mixtures in rotating cylinders. *Phys Fluids* **9**, 3600 (1997)
- Hill, K., Caprihan, A., Kakalios, J.: Bulk segregation in rotated granular material measured by magnetic resonance imaging. *Phys. Rev. Lett.* **78**(1), 50–53 (1997)
- Mobius, M., Lauderdale, B., Nagel, S., Jaeger, H.: Brazil-nut effect: size separation of granular particles. *Nature* **414**(6861), 270 (2001)
- Baxter, G., Behringer, R.: Cellular automata models of granular flow. *Phys. Rev. A* **42**(2), 1017–1020 (1990)
- Kozicki, J., Tejchman, J.: Application of a cellular automaton to simulations of granular flow in silos. *Granul. Matter* **7**(1), 45–54 (2005)
- Fitt, A., Wilmott, P.: Cellular-automaton model for segregation of a two-species granular flow. *Phys. Rev. A* **45**(4), 2383–2388 (1992)
- Yanagita, T.: Three-dimensional cellular automaton model of segregation of granular materials in a rotating cylinder. *Phys. Rev. Lett.* **82**(17), 3488–3491 (1999)
- Cizeau, P., Makse, H., Stanley, H.: Mechanisms of granular spontaneous stratification and segregation in two-dimensional silos. *Arxiv preprint cond-mat/9809430* (1998)
- May, L., Shearer, M., Daniels, K.: Scalar conservation laws with nonconstant coefficients with application to particle size segregation in granular flow. *J. Nonlinear Sci.* **20**, 1–19 (2010)
- Silbert, L.E., Ertas, D., Grest, G.S., Halsey, T.C., Levine, D., Plimpton, S.J.: Granular flow down an inclined plane: Bagnold scaling and rheology. *Phys. Rev. E* **64**(5), 051302 (2001)
- MiDi, G.: On dense granular flows. *Eur. Phys. J. E Soft Matter Biol. Phys.* **14**(4), 341–365 (2004)
- Rognon, P., Roux, J., Naaim, M., Chevoir, F.: Dense flows of bi-disperse assemblies of disks down an inclined plane. *Phys. Fluids* **19** (2007)
- Bridgwater, J., Ingram, N.D.: Rate of spontaneous inter-particle percolation. *Chem. Eng. Res. Des.* **49a**, 163–169 (1971)
- Toffoli, T.: Cellular automata as an alternative to (rather than an approximation of) differential equations in modeling physics. *Physica D* **10**(1–2), 117–127 (1984)
- LeVeque, R.: *Finite volume methods for hyperbolic problems*. Cambridge University Press, Cambridge (2002)



## Population balance models

---

### 4.1 Cellular automaton

The previous Chapter presented a simple cellular automata. This model was able to replicate the behaviour of similar continuum and probabilistic theories, and captured the essence of the segregation mechanism in terms of conservation of mass. To extend the previous system, this Chapter shows how conservation of momentum can be included in the field equations describing segregation. It also adds diffusive remixing as a phenomenon which more accurately represents both physical experiment and numerical simulations.

### 4.2 Continuum description

In addition to the predictive capability of the cellular automaton, we wish to have access to the kinematics of the system, while simultaneously describing systems with arbitrary grainsize distributions. To do this, the model needs to be enriched with a statement of conservation of momentum.

In the previous cellular automaton, the shear strain rate was shown to govern the evolution of the segregation patterns. By including conservation of momentum, the segregation patterns can be directly coupled to the boundary conditions by a constitutive model. Additionally, the description of the system can be extended to many spatial dimensions.

To allow arbitrary grainsize distributions, the continuum model is enriched with an internal coordinate that describes the grainsize distribution explicitly. With this inclusion, the extension to describe polydisperse systems and their interactions is made simple.

This form of mathematical description is known as a population balance equation (Ramkrishna 2000). This class of equation has been used to describe the conservation of mass of many particulate systems in chemical and mechanical engineering, and has a very wide applicability (Ramkrishna and Mahoney 2002). It will be employed here to describe both mass and momentum conservation of a system of dry grains of arbitrary grainsize distribution.

A population balance model describes the evolution of one or more quantities over time  $t$ , and  $n$  spatial dimensions  $\mathbf{r} = \{r_1, r_2, \dots, r_n\}$ . Additionally,  $m$  internal coordinates,  $\mathbf{x} = \{x_1, x_2, \dots, x_m\}$ , are generally included in the analysis to represent particle size, age, strength, or any other variable of interest. The general form of a population balance for some variable  $f_1$  is described in (Ramkrishna 2000) as

$$\frac{\partial}{\partial t} f_1 + \nabla_{\mathbf{x}} \cdot \dot{\mathbf{X}} f_1 + \nabla_{\mathbf{r}} \cdot \dot{\mathbf{R}} f_1 = h. \quad (4.1)$$

Here the spatial velocities are  $\dot{\mathbf{R}}$ , and the velocities in the internal coordinate directions are  $\dot{\mathbf{X}}$ . Additionally, the net birth rate of  $f_1$  is  $h$ . This balance equation then relates the change in quantity of  $f_1$  due to movement in either an external (spatial) or internal direction, or due to the spontaneous birth/death of that quantity. To describe the evolution of this system, this equation must be coupled with some initial and boundary conditions, then solved either analytically or numerically.

### 4.3 Contribution towards paper

For the following paper, I conducted all of the research and analysis, as well as writing the paper itself. I was assisted with the discrete element and constitutive modelling by Dr Pierre Rognon, and in everything else by Professor Itai Einav.

## 4.4 Post processing

Detailed post processing routines for the discrete element method are not contained in this paper, and so have been placed in Appendix A. This Appendix covers how the particulate data has been homogenised such that data from the whole simulation can be plotted as a function of either height above an inclined plane, or as a function of grainsize. This method of homogenisation of polydisperse particulate data is consistent with previous work (Weinhart et al. 2012a; Thornton et al. 2012).

# Grainsize dynamics of polydisperse granular segregation down inclined planes

Benjy Marks, Pierre Rognon and Itai Einav<sup>†</sup>

Particles and Grains Laboratory, School of Civil Engineering, The University of Sydney, Sydney, NSW 2006, Australia

(Received 1 July 2011; revised 2 September 2011; accepted 12 October 2011;  
first published online 14 November 2011)

Granular materials segregate by size when sheared, which increases the destructive power in avalanches and causes demixing in industrial flows. Here we present a concise theory to describe this phenomenon for systems that for the first time include particles of arbitrary size. The evolution of the grainsize distribution during flow is described based on mass and momentum conservation. The theory is derived in a five-dimensional space, which besides position and time, includes a grainsize coordinate. By coupling the theory with a simple constitutive law we predict the kinematics of the flow, which depends on the grainsize dynamics. We show that the underpinning mechanism controlling segregation is a stress variation with grainsize. The theory, solved by a finite difference scheme, is found to predict the dynamics of segregation consistent with results obtained from discrete element simulations of polydisperse granular flow down inclined planes. Moreover, when applied to bimixtures, the general polydisperse theory reveals the role of grainsize contrast.

**Key words:** granular media, pattern formation, granular mixing

---

## 1. Introduction

One of the most distinct forms of pattern formation in granular materials is that observable in flows with particles of different size or density. As they flow the grains segregate, forming complex patterns. This is a concern for industrial applications where generally particles are required to be well mixed. Segregation occurs in flows down planes and in rotating cylinders, drums and blenders (Bridgwater 1976; Shinbrot, Alexander & Muzzio 1999; Ottino & Khakhar 2000), which are used for a variety of applications in the pharmaceutical, chemical, food, ceramic and construction industries. For a recent comprehensive review of the subject see Gray & Ancy (2011).

It has been noted for some time (Bridgwater & Ingram 1971; Savage & Lun 1988) that segregation down inclined planes occurs due to fluctuations in the local pores within the flow, a process termed ‘kinetic sieving’. With increasing shear strain rate, those fluctuations become more frequent. As new void spaces are created and grow, smaller particles are more likely to fit and fall into the pores. This results in a flux of small particles downwards through the bulk and a corresponding flux of large particles upwards. The segregation velocity, therefore is expected to increase with the rate of creation of voids, and therefore with the shear strain rate.

<sup>†</sup> Email address for correspondence: [itai.einav@sydney.edu.au](mailto:itai.einav@sydney.edu.au)

Here we present a theory that describes this phenomenon for systems that for the first time include mixtures of arbitrary sizes. While this topic has been investigated for bimixtures (Savage & Lun 1988; Dolgunin, Kudy & Ukolov 1998; Gray & Thornton 2005; Gray & Chugunov 2006; May, Shearer & Daniels 2010), it has only recently been extended to ‘multicomponent’ systems (Gray & Ancey 2011), with  $n$  phases in the mixture. In that theory, particles are ranked from smallest to largest, without specifying the actual radii. Consequently, the number of free parameters increases quadratically with  $n$ , which are grouped into a single function that is not connected to the actual sizes. In the following section we introduce an alternative continuum theory that does include the actual sizes using a continuous grainsize coordinate. In § 4.4, we discuss the fundamental differences of the two approaches.

## 2. Continuum theory

We describe an avalanche of depth  $H$ , subjected to gravity  $g$ , where the largest particle has radius  $s_M$  and density  $\rho_0$ . The following theory is described non-dimensionally. Properties are non-dimensionalized as follows: length by  $H$ , grainsize by  $s_M$ , time by  $\sqrt{H/g}$ , velocity by  $\sqrt{Hg}$  and stress by  $\rho_0 g H$ .

### 2.1. A polydisperse mixture

Mixtures are generally described by accounting for the various constituents and their interactions during flow, such as in Morland (1992). These constituents are commonly fluids, gases and solids, and a finite number of such constituents are treated simultaneously. Here, only solid phases in the flow are considered and we replace the finite number of constituents with a single grainsize coordinate that maps the grain radii continuously. This allows us to describe a mixture made of arbitrarily sized solids. To do this, we introduce a volumetric grainsize distribution  $\phi(\mathbf{r}, s, t)$ , of a particular grainsize  $s$ , at some location in space  $\mathbf{r} = \{x, y, z\}$  and at time  $t$ :

$$\Phi[s_a < s < s_b] = \int_{s_a}^{s_b} \phi(s') ds', \quad (2.1)$$

where  $\Phi$  is the solid fraction of grains with grainsize above  $s_a$  and below  $s_b$ . Here  $\phi$  then represents a probability density function for the grainsize distribution at every point in space and time, which satisfies

$$\int \phi ds = 1, \quad \int \phi s ds = \bar{s}, \quad (2.2)$$

where  $\bar{s}(\mathbf{r}, t)$  is the average particle radius.

In the following, there is a distinction between intrinsic and partial properties. Intrinsic properties refer to a particular grainsize, whereas partial properties refer to the contribution of the intrinsic property of a particular grainsize to the average property.

### 2.2. Density

The intrinsic density,  $\rho^*(s)$ , is defined as the mass of a unit volume of particles with grainsize  $s$ . We allow particles belonging to a particular grainsize  $s$  to have different intrinsic density. Therefore, the partial density,  $\rho(\mathbf{r}, s, t)$ , and the bulk (or average) density,  $\bar{\rho}(\mathbf{r}, t)$ , are defined as

$$\rho = \phi \rho^*, \quad \bar{\rho} = \int \rho ds. \quad (2.3)$$

## 2.3. Stress

Stresses are defined in a similar manner to the densities. Accordingly, the intrinsic stress,  $\boldsymbol{\sigma}^*(\mathbf{r}, s, t)$ , is the Cauchy stress on the solid part of a representative volume–grainsize element, meaning an element that refers not only to grains that belong to a certain volume in space, but also to a certain grainsize bin. This stress could be measured, for example using discrete element simulations, as detailed in § 3, where it will be shown to depend on the grainsize. For this reason, we require that the intrinsic stress varies with grainsize  $s$  in such a manner that

$$\boldsymbol{\sigma}^* = \bar{\boldsymbol{\sigma}}f, \quad \boldsymbol{\sigma} = \phi\boldsymbol{\sigma}^*, \quad \bar{\boldsymbol{\sigma}} = \int \boldsymbol{\sigma} \, ds, \quad (2.4)$$

where the intrinsic stress scales about some average, or bulk stress  $\bar{\boldsymbol{\sigma}}(\mathbf{r}, t)$  with scaling  $f(\mathbf{r}, s, t)$ . We also define the partial stress of each constituent,  $\boldsymbol{\sigma}(\mathbf{r}, s, t)$ . For (2.4) to hold, we require that

$$\int f\phi \, ds = 1. \quad (2.5)$$

For a given size  $s$ , if  $f < 1$  the intrinsic stress felt by that size is less than the bulk stress, and if  $f > 1$  the intrinsic stress is greater than the bulk stress.

## 2.4. Conservation of mass

Following Ramkrishna (2000), we define a domain in the particle state space,  $\Lambda(t)$ , which contains a finite mass of particles which deforms over time. This domain can be split into two subdomains containing, first, the external physical space  $\Lambda_r$  and, second, the internal coordinate space  $\Lambda_s$ , where  $s$  is the grainsize coordinate. With the assumption that no particles enter or leave this domain, i.e. that there is no breakage or agglomeration, we may write in terms of the partial density  $\rho$ ,

$$\frac{d}{dt} \int_{\Lambda_s(t)} \int_{\Lambda_r(t)} \rho \, dV_r \, ds = 0, \quad (2.6)$$

where  $dV_r$  is an infinitesimal physical volume in real space and  $ds$  is the equivalent property in the grainsize direction. Using a generalization of Reynolds' transport theorem to general vector spaces,

$$\int_{\Lambda_s(t)} \int_{\Lambda_r(t)} \left[ \frac{\partial \rho}{\partial t} + \frac{\partial}{\partial s}(\rho \dot{S}) + \nabla_r \cdot (\rho \dot{\mathbf{R}}) \right] dV_r \, ds = 0, \quad (2.7)$$

where  $\dot{S}$  and  $\dot{\mathbf{R}}$  are the instantaneous velocities of material  $\rho$  in the  $s$  and  $\mathbf{r}$  directions, respectively, and  $\nabla_r = \{\partial/\partial x, \partial/\partial y, \partial/\partial z\}$ . Because the domain of these integrals is arbitrary, and the integral is continuous, we recover the population balance equation of the mass in a five-dimensional space  $\{\mathbf{r}, s, t\}$

$$\frac{\partial \rho}{\partial t} + \frac{\partial}{\partial s}(\rho \dot{S}) + \nabla_r \cdot (\rho \dot{\mathbf{R}}) = 0. \quad (2.8)$$

We set  $\dot{S} = 0$ , which implies that particles do not grow or reduce over time. This is contrasted with Ricard & Bercovici (2009), who explored growth and reduction via diffusion in grainy materials, where the physical motion of constituents was not explored. We also make the following assumption

$$\rho \dot{\mathbf{R}} = \rho \mathbf{u} - D \nabla_r \rho, \quad (2.9)$$

so that the fluxes in physical space are split into two components due to the advective flux,  $\rho \mathbf{u}$ , where  $\mathbf{u}(\mathbf{r}, s, t) = \{u, v, w\}$ , and the diffusive flux,  $D \nabla_r \rho$ , with some constant diffusion coefficient  $D$ , which we will discuss further in § 3. We can then write

$$\frac{\partial \rho}{\partial t} + \nabla_r \cdot (\rho \mathbf{u}) = \nabla_r \cdot (D \nabla_r \rho). \quad (2.10)$$

Considering a flow that is uniform in the downslope ( $x$ ) and cross-slope ( $y$ ) directions, and segregating in the normal ( $z$ ) direction, we retain a three-dimensional system in  $\{z, s, t\}$ , describing the evolution of the grainsize distribution  $\phi$  via

$$\frac{\partial \rho}{\partial t} + \frac{\partial}{\partial z}(\rho w) = D \frac{\partial^2 \rho}{\partial z^2}, \quad (2.11)$$

where it is noted that both  $\rho$  and  $w$  depend on the grainsize coordinate.

### 2.5. Conservation of momentum

Conservation of momentum for our system can be expressed as

$$\frac{d}{dt} \int_{\Lambda_s(t)} \int_{\Lambda_r(t)} \rho \dot{\mathbf{R}} dV_r ds = \int_{\Lambda_s(t)} \int_{\Lambda_r(t)} \phi \mathbf{F}^* dV_r ds, \quad (2.12)$$

where  $\mathbf{F}^*(\mathbf{r}, s, t)$  is the intrinsic force per representative volume–grainsize element. By again using Reynolds' transport theorem, and the arbitrariness of the intergrands,

$$\frac{\partial}{\partial t}(\rho \dot{\mathbf{R}}) + \nabla_r \cdot (\rho \dot{\mathbf{R}} \otimes \dot{\mathbf{R}}) = \phi \mathbf{F}^*, \quad (2.13)$$

where  $\otimes$  is the outer product. The left-hand side of the equality represents the material derivative of partial density  $\rho$ . Adapting the expressions in Gray & Thornton (2005) and Gray & Chugunov (2006), we set  $\mathbf{F}^*$  as

$$\mathbf{F}^* = -\nabla_r \cdot \boldsymbol{\sigma}^* + \rho^* \mathbf{g} - \frac{\bar{\rho} c}{\dot{\gamma}} (\mathbf{u} - \bar{\mathbf{u}}). \quad (2.14)$$

Note that unlike the work of Gray and colleagues, our definition of the partial force  $\phi \mathbf{F}^*$  was specified in a way that allows the identification of an intrinsic force  $\mathbf{F}^*$ , as was done for density and stress (see § 2.1). Specifically, the first term on the right-hand side represents a force due to the gradient of intrinsic stress. The second term represents the intrinsic body force due to gravity  $\mathbf{g}$ . The final term arises from the interaction of each species with the bulk. Here  $\bar{\mathbf{u}}(\mathbf{r}, t) = \int \phi \mathbf{u} ds$  and  $c$  is a coefficient of interparticle drag, with units of inverse time, to allow normalization by the shear rate  $\dot{\gamma}(\mathbf{r}, t)$ . Subsequently, drag force reduces with increasing fluctuation in local pore creation. The exact nature of the parameter  $c$  is poorly understood and is therefore taken as constant. At least, it represents the effects of particle shape, surface roughness and concavity in terms of their effect on the size segregation velocity.

For simplicity, we assume that the flow is quasisteady, and that the acceleration terms  $(\partial/\partial t)(\rho \dot{\mathbf{R}})$  and  $\nabla_r \cdot (\rho \dot{\mathbf{R}} \otimes \dot{\mathbf{R}})$  can be neglected. This implies that  $\mathbf{F}^* = 0$  with a weak form that can be expressed as  $\int \int \phi \mathbf{F}^* dV_r ds = 0$ . From this and (2.2)–(2.5) we obtain

$$\nabla_r \cdot \bar{\boldsymbol{\sigma}} = \bar{\rho} \mathbf{g}. \quad (2.15)$$

Considering a flow that is uniform in the downslope ( $x$ ) and cross-slope ( $y$ ) directions, and without stress at the free surface,

$$\bar{\sigma}_{xz} = \bar{\rho} g \sin \theta (1 - z), \quad \bar{\sigma}_{zz} = \bar{\rho} g \cos \theta (1 - z). \quad (2.16)$$

Then, after rearrangement,  $\mathbf{F}^* = 0$  becomes

$$w(s) = \dot{\gamma} \frac{g \cos \theta}{c} \left( f - \frac{\rho^*}{\bar{\rho}} \right), \quad (2.17)$$

where we have used the fact that  $\bar{w} = 0$ . This tells us that particles will move relative to other sizes for two reasons. The first, and the most important for this study, is if they feel a partial stress which is different from their neighbours. The second is if they feel either a positive or negative buoyancy.

For plug flow, where  $\dot{\gamma} = 0$ , we expect no segregation to occur because the velocity is constant everywhere and local voids should not be created.

We can now combine our segregation velocity (2.17) with (2.11) to conclude that our governing population balance equation for grainsize distribution  $\phi$  is

$$\frac{\partial \phi}{\partial t} + \frac{g \cos \theta}{c} \cdot \frac{\partial}{\partial z} \left( \phi \dot{\gamma} \left( f - \frac{\rho^*}{\bar{\rho}} \right) \right) = D \frac{\partial^2 \phi}{\partial z^2}. \quad (2.18)$$

## 2.6. Constitutive theory

We use a simple constitutive equation that is known to be reasonable for steady, dense flowing granular media down inclines (MiDi 2004; da Cruz *et al.* 2005), as a first-order approximation in  $\dot{\gamma}$

$$\frac{\bar{\sigma}_{xz}}{\bar{\sigma}_{zz}} = \mu_c + kt_i \dot{\gamma}, \quad (2.19)$$

where  $\mu_c$  is the angle of repose of our material,  $k$  is a non-dimensional constant and  $t_i$  is the inertial time. For quasimonodisperse systems, the inertial time represents the typical time for a particle to move a distance of its own radius, driven by the normal stress. Rognon *et al.* (2007) suggested that for bidisperse flows such a behaviour is still valid provided that the inertial time involves the average size of the mixture,  $\bar{s}$ . Although the precise dependence of the rheology on the polydispersity is still a matter of research (Yohannes & Hill 2010), we shall here employ the simplest hypothesis for polydisperse mixtures. Following Rognon *et al.* (2007), we equate the force due to  $\bar{\sigma}_{zz}$  with the inertial force on a particle of size  $\bar{s}$  with density  $\bar{\rho}$  and a typical acceleration  $2\bar{s}/t_i^2$ . This gives  $4\pi\bar{s}^2\bar{\sigma}_{zz} = \bar{\rho}(4\pi\bar{s}^3/3) \cdot (2\bar{s}/t_i^2)$ , from which the inertial time is  $t_i = \bar{s}\sqrt{2\bar{\rho}/3\bar{\sigma}_{zz}}$ . Considering the stress profile within a flow down a slope, (see (2.16)) the shear strain rate profile is

$$\dot{\gamma} = \frac{\tan \theta - \mu_c}{k\bar{s}} \sqrt{3/2g \cos \theta (1 - z)}. \quad (2.20)$$

Because  $\bar{s}$  varies with time, the shear strain rate does as well. This implies that segregating flows are non-steady, unlike our assumption employed to simplify the momentum conservation. Nevertheless, we will see in § 3 that this steadiness assumption is already very useful. Introducing this shear strain rate profile in (2.17) provides the segregation velocity as

$$w = \frac{C\sqrt{1-z}}{\bar{s}} \left( f - \frac{\rho^*}{\bar{\rho}} \right), \quad (2.21)$$

where  $C = (((\tan \theta - \mu_c)g \cos \theta)/kc)\sqrt{(3/2)g \cos \theta}$ .



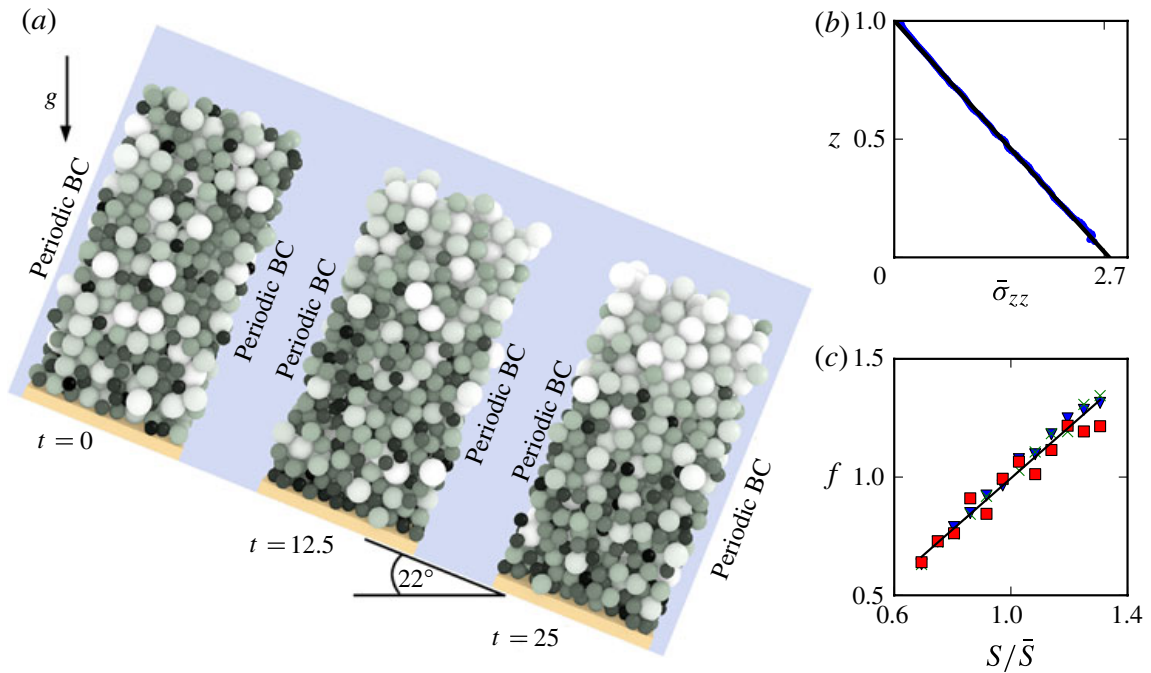


FIGURE 1. (Colour online available at [journals.cambridge.org/flm](http://journals.cambridge.org/flm)) Size segregation in a polydisperse discrete element method (DEM) sample. (a) At  $t = 0$ , an initial sample of 1550 particles begins flowing downslope. By  $t = 12.5$  the sample has begun to segregate by size, with larger particles collecting at the top of the flow, and smaller particles sinking to the base. By  $t = 25$  the sample has reached its final segregated state. (b) Bulk vertical stress  $\bar{\sigma}_{zz}$  is shown as a function of height, predicted by (2.16). (c) Size dependence of intrinsic stress expressed using the scaling function  $f$ . We split the simulation into three even layers by depth. The top ( $\nabla$ ), middle ( $\times$ ) and bottom ( $\square$ ) thirds are shown separately, yet all fit a linear scaling given by (3.1). For both right-hand plots, solid lines indicate linear fits to the data.

### 3. Discrete element method model

Looking at the population balance (2.18), we only require  $C$ ,  $D$  and  $f$  to complete the system. However, this Section demonstrates that the latter two are measurable, leaving  $C$  as the only free parameter.

To measure  $f$ , we would like to know how the intrinsic stress  $\sigma^*$  scales with grain size. To do this, we implemented a standard discrete element method (DEM) to simulate the flow down an inclined plane of a polydisperse mixture of spheres, with  $s \in [0.5, 1]$  distributed uniformly by volume (see figure 1). As usual, spheres interact by elastic (Hertzian) contacts, with some normal dissipation achieved through a dashpot element with coefficient of restitution of 0.6 and tangential friction (coefficient of friction of 0.4). There are 1550 particles in the sample: about 15 large particle diameters deep, 6 wide and 6 long, with periodic boundary conditions in the  $x$  and  $y$  directions. All of the particles have the same density. The base is a smooth plane inclined at an angle of  $\theta = 22^\circ$ . At lower angles, the flow stops; at higher angles, the flow accelerates with increasing diffusion. The plane has some rolling resistance, mimicking roughness, to avoid plug flow (the expression for rolling resistance used can be found in Rognon *et al.* 2010). The particles are initially set randomly with no contacts, which infers consolidation, and given initial down slope velocities near to their steady state speeds that are established from a preliminary simulation. Here  $t = 0$  is defined when the consolidation has completed (typically at times  $-0.2 < t < 0$ ). This initial condition was chosen to reach steady state rapidly, before significant segregation has occurred.

Since we are interested in polydisperse simulations, the numbers of particles within a given grainsize bin is very limited. Therefore, this process was repeated 15 times and the results were averaged across the simulations, in effect providing nearly 25 000 grains.

At a given time  $t$ , the intrinsic stress was measured by summing all contact forces  $\mathbf{F}_c$  acting at contacts  $c$  that belonged to particles in depth bin  $z$  and grainsize bin  $s$  as  $\boldsymbol{\sigma}^*(z, s) \approx (1/V) \sum_c \mathbf{F}_c \otimes \mathbf{r}_c$  where  $\mathbf{r}_c$  is the centre-to-centre vector and  $V$  is the total volume of particles in that bin. The bin dimensions were selected as small as possible while ensuring sufficient particles in each bin ( $\Delta z = 0.01$ ,  $\Delta s = 0.02$ ).

The bulk normal stress was calculated as the volume weighted average of the intrinsic stresses from all bins  $s$  at a particular height. As shown in figure 1, it follows that the bulk normal stress scales as  $\bar{\sigma}_{zz} \propto 1 - z$ , which is consistent with the prediction of (2.16). Moreover, we can measure at different depths the ratio between the intrinsic normal stress carried by one species  $\sigma_{zz}^*$  and the bulk stress  $\bar{\sigma}_{zz}$  of all species, to obtain the function  $f$  (see figure 1). It appears that  $f$  admits a simple linear scaling with the grainsize, which is consistent with the requirement discussed in § 2.3

$$f(\mathbf{r}, s, t) = \frac{s}{\bar{s}}. \quad (3.1)$$

A similar grainsize scaling has been observed during uniaxial compression by Einav (2007), which highlights its significance in polydisperse media.

We also measure the self-diffusion coefficient using the standard expression (see for example Campbell 1997):  $D = \langle \Delta z^2 / 2\Delta t \rangle$  where  $\Delta z$  represents a change in position during an time increment  $\Delta t = 0.01$ . The angle brackets denote an average made over all of the grains, and over some time. While  $D$  may in fact be a function of both  $\dot{\gamma}$  and  $s$  (Utter & Behringer 2004), for simplicity we only focus here on a constant mean value. In these simulations, we measure  $D \approx 0.007$  (the physical diffusion coefficient non-dimensionalized by  $\sqrt{H^3 g}$ ).

We can now rewrite (2.18) using (3.1) and (2.21) to give the governing population balance equation of polydisperse segregation down inclined planes:

$$\frac{\partial \phi}{\partial t} + C \frac{\partial}{\partial z} \left( \frac{\phi \sqrt{1-z}}{\bar{s}} \left( \frac{s}{\bar{s}} - \frac{\rho^*}{\bar{\rho}} \right) \right) = D \frac{\partial^2 \phi}{\partial z^2}. \quad (3.2)$$

Lastly, the only free parameter in our theory,  $C$ , was fitted such that the DEM simulation took the same physical time to reach steady state as the numerical solution of the continuum theory. The theory can now be implemented in a finite element code, because it contains a constitutive model, albeit a simple one. This could also be solved in five-dimensional  $\{\mathbf{r}, s, t\}$ -space without the quasisteady assumption, using a more elaborate constitutive model, defined in tensorial form rather than the scalar form employed in this paper.

## 4. Results

### 4.1. Solution of governing equation

Solving the governing equation (3.2) is done numerically using a finite difference method. Simple methods for solving this class of equation are known to exhibit large amounts of numerical dissipation (LeVeque 2002). For that purpose we use a slope-limited total variation diminishing upstream-centred scheme (Quarteroni & Valli 1997) to approximate the numerical solution of the general equation in  $\{z, s, t\}$ .

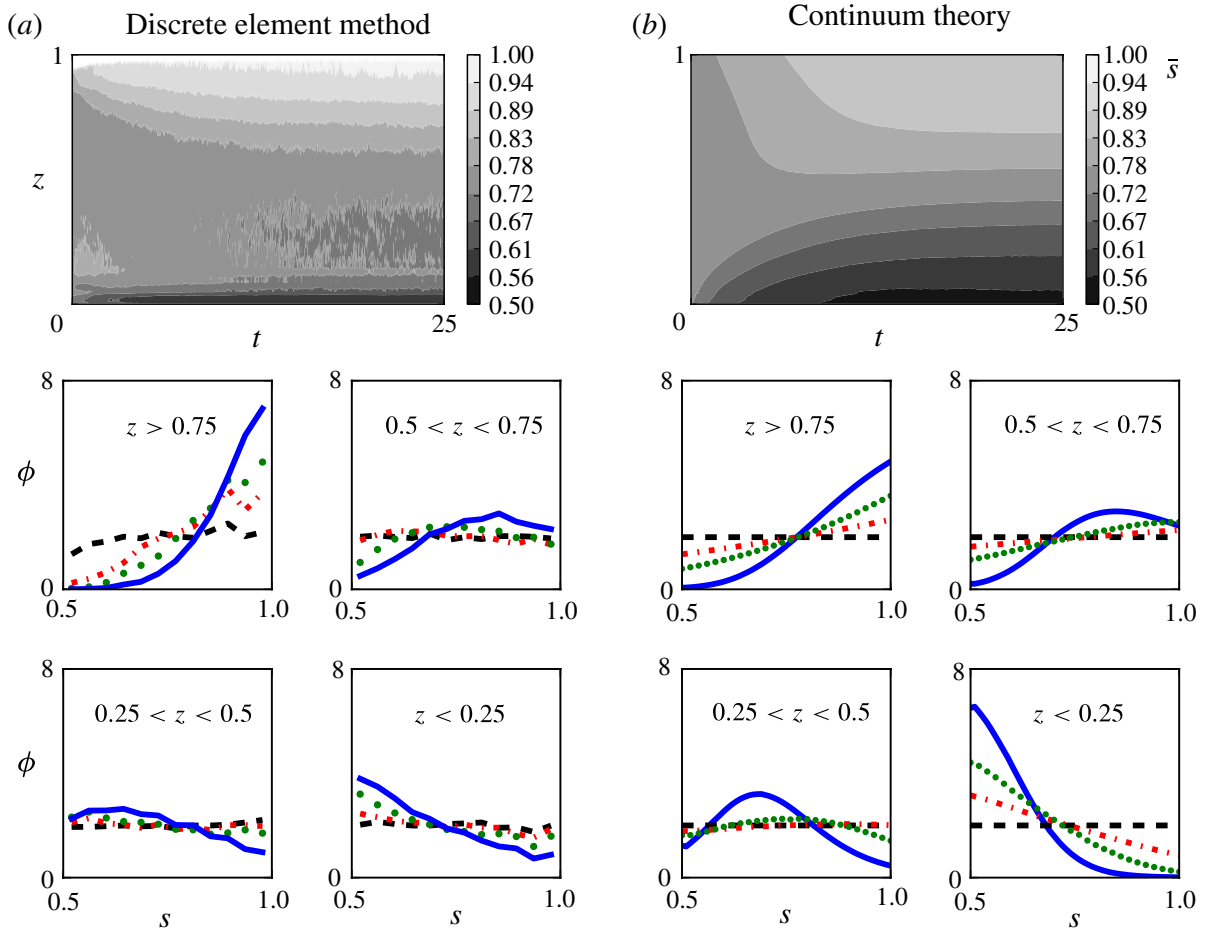


FIGURE 2. (Colour online) The DEM system (a) compared with an equivalent solution of the continuum theory. (b) Top: spatiotemporal plot of the average grainsize. Remaining: grainsize distributions at  $t = 0$  (dashed),  $t = 2$  (dash-dotted),  $t = 5$  (dotted) and  $t = 25$  (solid) averaged over different heights of the flow.

The system of equations is solved by discretizing along the  $z$  and  $s$  directions into a regularly spaced mesh, and a discretized set of grainsize distribution values  $\phi_{i,j}^k$  is defined at each height  $i$ , grainsize  $j$  and time  $k$ . The mesh is defined so that the edges between cells lie at the midpoints  $i \pm 1/2$ . Across these edges the total flux is the sum of the fluxes due to the diffusive term ( $\phi_{i,j}^k w_{i,j}^k$ ) and the advective term ( $-D(\partial\phi_{i,j}^k/\partial z)$ ) in (3.2). A SuperBee flux limiter is used to minimize dissipation near discontinuities in the solution, and the resultant numerical flux,  $h$ , is constructed from upwinded left and right going fluxes for each  $\phi_{i\pm 1/2,j}^k$  and then projected onto the solution at  $\phi_{i,j}^{k+1}$ . This can be summarized as

$$\phi_{i,j}^{k+1} = \phi_{i,j}^k - \frac{\Delta t}{\Delta z} (h_{i+1/2,j}^k - h_{i-1/2,j}^k), \quad (4.1)$$

and the whole scheme can be found in Quarteroni & Valli (1997, pp. 475–481). The solution for all grainsizes are coupled through the dependence of  $h$  on  $\bar{s}$  and  $\bar{\rho}$ , which are updated each time step by summing over the  $n$  discrete grainsizes as  $\bar{s}_i^k = \Delta s \sum_{j=1}^n \phi_{i,j}^k s_j$ . Lastly, we impose a no flux boundary condition

$$C \frac{\phi \sqrt{1-z}}{\bar{s}} \left( \frac{s}{\bar{s}} - \frac{\rho^*}{\bar{\rho}} \right) = D \frac{\partial \phi}{\partial z} \quad \text{on } z = 0, 1. \quad (4.2)$$

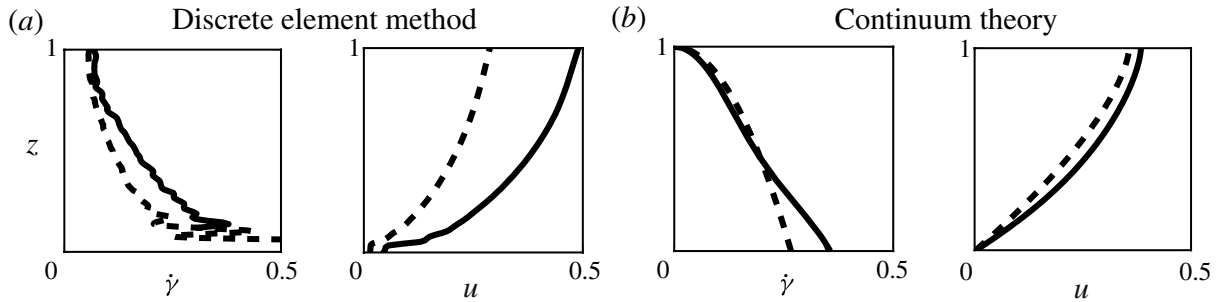


FIGURE 3. The DEM system (a) compared with an equivalent solution of the continuum theory. (b) For each system, the initial (dashed) and final (solid) shear strain rate and downslope velocity profiles are shown.

For the results shown here, we have used  $\Delta s = \Delta z = 0.05$  and  $\Delta t < \Delta z^2$ . This numerical method has been used extensively for similar problems, such as in Gray & Thornton (2005), and has been shown to be stable and accurate, with a minimal amount of numerical dissipation.

#### 4.2. Results from polydisperse system

On the left of figures 2 and 3 we represent the time evolution of the DEM sample shown in figure 1, and the equivalent solution of the analytic theory on the right. For that purpose, the theoretical model was solved with the values  $D = 0.007$  (measured directly from the DEM in § 3) and  $C = 0.2$  (to match the segregation time).

The theory predicts the grainsize distribution  $\phi(s)$  at any time of the flow, here shown for four times, ranging from the initial to final stages. It is clear from both analyses that there is significant segregation, which feeds back in a way that intensifies the downslope velocity. Also, it appears that at steady state, diffusion prohibits stratification into layers of uniform grainsizes. Instead, the grainsize distribution has a non-trivial shape that varies with time and position. Nevertheless, the theory predicts qualitative agreement with the DEM realization.

In figure 3, the predictions of the continuum theory for  $\dot{\gamma}$  and  $u$  are compared with the DEM, which shows comparable shear strain rate next to the basal plane, with both decaying strongly towards the free surface. The curvature of the strain rate profile is different. However, this discrepancy is likely related to the linear approximation of the constitutive law for dry granular flow (2.19). This is also known to be affected by the proximity of the plane (see for instance Rognon *et al.* 2007).

#### 4.3. Reduction to bimixture theory

There are many theories describing kinetic sieving in bimixtures. The first such theory was that of Savage & Lun (1988), where statistical mechanics was employed to model the segregation. Later, Dolgunin & Ukolov (1995) and Gray & Thornton (2005) developed continuum models for non-diffusive flow by considering a bimixture with shared solid fraction between the two phases in the flow. More recently, Gray & Chugunov (2006) added diffusion to the previous continuum theories.

For the case of bimixtures, which involve only two distinct grainsizes, with the same intrinsic density, the grainsize distribution  $\phi$  can be represented as a polydisperse mixture with the help of two dirac  $\delta$ -functions. For two grainsizes  $s = \{s_a, s_b\}$  the bidisperse case takes the following grainsize distribution

$$\phi = \Phi_a \delta(s - s_a) + \Phi_b \delta(s - s_b), \quad \Phi_a + \Phi_b = 1, \quad (4.3)$$

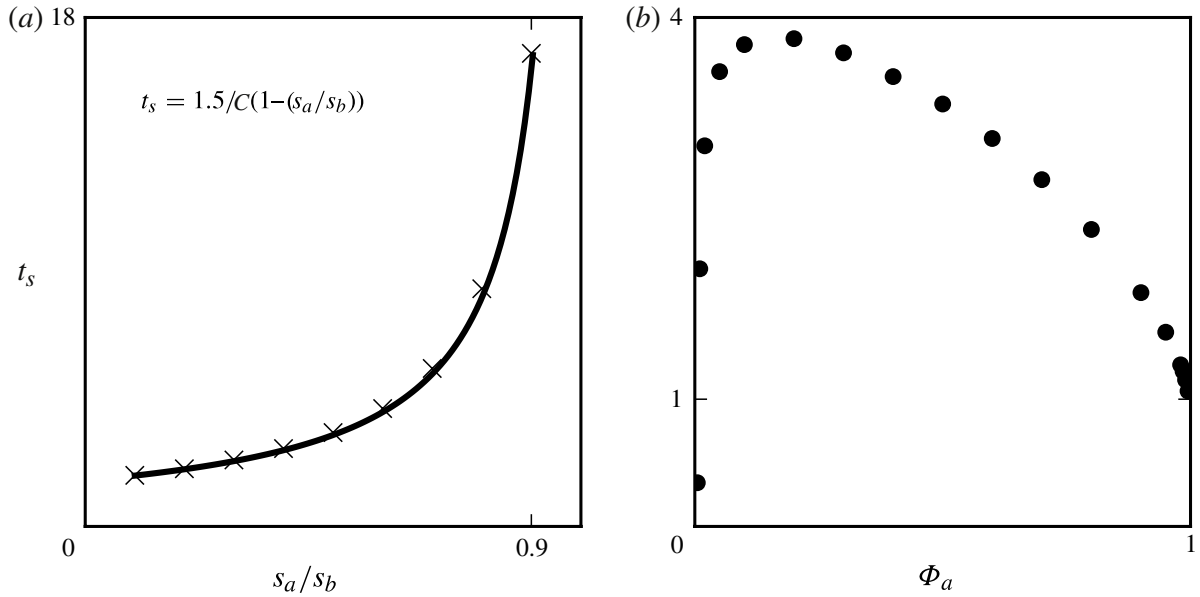


FIGURE 4. The time for complete segregation in bidisperse systems. (a) The time as a function of small grainsize  $s_a$ , with  $s_b = 1$  and  $\Phi_a = 0.5$ . The solid line indicates a hyperbolic trend for the segregation time. (b) The time for complete segregation as a function of small particle concentration,  $\Phi_a$ , for two grainsizes  $s_a = 0.5$  and  $s_b = 1$ .

where  $\Phi_a$  and  $\Phi_b$  are the solid fractions of the two species. For this case, using (2.17) and (3.1), the segregation velocity of the large particles ( $s = s_b$ ) becomes

$$w(s_b) = \dot{\gamma} \left( \frac{g \cos \theta}{c} \right) \left( \frac{s_b - s_a}{\bar{s}} \right) (1 - \Phi_b), \quad (4.4)$$

where  $\bar{s} = s_a \Phi_a + s_b \Phi_b$ . Compare this with equation (3.11) of Gray & Thornton (2005):  $w^b = ((Bg \cos \theta)/c)(1 - \Phi_b)$ , where  $B/c$  controls the rate of segregation in their model. As in May *et al.* (2010), our formulation explicitly represents the role of the shear rate. Unlike the previous works of Gray & Thornton (2005) and May *et al.* (2010), we capture the effects of grainsize difference and the time-dependent local average grainsize.

Experiments by Wiederseiner *et al.* (2011) have shown good agreement with the theory presented by Gray & Chugunov (2006) for one set of particle sizes ( $s_a = 1$  mm,  $s_b = 2$  mm). Using this new formulation, it is now possible to explore the sensitivity of such systems to alternative grainsizes.

We use  $\int_0^1 \int_0^1 |\partial \phi / \partial t| dz ds \leq 0.01$  as a criterion for a steady-state solution, applied for the case of  $D = 0$ . Using this definition, in figure 4 we represent this segregation time,  $t_s$ , as a function of initial conditions for a variety of bimixtures. On the left, increasing the size contrast between the particle species reduces the time for segregation. On the right, for a mixture with grainsize ratio of two, and  $C = 1$ , there is a maximum in the time for segregation at a concentration of approximately 20% small particles. These results await experimental validation. However, an explanation for this has already been proposed using a simple cellular automaton, as being due to the asymmetry of the shear strain rate (Marks & Einav 2011).

#### 4.4. Reduction to multicomponent theory

Recently, Gray & Ancy (2011) proposed a multicomponent theory which extends the work presented in Gray & Thornton (2005) to many dirac  $\delta$ -functions. For this case,



which involves a discrete number of grainsizes,  $n$ , with the same intrinsic density, the grainsize distribution  $\phi$  can be represented as a sum of dirac  $\delta$ -functions. For grainsizes  $i = \{1, 2, \dots, n\}$  the multicomponent case takes the following grainsize distribution

$$\phi = \sum_{i=1}^n \Phi_i \delta(s - s_i), \quad \sum_{i=1}^n \Phi_i = 1, \quad \bar{s} = \sum_{i=1}^n \Phi_i s_i, \quad (4.5)$$

where  $\Phi_i$  is the solid fraction of species  $i$ , and each  $i$  is chosen to perfectly tessellate the grainsize distribution. For this case, using (2.17) and (3.1), the segregation velocity of grainsize  $s_i$  becomes

$$w(s_i) = \dot{\gamma} \left( \frac{g \cos \theta}{c} \right) \left( \frac{s_i}{\sum_{i=1}^n \Phi_i s_i} - 1 \right), \quad (4.6)$$

which is not immediately comparable to the result produced by Gray & Ancy (2011). As a means of drawing a reasonable comparison, let us specify a geometrical sequence for the discrete size bins, such as the  $j$ th bin being twice the size of the  $(j - 1)$ th bin, or  $s_j = s_0 \cdot 2^j$ , for some smallest size  $s_0$ . This set of bin sizes was found to be useful for defining grading entropy (Lorincz *et al.* 2005). Equation (4.6) then becomes

$$w(s_i) = \dot{\gamma} \left( \frac{g \cos \theta}{c} \right) \sum_{j=1}^n B_{ij} \Phi_j, \quad (4.7)$$

where  $B_{ij} = (1 - 2^{j-i}) / (\sum_{m=1}^n \Phi_m 2^{m-i})$ . Similarly, distributing the grainsize bins linearly,  $s_j = s_0 + \Delta s \cdot j$ , gives  $B_{ij} = (i - j) / (\sum_{m=1}^n \Phi_m ((s_0/\Delta s) + m))$ . Compare these with equations (2.22)–(2.23) of Gray & Ancy (2011), with no diffusion ( $D_r = 0$ ) where  $w_i = ((g \cos \theta)/c) \sum_{j=1}^n B_{ij} \Phi_j$ . Gray & Ancy (2011) introduced  $(1/2)n(n - 1)$  constants  $B_{ij}$ , as a means to construct analytic solutions. According to our theory these coefficients are not constant, but vary with time through  $\Phi_m$ . Furthermore, they also depend on the allocation of the grainsize bins, which is now obtained naturally by associating each  $w_i$  with a grainsize  $s_i$ , without requiring additional parameters.

## 5. Conclusions

In this paper we have derived a polydisperse theory for granular segregation, where we have introduced the notion of a grainsize coordinate. The result of this is a five-dimensional population balance equation. By specifying this for inclined plane flows, this equation simplifies to three dimensions. Pivotal to our theory is the description of intrinsic stresses that scale with grainsize and control the segregation dynamics. The use of a simple constitutive equation that relates the shear stress and the shear strain rate enables us to connect the kinematics to the variation of grainsize distribution. We predict a grainsize distribution and a shear strain rate at any time and at any point in space.

Using this theory we have been able to model the segregation in systems of arbitrary grainsize distributions. Numerical solutions of the resulting nonlinear population balance equation are solved using a finite difference scheme. Comparison has been made with DEM simulations and consistent results have been found.

By employing our polydisperse theory to describe segregation in a bidisperse system, we have been able to compare our formulation with previous predictions (Gray & Thornton 2005). In this bidisperse limit, we now understand the role of size contrast between the constituents, and how that affects both the time for segregation, and the kinematics of the flow. We have also shown how multicomponent systems can be expressed in terms of the polydisperse theory, and how the fitting parameters used vary with time and with the choice of grainsize bins.

It is now possible to predict the time for segregation in geophysical and industrial flows and then to tailor conditions to either reduce or increase the extent of segregation as necessary. This has relevance for industrial applications that use granular materials, such as pharmaceuticals, agriculture and mining. This can also increase our understanding of long run out landslides, since we predict a shear strain rate profile, and hence a downslope velocity profile. Also, these dynamics, with the added ingredient of momentum conservation, could be used for the design of protection structures.

### Acknowledgements

We would like to thank the members of the Particles and Grains Laboratory at The University of Sydney. I.E. acknowledges grant DP0986876 from the ARC.

### REFERENCES

- BRIDGWATER, J. 1976 Fundamental powder mixing mechanisms. *Powder Technol.* **15** (2), 215–236.
- BRIDGWATER, J. & INGRAM, N. D. 1971 Rate of spontaneous inter-particle percolation. *Chem. Engng Res. Des.* **49a**, 163–169.
- CAMPBELL, C. S. 1997 Self-diffusion in granular shear flows. *J. Fluid Mech.* **348**, 85–101.
- DA CRUZ, F., EMAM, S., PROCHNOW, M., ROUX, J-N. & CHEVOIR, F. 2005 Rheophysics of dense granular materials: discrete simulation of plane shear flows. *Phys. Rev. E* **72**, 021309.
- DOLGUNIN, V. N. & UKOLOV, A. A. 1995 Segregation modelling of particle rapid gravity flow. *Powder Technol.* **83** (2), 95–104.
- DOLGUNIN, V. N., KUDY, A. N. & UKOLOV, A. A. 1998 Development of the model of segregation of particles undergoing granular flow down an inclined chute. *Powder Technol.* **96** (3), 211–218.
- EINAV, I. 2007 Breakage mechanics – part 1: theory. *J. Mech. Phys. Solids* **55** (6), 1274–1297.
- GRAY, J. M. N. T. & ANCEY, C. 2011 Multi-component particle-size segregation in shallow granular avalanches. *J. Fluid Mech.* **678**, 535–588.
- GRAY, J. M. N. T. & CHUGUNOV, V. A. 2006 Particle-size segregation and diffusive remixing in shallow granular avalanches. *J. Fluid Mech.* **569**, 365–398.
- GRAY, J. M. N. T. & THORNTON, A. R. 2005 A theory for particle size segregation in shallow granular free-surface flows. *Proc. R. Soc. A* **461** (2057), 1447–1473.
- LEVEQUE, R. J. 2002 *Finite Volume Methods for Hyperbolic Problems*. Cambridge University Press.
- LORINCZ, J., IMRE, E., GLOS, M., TRANG, Q. P., RAJKAI, K., FITYUS, S. & TELEKES, G. 2005 Grading entropy variation due to soil crushing. *Intl J. Geomech.* **5** (4), 311–319.
- MARKS, B. & EINAV, I. 2011 A cellular automaton for segregation during granular avalanches. *Granul. Matt.* **13**, 211–214.
- MAY, L. B. H., SHEARER, M. & DANIELS, K. E. 2010 Scalar conservation laws with non-constant coefficients with application to particle size segregation in granular flow. *J. Nonlinear Sci.* 1–19.
- MIDI, G. D. R. 2004 On dense granular flows. *Eur. Phys. J. E* **14** (4), 341–365.
- MORLAND, L. 1992 Flow of viscous fluids through a porous deformable matrix. *Surv. Geophys.* **13** (3), 209–268.

- OTTINO, J. M. & KHAKHAR, D. V. 2000 Mixing and segregation of granular materials. *Annu. Rev. Fluid Mech.* **32** (1), 55–91.
- QUARTERONI, A. & VALLI, A. 1997 *Numerical Approximation of Partial Differential Equations*. Springer.
- RAMKRISHNA, D. 2000 *Population Balances: Theory and Applications to Particulate Systems in Engineering*. Academic.
- RICARD, Y. & BERCOVICI, D. 2009 A continuum theory of grain size evolution and damage. *J. Geophys. Res. (Solid Earth)* **114** (13), 01204.
- ROGNON, P., EINAV, I., BONIVIN, J. & MILLER, T. 2010 A scaling law for heat conductivity in sheared granular materials. *EPL* **89** (5), 58006.
- ROGNON, P. G., ROUX, J. N., NAAÏM, M. & CHEVOIR, F. 2007 Dense flows of bidisperse assemblies of disks down an inclined plane. *Phys. Fluids* **19**, 058101.
- SAVAGE, S. B. & LUN, C. K. K. 1988 Particle size segregation in inclined chute flow of dry cohesionless granular solids. *J. Fluid Mech.* **189**, 311–335.
- SHINBROT, T., ALEXANDER, A. & MUZZIO, F. J. 1999 Spontaneous chaotic granular mixing. *Nature* **397**, 675–678.
- UTTER, B. & BEHRINGER, R. P. 2004 Self-diffusion in dense granular shear flows. *Phys. Rev. E* **69** (3), 031308.
- WIEDERSEINER, S., ANDREINI, N., ÉPELY-CHAUVIN, G., MOSER, G., MONNEREAU, M., GRAY, J. M. N. T. & ANCEY, C. 2011 Experimental investigation into segregating granular flows down chutes. *Phys. Fluids* **23** (1), 013301.
- YOHANNES, B. & HILL, K. M. 2010 Rheology of dense granular mixtures: particle-size distributions, boundary conditions, and collisional time scales. *Phys. Rev. E* **82** (6), 061301.



## CHAPTER 5

### **Bulk, mean and grainsize dynamics**

---

In the previous Chapter, a continuum approach was developed so that the grainsize distribution could be included as an internal coordinate. This was then solved in a single spatial dimension, and the evolution of the system subject to simple boundary conditions was analysed. For the future, beyond the scope of this thesis, it is necessary to have a description of the material that can be included in a numerical analysis.

For this purpose, the mean dynamics must be decoupled from the grainsize dynamics, as shown in Figure 5.1. This will allow the use of conventional continuum analysis software, such as the finite element, finite volume or material point methods. To facilitate this, the current Chapter is devoted to showing how a mean and fluctuation decomposition can be used to partition the solution space into the mean behaviour of the material and the grainsize dynamics.

In the field of fluid mechanics, Reynolds decomposition is often used to account for turbulent behaviour, by averaging over the velocity field to find mean and fluctuating parts (Reynolds 1895). This gives rise to the Reynolds-averaged Navier-Stokes equations, which represent the time-averaged equations for fluid flow. In this Chapter turbulence is not considered and fluctuations introduced by the internal coordinate of grainsize create segregation and mixing instead.

For simplicity, this Chapter treats all of the material as being the same density, so that  $\rho = \phi\bar{\rho}$ . As a continuum quantity, the intrinsic density of a particular size of particles is defined as the mass of those particles divided by the volume of tessellated cells surrounding them. This simplification may not be realistic, as it does not allow changes in volume of the soil skeleton,

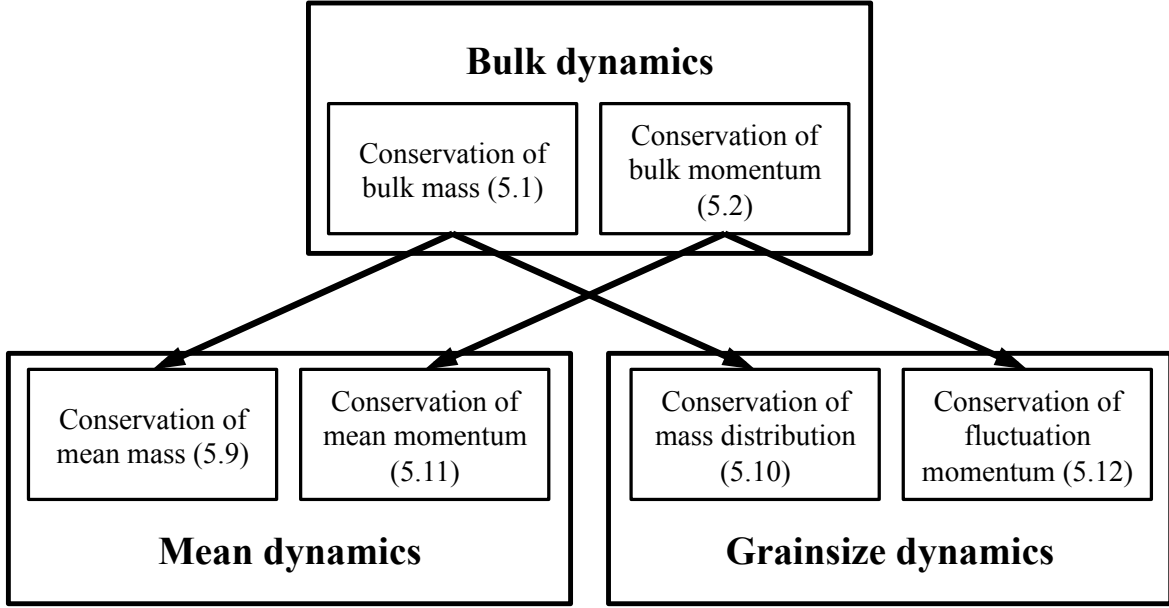


FIGURE 5.1: Dynamics hierarchy in the system. The bulk dynamics can be decomposed into the mean and grainsize dynamics, all of which include conservation of mass and momentum.

whether due to shearing, compression or grain crushing. This simplification should be relaxed in further research, and deserves investigation.

To begin, we can split the velocity into a mean  $\bar{\mathbf{u}}$  and a fluctuating part  $\hat{\mathbf{u}}$  as  $\mathbf{u} = \bar{\mathbf{u}} + \hat{\mathbf{u}}$ , where  $\bar{\mathbf{u}} = \int \phi \mathbf{u} ds$ . The bulk material will move with velocity  $\bar{\mathbf{u}}$ , and we can track this mean component of the dynamics with a traditional continuum solver. The other component, the grainsize dynamics, must be tracked separately. As shown in Chapter 4, conservation of bulk mass and momentum can in this case be written as

$$\frac{\partial \rho}{\partial t} + \nabla \cdot (\rho \bar{\mathbf{u}}) + \nabla \cdot (\rho \hat{\mathbf{u}}) = 0, \quad (5.1)$$

$$\frac{D}{Dt}(\rho \bar{\mathbf{u}}) + \frac{D}{Dt}(\rho \hat{\mathbf{u}}) = \rho \mathbf{g} - \phi f \nabla \cdot \bar{\boldsymbol{\sigma}} - D \bar{\rho} \nabla \phi - \frac{\phi \bar{\rho} c \hat{\mathbf{u}}}{\dot{\gamma}}. \quad (5.2)$$

It should be noted that the diffusion term is now included in the momentum equation, rather than in conservation of mass. As there is no longer an assumption of steady state flow, it cannot be assumed that diffusion is independent of velocity. Additionally, the term  $f$  has been

moved outside of the stress gradient, to be more consistent with Darcy's law, such that the system is not driven by partial pressure gradients (Bear 1972).

## 5.1 Conservation of mass

The purpose of this Section is to split (5.1) into two equations. The first will represent conservation of mass of the material, and the second will describe the evolution of the grainsize distribution. If we integrate (5.1) over the grainsize direction  $s$  we get

$$\int \frac{\partial \rho}{\partial t} ds + \int \nabla \cdot (\rho \bar{\mathbf{u}}) ds + \int \nabla \cdot (\rho \hat{\mathbf{u}}) ds = 0,$$

or by introducing the integrals into the differentiation and using the fact that  $\int \phi \hat{\mathbf{u}} ds = 0$ ,

$$\frac{\partial \bar{\rho}}{\partial t} + \nabla \cdot (\bar{\rho} \bar{\mathbf{u}}) = 0, \quad (5.3)$$

which represents the mean conservation of mass without a grainsize direction. Expanding (5.1) and using (5.3), and subsequently applying the product rule gives

$$\bar{\rho} \frac{\partial \phi}{\partial t} = \phi \nabla \cdot (\bar{\rho} \bar{\mathbf{u}}) - \nabla \cdot (\bar{\rho} \phi \bar{\mathbf{u}}) - \nabla \cdot (\bar{\rho} \phi \hat{\mathbf{u}}). \quad (5.4)$$

Applying the product rule again we can state that

$$\nabla \cdot (\bar{\rho} \phi \bar{\mathbf{u}}) = \phi \nabla \cdot (\bar{\rho} \bar{\mathbf{u}}) + \bar{\rho} \bar{\mathbf{u}} \cdot \nabla \phi,$$

or by rearrangement

$$\phi \nabla \cdot (\bar{\rho} \bar{\mathbf{u}}) - \nabla \cdot (\bar{\rho} \phi \bar{\mathbf{u}}) = -\bar{\rho} \bar{\mathbf{u}} \cdot \nabla \phi.$$

Putting this in (5.4) gives

$$\frac{\partial \phi}{\partial t} + \bar{\mathbf{u}} \cdot \nabla \phi = -\frac{1}{\bar{\rho}} \nabla \cdot (\bar{\rho} \phi \hat{\mathbf{u}}). \quad (5.5)$$

This gives us a description of the evolution of the grainsize distribution as a function of its material derivative. The term on the right hand side will cause changes in the grainsize distribution due to material flowing at the fluctuation velocity, and not at the mean velocity. We have partially decoupled the mean mass conservation (5.3) and the mass distribution conservation (5.5).

## 5.2 Conservation of momentum

To complete the description of the system in a decoupled state, we can now express the momentum equations in the same mean and fluctuation decomposition. Integrating (5.2) over all sizes

$$\int \frac{D}{Dt}(\rho \bar{\mathbf{u}}) ds + \int \frac{D}{Dt}(\rho \hat{\mathbf{u}}) ds = \int \rho \mathbf{g} ds - \int \frac{\phi s}{\bar{s}} \nabla \cdot \bar{\boldsymbol{\sigma}} ds - \int D\bar{\rho} \nabla \phi ds - \int \frac{\phi \bar{\rho} c \hat{\mathbf{u}}}{\dot{\gamma}} ds.$$

By again moving the integrals into the differentiation, this reduces to

$$\frac{D}{Dt}(\bar{\rho} \bar{\mathbf{u}}) = \bar{\rho} \mathbf{g} - \nabla \cdot \bar{\boldsymbol{\sigma}}. \quad (5.6)$$

This is the traditional conservation of mean momentum statement solved for in numerical inertial methods. The final expression required to close the system is a statement of conservation of fluctuation momentum. To derive this, we can use the product rule to state that

$$\frac{D}{Dt}(\phi \bar{\rho} \bar{\mathbf{u}}) = \frac{D\phi}{Dt} \cdot \bar{\rho} \bar{\mathbf{u}} + \frac{D}{Dt}(\bar{\rho} \bar{\mathbf{u}}) \cdot \phi. \quad (5.7)$$

Substituting (5.6) into this equation gives

$$\frac{D}{Dt}(\phi\bar{\rho}\bar{\mathbf{u}}) = \frac{D\phi}{Dt} \cdot \bar{\rho}\bar{\mathbf{u}} + \phi\bar{\rho}\mathbf{g} - \phi\nabla \cdot \bar{\boldsymbol{\sigma}}, \quad (5.8)$$

and putting this into the previous conservation of momentum (5.2) gives, after rearrangement

$$\frac{D}{Dt}(\bar{\rho}\hat{\mathbf{u}}) = \left(1 - \frac{s}{\bar{s}}\right)\nabla \cdot \bar{\boldsymbol{\sigma}} - \frac{D\bar{\rho}}{\phi}\nabla\phi - \frac{\bar{\rho}c\hat{\mathbf{u}}}{\dot{\gamma}} - \bar{\rho}\mathbf{u}\frac{D\phi}{Dt}.$$

which represents conservation of fluctuation momentum, only weakly coupled to the mean dynamics. The first term on the right hand side is the splitting of the mean stress across the grain size distribution, giving gradients in space and the grain size direction. The second term is the diffusive momentum, which causes remixing of particles to minimise spatial gradients in the grain size distribution. The third term is a drag force, creating an interaction between the sizes, as introduced in Chapter 4. The final term is a convective term, describing the change in fluctuation momentum due to mean movement of the material.

### 5.3 Summary of governing equations

We now have four governing equations, two for mass and two for momentum. They are

$$\frac{\partial\bar{\rho}}{\partial t} + \nabla \cdot (\bar{\rho}\bar{\mathbf{u}}) = 0, \quad (5.9)$$

$$\frac{\partial\phi}{\partial t} + \bar{\mathbf{u}} \cdot \nabla\phi + \frac{1}{\bar{\rho}}\nabla \cdot (\bar{\rho}\phi\hat{\mathbf{u}}) = 0, \quad (5.10)$$

$$\frac{D}{Dt}(\bar{\rho}\bar{\mathbf{u}}) = \bar{\rho}\mathbf{g} - \nabla \cdot \bar{\boldsymbol{\sigma}}, \quad (5.11)$$

$$\frac{D}{Dt}(\bar{\rho}\hat{\mathbf{u}}) = \left(1 - \frac{s}{\bar{s}}\right)\nabla \cdot \bar{\boldsymbol{\sigma}} - \frac{D\bar{\rho}}{\phi}\nabla\phi - \frac{\bar{\rho}c\hat{\mathbf{u}}}{\dot{\gamma}} + \mathbf{u}\nabla \cdot (\bar{\rho}\phi\hat{\mathbf{u}}). \quad (5.12)$$

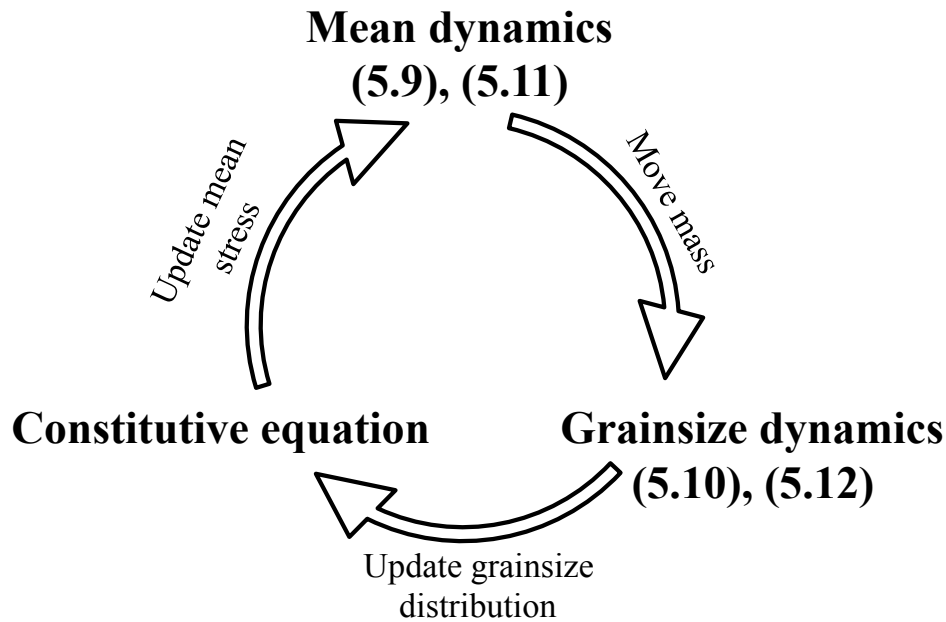


FIGURE 5.2: Numerical implementation of a grain size dynamics solver. A traditional solver alternates between the mean dynamics and a constitutive equation. In this scheme, the grain size dynamics are updated between these two steps so that the constitutive equation can use the local grain size distribution as a state variable.

These four coupled equations describe the evolution of mass and momentum for the mean and grain size dynamics. These equations are now ready to be implemented into a two or three spatial dimensional model, to capture the flow of material and the inherent grain size dynamics.

## 5.4 Towards numerical implementation of grain size dynamics

For the purpose of solving this set of equations numerically, as indicated schematically in Figure 5.2, (5.9) and (5.11) can be solved to find the mean behaviour of the system, neglecting the grain size coordinate. Once the material has advected in space, the equations (5.10) and (5.12) can be updated to find the grain size distribution at each point in space.

A constitutive model can then be used which takes advantage of the local grain size distribution, such as the one motivated in Chapter 4. This could easily be extended to a three

dimensional model by replacing the scalar shear strain rate with the strain rate tensor, as done for monodisperse flows in Jop et al. (2006).

The mean material advection could be implemented into a numerical code that is able to handle large deformation problems, such as the material point method (Sulsky et al. 1995). Solving the grainsize dynamics equations could be done with a separate solution scheme that advected grainsize between the existing material points.

As will be discussed at length in Chapter 8, these equations can also be extended to describe other processes that feature changes in the grainsize distribution, such as agglomeration, crushing, melting, thermal expansion and erosion. The possible uses for such a code are very exciting, and will necessitate much further research.

## CHAPTER 6

### **Steady State Solutions**

---

The prediction of segregation patterns in granular flow problems are generally treated separately for different geometries. This Chapter presents a method for determining the grainsize distribution of arbitrary mixtures of granular materials at steady state regardless of the flow geometry. The grainsize distribution at any point in space is shown to be a function of the normal stress gradient and the diffusivity only. Solutions are presented for one dimensional flows only.

Segregation can occur quickly in many systems, such as in avalanches, debris flows and rotating tumblers. In these cases, the time evolution of the segregation is often unimportant. While models are not yet available to predict the time for full segregation to occur, it is for these cases only the final extent of segregation that is important for physical modelling. It is then of interest to find the steady state solution to the problem posed in the previous Chapter.

As this removes the temporal coordinate from the solution, we will be able to solve this system without the use of complicated partial differential equation solvers. Steady state solutions of previous theories have shown to be of a similar form to those presented below, but neglecting information about the physical size of the particles (Gray and Thornton 2005; Shearer et al. 2008).



## 6.1 Continuum description

Following on from the statement of conservation of momentum for the grainsize direction, (5.12), and considering a flow that has reached some form of quasi-steady state where  $\frac{\partial \phi}{\partial t} = 0$  and  $\hat{\mathbf{u}} = \mathbf{0}$ ,

$$\nabla \phi = \frac{\phi}{D\bar{\rho}} \left(1 - \frac{s}{\bar{s}}\right) \nabla \cdot \bar{\boldsymbol{\sigma}}. \quad (6.1)$$

We now have a direct competition between stress gradients and diffusion. Stress gradients will create spatial gradients in the grainsize distribution, and diffusion will attempt to remove them. It is therefore sufficient to know the grainsize distribution, stress gradient and diffusivity to be able to predict the steady state grainsize distribution for any flow, in any geometry.

The simplification presented in (6.1) has taken the fluctuation velocity to be zero, and so neglects solutions where stable recirculation of grainsize could reach other steady state solutions, such as with a vortex. For the case of a system which can be represented in one spatial dimension, we can find an explicit analytic solution to the steady state grainsize distribution presented above. In this  $x$  direction, which we take normal to the boundary, and assuming no variation in the  $y$  or  $z$  directions, the steady state solution becomes

$$\frac{\partial \phi}{\partial x} = \frac{\phi}{D\bar{\rho}} \left(\frac{s}{\bar{s}} - 1\right) \frac{d\bar{\sigma}_{xx}}{dx}. \quad (6.2)$$

For a bidisperse system with grainsize  $s = \{s_a, s_b\}$ , this can be expressed in terms of the solid fraction  $\Phi_a$  of species  $s_a$  as

$$\frac{d\Phi_a}{dx} = \frac{\Phi_a}{D\bar{\rho}} \left(\frac{s_a}{s_a\Phi_a + s_b(1 - \Phi_a)} - 1\right) \frac{d\bar{\sigma}_{xx}}{dx}, \quad (6.3)$$

which has the following analytic solution

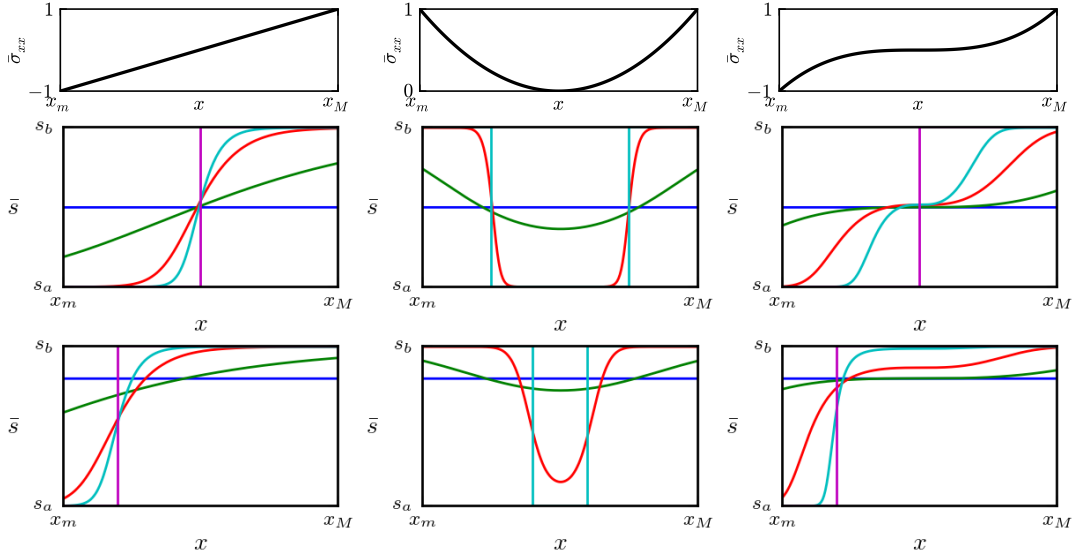


FIGURE 6.1: Steady state solution for bidisperse chute flow problems. For all cases  $x_m = -1$  and  $x_M = 1$ . *Left*: Inclined chute flow.  $\bar{\sigma}_{xx} = \bar{\rho}g \cos \theta(1 - x)/2$ .  $D\bar{\rho} = \{\infty, 0.5, 0.1, 0.05, 0\}$ . *Middle*: Possible vertical chute flow.  $\nu = 0.6$ ,  $\bar{\sigma}_{xx} \propto x^2$ .  $D\bar{\rho} = \{\infty, 0.2, 0.02, 0\}$ . *Right*: Possible vertical chute flow.  $\nu = 0.3$ ,  $\bar{\sigma}_{xx} \propto x^3$ .  $D\bar{\rho} = \{\infty, 0.5, 0.05, 0.01, 0\}$ . *Top*: Stress condition. *Middle*: 50% small particles. *Bottom*: 20% small particles.

$$\frac{s_b \log \frac{\Phi_a}{k} - s_a \log \left( \frac{1 - \Phi_a}{1 - k} \right)}{(s_a - s_b)} = \frac{1}{D\bar{\rho}} \int_{x_m}^x \frac{d\bar{\sigma}_{x'x'}}{dx'} dx', \quad (6.4)$$

where  $k = \Phi_a|_{x_m}$ , i.e. the solid fraction of species  $a$  at the bottom boundary. This can also be expressed as

$$\Phi_a^{s_a/s_b} k e^{f(x)(s_a - s_b)/s_b} + \Phi_a (1 - k)^{s_a/s_b} - k e^{f(x)(s_a - s_b)/s_b} = 0, \quad (6.5)$$

where  $f(x) = \frac{1}{D\bar{\rho}} \int_{x_m}^x \frac{d\bar{\sigma}_{x'x'}}{dx'} dx'$  represents the coupled stress/diffusion state. If  $s_a = 0.5$  and  $s_b = 1$ , this further simplifies to

$$\Phi_a = \frac{-k^2 \pm \sqrt{k^4 + 4k^2 e^{f(x)}(1 - k)}}{2e^{f(x)}(1 - k)}. \quad (6.6)$$

Examples of predictions using this ordinary differential equation are shown in Figure 6.1. Shown are three different potential stress fields, and a variety of diffusivities. For each case,

two different grainsize distributions are shown, one with 50% small particles, and the second with 20% small particles. It is evident that we can find complex stratigraphy resulting from any type of one dimensional flow with minimal computational effort. This is a promising tool for future analysis of avalanche, landslide and debris flow runout, or cases where the topography of the system does not vary significantly.

## Chute experiment

---

As show in Figure 3 in Chapter 4, we observe in both the discrete element model and the analytic theory an increase in down slope velocity due to segregation. As small particles migrate towards the base of the flow, the shear strain rate at the base increases, and a lubrication layer forms, accelerating the bulk of the flow.

### 7.1 Lubrication effect

The lubrication effect can be quantified coarsely by making the assumption that we can consider the one dimensional avalanche presented in Chapter 4 to be a model for a natural avalanche. Now assuming that the avalanche hits a rigid wall and all of the kinetic energy in the avalanche is converted into spring energy behind the wall, we can state that

$$\frac{1}{2}k\Delta x^2 = \int \frac{1}{2}mu^2 dz,$$

where  $k$  is the stiffness of the wall,  $\Delta x$  is the displacement of the wall,  $m$  is the mass of the material and  $u(z)$  is the down slope velocity. We can then find the elastic force  $F$  contained within the wall as

$$F = k\Delta x = \sqrt{km \int u^2 dz}.$$

We now consider two cases. The first case is when the material has not had a chance to segregate, and has a homogeneous spatial distribution of grainsize. For this case, let the

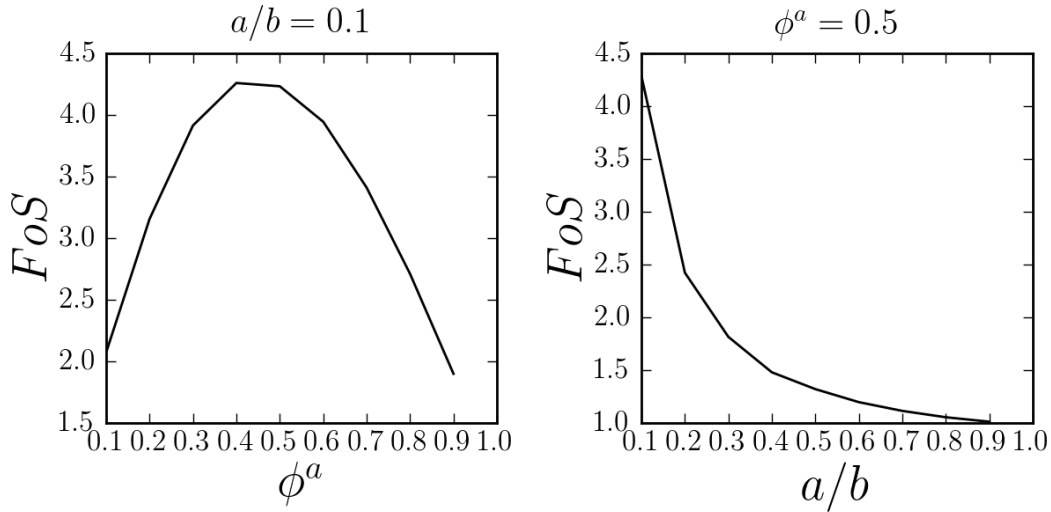


FIGURE 7.1: Factors of safety due to lubrication effect for a bimixture with sizes  $a$  and  $b$ . *Left*: Varying factor of safety with concentration of small particles for a size ratio of 10. This has a peak at approximately 40-50% concentration. *Right*: Varying factor of safety with size ratio, and constant initial concentration of small particles of 50%.

down slope velocity distribution be called  $u_i(z)$ . After some time, when segregation has occurred, and the system has reached its steady state, the velocity distribution will be  $u_f(z)$ . By comparing the forces exerted by these two cases, we can consider a factor of safety,  $FoS$ , which describes the increase in force due to segregation. This can be expressed as

$$FoS = \sqrt{\frac{\int u_f^2 dz}{\int u_i^2 dz}}.$$

For the case of bidisperse material with sizes  $a$  and  $b$ , and volumetric concentration of species  $\phi^a$ , we predict the factors of safety according to Figure 7.1. At a concentration of 50% small particles, and a size ratio of 10, we expect around 4 times more force on a rigid obstacle.

Because of this prediction, an experiment was designed and conducted in ETH Zürich under the supervision of Professor Alexander Puzrin, and assisted by Mr Aurelio Valaulta, who conducted the experimental work for his Masters thesis Valaulta 2012. The aim of the experiment was to capture the effect that this lubrication layer may have on a protection structure, such as when an avalanche impacts a building.

## **7.2 Contribution towards paper**

The experimental work described in the following in press conference proceeding was primarily conducted by a Masters research student, Aurelio Valaula, at ETH Zürich, and supervised by Professor Alexander Puzrin. Aurelio's dissertation was submitted in July 2012 (Valaula 2012). My role in this work was as designer, co-supervisor and author.

# Design of protection structures: the role of the grainsize distribution

Benjy Marks\*, Aurelio Valaula<sup>†</sup>, Alexander Puzrin<sup>†</sup> and Itai Einav\*

\*The University of Sydney

<sup>†</sup>ETH Zürich

**Abstract.** Granular avalanches are a natural hazard which pose a serious threat to human safety, especially in remote areas. These avalanches are generally modelled as being composed of particles of uniform size. However, recent analytic work on size segregation during flow indicates that this is a non-conservative way to model avalanche kinematics, as the segregation creates a lubrication layer at the base of the flow that can greatly accelerate the system. In this experimental work, we have analysed the importance of the grainsize distribution on the flow kinematics of a granular avalanche occurring down an inclined chute. We show that varying the size of the particles in the avalanche changes the shape and magnitude of the velocity profile, the depth of flow and the shape of the pile retained by a rigid wall in the path of an avalanche. These effects create additional loads on the protection structure, which are not observed for monodisperse flow.

**Keywords:** Avalanches, Granular Materials, Polydispersity

**PACS:** 45.70.Ht, 47.60.Dx, 83.80.Fg

## INTRODUCTION

Rockfalls, landslides and debris flows cause approximately 5000 fatalities per year globally, and this number appears to be increasing [1]. The main method of protecting both people and buildings from these flows is with the installation of upstream protection structures to divert or impede the flow. The design of such protection structures is reliant on knowledge of the kinematics of the flowing material, and the forces created as a result of impact.

To inform our understanding of these concepts, small scale laboratory chute flows are often conducted [2]. Typically, the size of the constituent granular material is carefully controlled to stop "unwanted" effects, such as segregation. The effect of this segregation on the avalanche kinematics is largely unknown, although it can induce additional mobility [3]. The effect of segregation on the forces exerted on an obstacle have not previously been investigated.

When dry granular material flows down a roughened inclined plane, there is a tendency for small particles to migrate in a direction perpendicular to the slope, towards the base, with a corresponding rise of large particles upwards towards the free surface [4]. This is referred to as segregation, or inverse grading.

The model we use to explain this phenomenon is known as kinetic sieving [5]. As particles collide within the flow, new void spaces are created, which are more likely to be filled with a small particle than a large one. As a result, we observe a net movement of small particles towards the base of the flow and large ones upwards towards the free surface. Under ideal conditions — flow

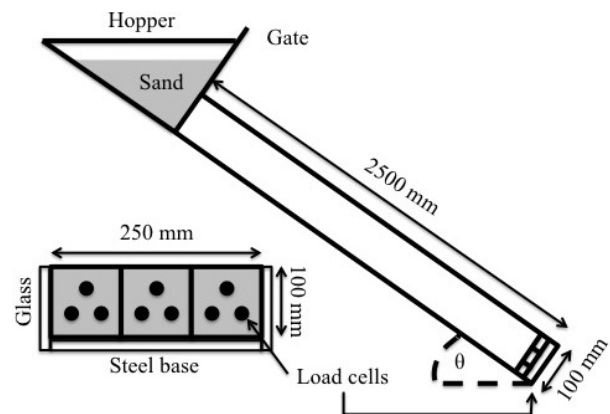


**FIGURE 1.** Schematic representation of the experimental apparatus. A hopper is attached to the upper end of a chute with variable inclination angle, of length 2.5 m, width 250 mm and depth 100 mm. At the bottom end, 9 load cells are attached to three separate aluminium plates which span the 250 mm cross section of the chute, as pictured on the left of the Figure. The chute has glass side walls and a steel base, which is coated with sand to mimic roughness.

near the angle of repose and a bidisperse mixture with a large size contrast — the large and small phases can separate completely into layers of uniform size.

A continuum model has been proposed to model this effect in a bidisperse media [6, 7]. In experimental tests, it has been shown to correctly reproduce segregation patterns [8]. Recently, this theory has been extended to multi-component flows [9] which captures segregation in systems with arbitrary numbers of particle sizes. How-

ever, these theories do not explicitly state the sizes of the particles considered, and so give no information as to how the size contrast between particle species affects the segregation, and hence the avalanche kinematics.

To gain information related to the physical size of the particles, another continuum model was proposed [10], which explicitly includes the particle sizes as an internal coordinate,  $s$ , the grainsize. In this theory, a grainsize distribution  $\phi(s)$  is defined at every point in space. A conclusion of this theory, when solved for inclined plane flow of material with constant density, is that the segregation velocity  $w(z)$  obeys the following law

$$w = \dot{\gamma} \frac{g \cos \theta}{c} \left( \frac{s}{\bar{s}} - 1 \right), \quad (1)$$

where  $z$  is the perpendicular distance from the base of the chute upwards,  $\dot{\gamma}(z)$  is the shear strain rate,  $g$  is the acceleration due to gravity,  $\theta$  the inclination angle,  $\bar{s}$  the local average grainsize and  $c$  is a parameter controlling the rate of segregation, with units of inverse time squared. This equation predicts that as the size contrast between particles increases, segregation will occur more rapidly. The shear strain rate is also predicted by assuming the granular media acts as a yield stress fluid, giving

$$\dot{\gamma} = \frac{\tan \theta - \mu_c}{k \bar{s}} \sqrt{3/2 g \cos \theta (1 - z)}. \quad (2)$$

where  $\tan^{-1} \mu_c$  is the angle of repose and  $k$  is a non-dimensional constant controlling the viscosity. Because the shear strain rate is inversely proportional to the local average grainsize, this equation predicts that as segregation occurs, and small particles collect near the base of the flow, a lubrication layer will form there. Here we attempt to measure this effect for a range of chute flow experiments.

Many experiments in this geometry have been conducted for monodisperse tests on dry sand [2, 11], as well as using discrete element modelling [12, 13]. From these we understand that in terms of chute inclination there is a

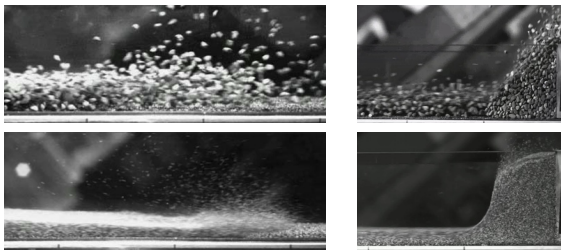


**FIGURE 2.** Images of avalanche flow recorded using a high speed camera, taken through a side wall. Flow direction is left to right. *Left:* Saltation of particles at the avalanche front. *Right:* Granular jump formed when a deposit builds against a wall. All are during monodisperse tests at  $42^\circ$ . *Top:* 4–4.75 mm particles. *Bottom:* 0.5–0.6 mm particles.

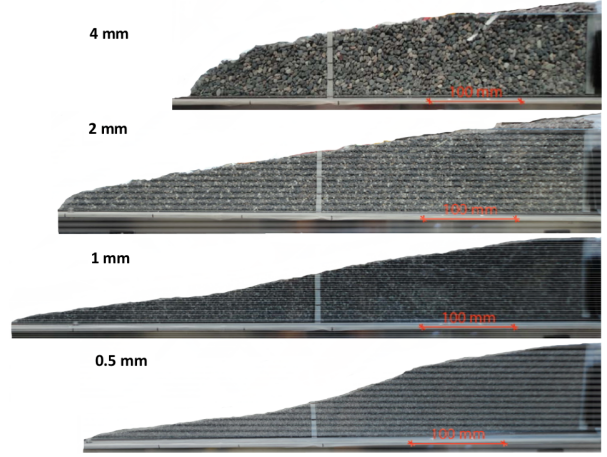


**FIGURE 3.** Residual deposition from monodisperse tests at  $\theta = 42^\circ$ . *Top to bottom:* 4, 2, 1 and 0.5 mm particles.

minimum threshold below which flow will not occur, and that the depth of flow increases with inclination above this threshold. From other experiments [14], we know that this threshold value, which is related to the angle of repose, varies with particle size. So for a set of monodisperse tests at the same inclination angle, with the same amount of material, we expect a different depth of flow for each size fraction used.

When a flowing avalanche impacts a rigid obstacle, the force applied to the obstacle increases over time as a static pile builds up. If the wall height is smaller than the granular jump (see Figure 2), the avalanche will eventually flow over the wall. As the pile reaches its maximum height, and the avalanche continues to overtop the obstacle, the force reaches a maximum, or peak force  $F_p$ , dying down to a residual static force  $F_r$ , as the avalanche abates. For vigorous flows, well above the angle of repose of the material, we have  $F_p \gg F_r$ , but at lower angles, where the pile builds gradually on the obstacle, we see that  $F_p = F_r$  [2].

## EXPERIMENTAL APPARATUS

Here we model a dry avalanche flowing down an inclined chute of dimensions 2.5 m long by 250 mm wide, as shown in Figure 1. The side walls are 100 mm high and are made of 10 mm thick transparent glass. At the upper end of the chute is a hopper, and at the lower end is a rigid aluminium wall, 100 mm high, filling the full width of the chute, as shown in Figure 1.

Nine load cells are arranged on three separate aluminium plates, which record the impact force of the granular flow. Each plate is 100 mm high and 83 mm wide. They each consist of a 10 mm thick movable rigid alu-



minium plate, which is connected via three load cells to a fixed 40 mm thick aluminium plate. The bottom left of Figure 1 shows the arrangement of load cells on the three plates.

A high speed camera is also used to record images through the side walls of the avalanche flow. We capture images at 525 Hz and record the evolving flow properties as the avalanche passes. To process these images we use the package OpenPIV [15] to do digital image correlation to find displacements and velocities between camera images.

To model a real dry landslide, we use a Lenzhurd quarry sand sieved into the following size fractions,  $s = 0.5 - 0.6, 1 - 1.18, 2 - 2.26$  and  $4 - 4.75$  mm, with corresponding angles of repose  $\theta_r = 30, 32, 35$  and  $38$  degrees, measured from heap tests.

Sand in the remaining size fraction 1.18–2 mm was glued a single particle deep to the steel base to give roughness. A small amount of scouring of the base was observed during tests, but dislodged base particles were sieved from the other grainsize fractions after each test.

## RESULTS

Experiments were conducted using 20 kg of material for all cases, at a slope inclination of  $\theta = 42^\circ$ , where steady flow is observed down the length of the chute with minimal saltation of particles. This slope angle is  $5-10^\circ$  above the angle of repose for the considered sands. The gate is released rapidly (typically in under 0.1s), whereupon the granular mass begins to flow down the chute. Initially a spray of particles flows down slope, followed by a granular front of much denser sand. This front has a shape and characteristics which vary with the grainsize fraction used, as shown in Figure 2.

At the base of the chute, the avalanche impacts a rigid wall. Load cells measure the normal load on the wall. As

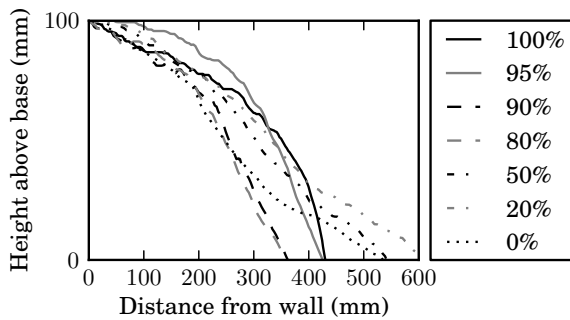


**FIGURE 4.** Residual deposition from bidisperse tests of 20 kg of mixed 1 mm and 4 mm sand at  $\theta = 42^\circ$ . *Top to bottom:* 100%, 95%, 90%, 80%, 50%, 20% and 0% 4 mm particles.

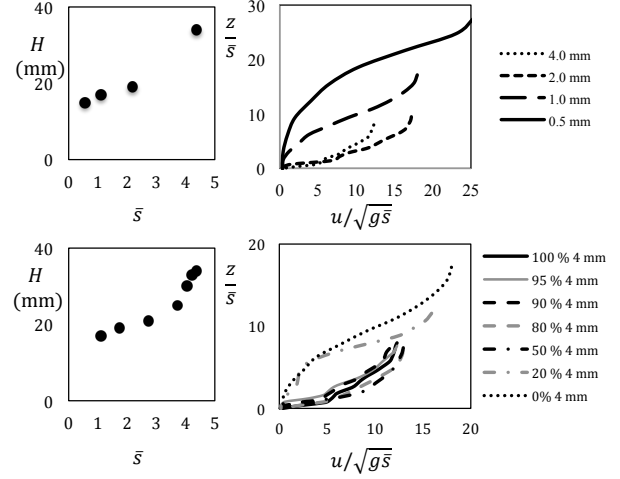


**FIGURE 5.** Kinematics after 1.5 m of flow in the chute. *Left:* Typical depth  $H$  of the avalanche. *Right:* Typical down slope velocity profiles  $u$  over height  $z$ . *Top:* Monodisperse tests for four different grainsizes. *Bottom:* Bidisperse tests with 1 mm and 4 mm particles.

a pile begins to form, a granular jump [16] is observed which reaches the full height of the wall, as on the right hand side of Figure 2. This jump propagates backwards from the wall, leaving a large wedge-shaped deposit once flow has stopped.

The shape of this deposit is convex for large particle sizes and concave for smaller sizes, as shown in Figure 3. We attribute this to the choice of basal roughness, which lies in the size range 1.18–2 mm. Particles larger than this are not trapped significantly in the basal void spaces, and see a smaller base roughness with increasing size. Conversely, sand smaller than the base particles gets trapped in the rough bed, at first depositing a base layer of intruder particles, and then behaving as if flowing over an erodible base. Bidisperse tests (see Figure 4) show a gradual scaling between the depositions formed in the two monodisperse cases.

Typical down slope velocity profiles,  $u(z)$  and flow depths,  $H$ , are shown in Figure 5 for the case of quasi-steady flow far from the wall at the bottom of the chute. The flow depth increases with increasing particle size in millimetres, but decreases in terms of particle diameters. The velocity profiles of the 2 and 4 mm particles fit a Bagnold-like scaling [17], ( $u \propto 1 - (1 - z/H)^{3/2}$ ), which is common for flows over a rough base, whereas the smaller sizes behave as if flowing over an erodible bed [18].

Bidisperse tests show a similar pattern, scaling between the two monodisperse cases. A marked change occurs above 20% 4 mm grains, where the behaviour rapidly changes from Bagnold-like to Takahashi-like flow.

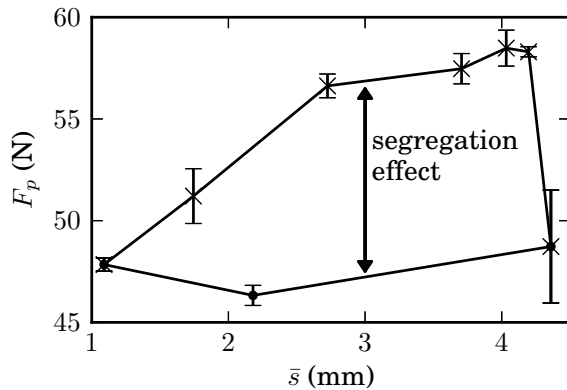


**FIGURE 6.** Peak force on the wall. Filled circles (●) are monodisperse tests, crosses (×) are bidisperse tests. Error bars indicate one standard deviation.

Peak forces from each case are shown in Figure 6, and a clear deviation between monodisperse and bidisperse cases is evident. This can be explained simply as a result of segregation creating a lubrication layer, increasing the destructive force of the avalanche. As shown in [19, 10], the shear strain rate is in fact locally a function of the average grain size. At the base of the flow, where the small particles accumulate via segregation, a region of high shear strain rate is created. This high shear strain rate at the base of the flow accelerates all material above it, resulting in this lubrication effect.

## CONCLUSIONS

We have shown that the peak forces measured on a rigid obstacle depend strongly on the grain size distribution. At approximately 5% fine particles a bidisperse avalanche of this sand reaches the largest peak force, 20% larger than if modelling with a monodisperse sand. To safely design protection structures, this effect must be considered, as monodisperse tests will give non-conservative estimates of the peak force.

How to predict this peak force is still an open question, but should be answered by posing the problem in terms of a spatially variable grain size distribution. As in [10], theory needs to capture the changes in the grain size distribution during flow, and to use constitutive laws that depend on the local grain size distributions. In this way internal rheology, basal roughness effects, and wall interaction can all be expressed in terms of their dependence on the grain size distribution.

Only once we have this level of understanding of the kinematics of flowing granular material will we be able to safely design protection structures to impede the flow of avalanches, debris flows and landslides.

## ACKNOWLEDGMENTS

The authors would like to thank Ernst Bleiker, Rene Rohr, Adrian Zweidler and Heinz Richner.

## REFERENCES

1. D. Petley, *Geology* (2012).
2. S. Moriguchi, R. Borja, A. Yashima, and K. Sawada, *Acta Geotechnica* **4**, 57–71 (2009).
3. F. Moro, T. Faug, H. Bellot, and F. Ousset, *Cold Regions Science and Technology* **62**, 55–66 (2010).
4. J. Bridgwater, and N. D. Ingram, *Chemical Engineering Research and Design* **49a**, 163–169 (1971).
5. S. Savage, and C. Lun, *Journal of Fluid Mechanics* **189**, 311–335 (1988).
6. J. Gray, and A. Thornton, *Proceedings of the Royal Society A: Mathematical, Physical and Engineering Sciences* **461**, 1447–1473 (2005).
7. J. M. N. T. Gray, and V. A. Chugunov, *Journal of Fluid Mechanics* **569**, 365–398 (2006).
8. S. Wiedersheimer, N. Andreini, G. Épely-Chauvin, G. Moser, M. Monnereau, J. Gray, and C. Ancey, *Physics of Fluids* **23**, 013301 (2011).
9. J. M. N. T. Gray, and C. Ancey, *Journal of Fluid Mechanics* **678**, 535–588 (2011).
10. B. Marks, P. Rognon, and I. Einav, *Journal of Fluid Mechanics* **690**, 499–511 (2012).
11. B. Chanut, T. Faug, and M. Naaïm, *Physical Review E* **82**, 041302 (2010).
12. G. MiDi, *The European Physical Journal E: Soft Matter and Biological Physics* **14**, 341–365 (2004).
13. T. Faug, R. Beguin, and B. Chanut, *Physical Review E* **80**, 021305 (2009).
14. A. Van Burkalow, *Geological Society of America Bulletin* **56**, 669–707 (1945).
15. Z. Taylor, R. Gurka, G. Kopp, and A. Liberzon, *Instrumentation and Measurement, IEEE Transactions on* **59**, 3262–3269 (2010).
16. T. Faug, “Jumps and bores in bulky frictional granular flows,” in *Powders and Grains*, edited by S. Nakagawa, Masami; Luding, AIP Conference Proceedings, 2013.
17. L. E. Silbert, D. Ertas, G. S. Grest, T. C. Halsey, D. Levine, and S. J. Plimpton, *Physical Review E* **64** (2001).
18. T. Takahashi, *Debris Flow*, IAHR monograph series, Balkema, 1991.
19. P. Rognon, J. Roux, M. Naaïm, and F. Chevoir, *Phys. Fluids* **19**, 058101 (2007).

## CHAPTER 8

### **Comminution during flow**

---

In nature we observe two limiting cases of particle crushing. The first is confined comminution, where a set of particles is maintained in a particular arrangement, and subsequently crushed. Under these conditions, fractal grainsize distributions are often measured. This is a signature of a system with no typical internal length or time scale. Conversely, when measurements are taken of the grainsize distribution of in-situ material in avalanche runout, we often measure log-normal grainsize distributions. There is a stark difference in this grainsize distribution, which is still spread over many orders of magnitude, but now containing a typical size.

Prior to this work, no theories existed which could explain the evolution and behaviour of these two types of limiting behaviour in a unified manner. What I will show in this Chapter is that the transition to log-normal gradings is due to segregation, and the interaction of segregation with comminution, and to a lesser extent remixing.

These ideas are formulated in terms of another cellular automata, which extends the previous one described in Chapter 3 to polydisperse systems, undergoing not just one process, but simultaneously segregation, mixing and comminution.

#### **8.1 Contribution towards paper**

In the following arXiv manuscript, I was the primary researcher and author, being supervised by Professor Itai Einav.

# The interactions between comminution, segregation and remixing in granular flows

Benjy Marks · Itai Einav

August 28, 2013

**Abstract** Granular segregation is an important mechanism for industrial processes aiming at mixing grains. Additionally, it plays a pivotal role in determining the kinematics of geophysical flows. Because of segregation, the grainsize distribution varies in space and time. Additional complications arise from the presence of comminution, where new particles are created, enhancing segregation. This has a feedback on the comminution process, as particles change their local neighbourhood. Simultaneously, particles are generally undergoing remixing, further complicating the segregation and comminution processes. The interaction between these mechanisms is explored using a cellular automaton with three rules: one for each of segregation, comminution and mixing. The interplay between these rules creates complex patterns, as seen in segregating systems, and depth dependent grading curves, which have been observed in avalanche runout. At every depth, log-normal grading curves are produced at steady state, as measured experimentally in avalanche and debris flow deposits.

**Keywords** Segregation · Comminution · Mixing · Cellular automata

## 1 Introduction

Flowing granular material exhibits complex behaviour, including many phenomena that cannot be described in the context of a conventional fluid. For example size segregation, comminution and agglomeration all have

---

B. Marks  
Particles and Grains Laboratory, The University of Sydney  
E-mail: benjy.marks@sydney.edu.au

I. Einav  
Particles and Grains Laboratory, The University of Sydney

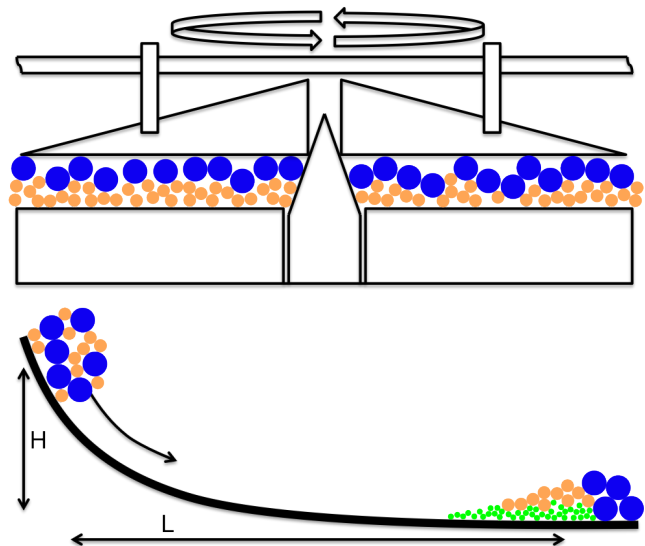


**Fig. 1** *Top:* A mill stone — the grinding of grain using a mill stone is one of the oldest industrial problems in human history, yet still mathematically unsolved. Particles of grain are crushed to a fine powder by very large deformation shearing at high normal stress. The fine powder segregates out of the shear zone into cavities built into the mill stone, and then under the action of centripetal forces migrates out to a collection bin. *Bottom:* A long run-out landslide, where the ratio of  $L/H$  can be up to 10.  $L$  and  $H$  are the change in horizontal position and height respectively of the centre of mass of an avalanche during run-out. Large values of  $L/H$  are possible indicators of lubrication by a layer of very small particles at the base of the flow, which have been created as a result of comminution and percolated downwards through segregation.

no analogue in traditional fluids. To describe these phenomena the grainsize distribution has to be involved as a dynamic property.

The dynamics of granular material are important in many natural processes, such as debris flows, landslides,

rockfalls and shear banding. Industrial processing also requires many granular flows, such as rotating or tumbling mills, chute flows and hopper filling or discharge. In these types of flow processes, breakage of particles can be important. As yet, there are no temporo-spatial continuum models for measuring changes in the grain-size distribution for such open systems where particles can advect in space.

This is especially important in two poorly understood systems, shown in Figure 1. The first is ancient grain milling, where combined normal and shear stresses crush wheat grains, dynamically sieving the resultant mix. The second is long run out avalanches, where it is unclear why these incredibly destructive natural phenomena can travel enormous distances, up to 10 times their vertical fall [1, 2].

With regards to natural flows, it has been understood for some time that there is a need to model spatial and temporal variability in the grainsize distribution of flowing material to be able to implement appropriate rheological models [3].

Here we tackle this problem using a cellular automaton [4] with three distinct rules of operation: segregation, remixing and comminution. As has been shown previously [5] for bidisperse systems, we can describe segregation in terms of the swapping of cells in a cellular automaton. Comminution rules have also been developed [6, 7], but these are limited to closed systems. Here we will present rules which can apply in open systems to arbitrarily polydisperse materials.

As in [8] we denote the grainsize,  $s$ , as an internal coordinate of the system such that every point in space has a grainsize distribution. We then describe this continuous grainsize distribution  $\phi(s)$  of the system in terms of the solid fraction  $\Phi(s)$  of particles between grainsizes  $s_a$  and  $s_b$  as

$$\Phi[s_a < s < s_b] = \int_{s_a}^{s_b} \phi(s') ds'. \quad (1)$$

Conservation of mass at a point in space  $\mathbf{r} = \{x, y, z\}$  can then be expressed as [8–10]

$$\frac{\partial \phi}{\partial t} + \nabla \cdot (\phi \mathbf{u}) = h^+ - h^-, \quad (2)$$

where  $\mathbf{u}(\mathbf{r}, s, t) = \{u, v, w\}$  is the material velocity,  $h^+(\mathbf{r}, s, t)$  is the birth rate, describing the creation of new particles of grainsize  $s$  at time  $t$ , and  $h^-(\mathbf{r}, s, t)$  is the death rate, at which particles of grainsize  $s$  are destroyed.

The second term in Equation 2 describes the advection of mass, such as characterises open systems,

where material can move spatially. The right hand side of the same Equation represents mechanisms traditionally treated as closed systems, such as agglomeration, crushing and abrasion. Each of these systems — open and closed — has been the subject of much study, but the coupling of such processes using a continuum description has yet to be achieved.

## 2 Cellular automata and continua

To model these systems we use a cellular automaton in two spatial dimensions. It is a series of cells on a 2D regular cartesian lattice of size  $N_x$  by  $N_z$ , with directions  $x$  and  $z$ , and cell spacing  $\Delta x$  and  $\Delta z$  in the respective directions. The  $z$  direction is perpendicular to the shear direction, such that for inclined plane flow it points normal to the slope. The  $x$  direction represents a micro scale internal coordinate.

We allow the grainsize distribution to be a function of this internal spatial coordinate such that  $s = s(x)$ . By discretising the grainsize distribution  $\phi(s)$  into  $N_x$  monodisperse components of equal volume, they can be arranged in the  $x$  direction such that summing over this coordinate would recover the full grainsize distribution. We consider the local neighbourhood of a particular particle as those that are adjacent in the  $x$  direction. The  $x$  direction now contains more information than the grainsize distribution alone, as the local orientation of particles is preserved, below the resolution of the analogous continuum scale.

We number the cells from the bottom-left corner of the grid so that position on the grid can be expressed using the pair  $\{i, j\}$ , where  $i$  and  $j$  indicate the number of cells across in the respective  $z$  and  $x$  directions. In all cases the system is considered to be periodic in the  $j$  direction.

Each cell contains a single number,  $s_{i,j}$ , which dictates the grainsize of the particles in the representative volume element defined by the cell  $\{i, j\}$ .

We can define a discretised grainsize distribution  $\phi_i$  at any height  $i$  as a histogram of the number of cells within a discrete grainsize fraction with centre  $s_a$  and width  $\Delta s$  in all  $N_x$  neighbours taken in the  $j$  direction:

$$\phi_i(s_a) = \frac{1}{N_x \Delta s} \sum_{k=1}^{N_x} \begin{cases} 1 & \text{if } s_a - \frac{\Delta s}{2} < s_{i,k} \leq s_a + \frac{\Delta s}{2}, \\ 0 & \text{otherwise.} \end{cases} \quad (3)$$

We also define the local average grainsize over the nearest neighbours in the  $j$ -direction as

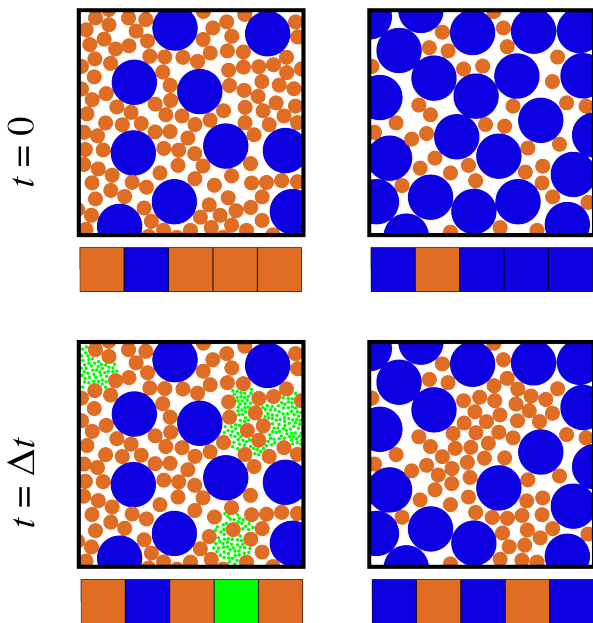


**Fig. 2** The cushioning effect and nearest neighbour rule. *Left:* Large particles are cushioned such that they will not break because of an abundance of small particles. *Right:* Small particles do not carry a significant amount of load as they are free to move in interstitial pore spaces. *Top:* Initial conditions. *Bottom:* Result after one iteration of the cellular automata rule, where on the left the small particles in a cell (orange) become even smaller (green), and on the right the large particles in a cell (blue) become smaller.

$$\bar{s}_{i,j} = (s_{i,j-1} + s_{i,j+1})/2, \quad (4)$$

and similarly for the  $i$ -direction. For the cellular automata rules defined below, we need to define two new operators:  $s_a \Leftrightarrow s_b$  represents the swapping of values  $s_a$  and  $s_b$  between their respective cells, and  $s_a \Rightarrow s_b$  represents a change in grainsize in the cell containing  $s_a$  to the new value of  $s_b$ .

In the limit of infinitesimal cell size, the cellular automaton may be regarded as a first order partial differential solver [11]. In fact, there are many ways to recover continuous results from such a cellular automaton [12].

### 3 Closed systems

We begin by considering closed systems, which are those in which material does not advect in space such that  $\mathbf{u} = \mathbf{0}$ . There are many processes that have previously been represented as closed systems, such as comminution, agglomeration and abrasion. We here look only at comminution, where particles are crushed to form fragments of smaller sizes.

Following the formulation in [10], for the case where particles are created only by the fragmentation of larger particles, we can express the death rate as

$$h^-(s, t) = b(s)\phi(s, t), \quad (5)$$

where  $b(s)$  is some specific breakage rate which governs the frequency at which particles of grainsize  $s$  break into smaller fragments. The birth rate is then the sum of breakages into size  $s$  over all particles larger than  $s$ , which can be expressed as

$$h^+(s, t) = \int_s^\infty b(s')P(s|s')\phi(s', t) ds', \quad (6)$$

where  $P(s|s')$  is a probability density function which dictates the probability of creating grainsize  $s$  from crushing a particle of grainsize  $s'$ . We can then express conservation of mass as

$$\frac{\partial\phi(s, t)}{\partial t} = \int_s^\infty b(s')P(s|s')\phi(s', t) ds' - b(s)\phi(s, t). \quad (7)$$

In a discrete sense, such as that defined in the cellular automaton, we can rewrite this equation as the conservation of a grainsize fraction with centre  $s_a$  and width  $\Delta s$ , over a time step  $\Delta t$  as

$$\frac{\Delta\phi_i(s_a)}{\Delta t} = \sum_{k=a+\Delta s}^{N_s} \left( b_i(s_k)P(s_a|s_k)\phi_i(s_k)\Delta s \right) - b_i(s_a)\phi_i(s_a), \quad (8)$$

where  $N_s$  is the total number of evenly spaced bins of size  $\Delta s$ . These equations have been considered many times before [13–16], and solutions have been proposed for many mechanisms of comminution, such as grinding, cleavage and abrasion. However, breakage mechanisms are normally assumed with a priori knowledge of power law distributions [9, 13]. In fact, in most models, either the breakage rate  $b$ , the fragment probability distribution  $P$ , or both, are generally assumed to be power law in nature from the outset [13].

Another method to model the problem has been proposed in various forms, and uses simple geometric analogies in a cellular automaton [6, 7] where power law patterns are found, not imposed, by assuming that particles with neighbours of the same size are likely candidates to crush.

We can unify these two approaches, of macroscopic grainsize distribution changes, and microscopic nearest neighbourhood behaviour, by including the grainsize distribution in a cellular automaton.

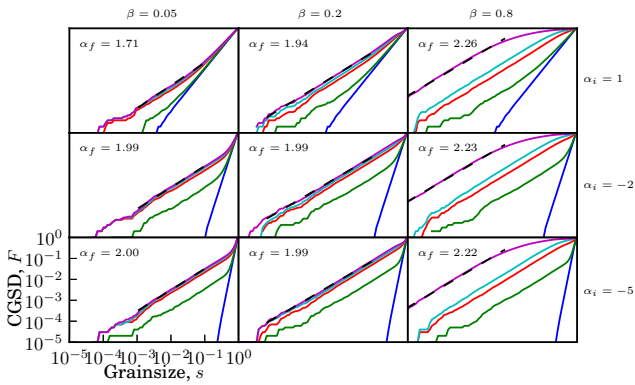


**Fig. 3** Evolving cumulative grain size distributions due to comminution. All simulations have  $N_z = 1$ ,  $N_x = 10^6$  and  $k_b = 1$ . Three initial conditions are considered, with  $\alpha_i = -5$ ,  $-2$  and  $1$ . Each initial condition is crushed at three values of  $\beta = 0.05, 0.2$  and  $0.8$ . Within each sub-plot, each line represents a different time  $t = 0, 0.05, 1, 2$  and  $10$ , from bottom right to top left.

### 3.1 The crushing mechanism

When a large particle is surrounded by small particles, it is cushioned from fracture by having many points of contact with neighbours, leading to a fairly isotropic loading state, as shown on the left of Figure 2. Also, when a small particle is surrounded by large particles, it does not carry significant load, as it is either able to fit in the pore spaces if sufficiently small, or is highly mobile, as on the right of Figure 2. Because of this, we consider fracture of particles only when they are surrounded by particles of a similar size. We then have a condition for fracture such that for a particle of size  $s_{i,j}$  and a local neighbourhood of particles of average grain size  $\bar{s}_{i,j}$ ,

$$s_{i,j} \Rightarrow (0, 1) \times s_{i,j}, \quad \text{if } |s_{i,j} - \bar{s}_{i,j}| \leq \beta s_{i,j}. \quad (9)$$

This rule states that all particles in the representative volume defined at  $s_{i,j}$  reduce in size by a randomly chosen factor between 0 and 1 if it is within  $\beta s_{i,j}$  of the local mean grain size. The non-dimensional factor  $\beta$  determines how similar particles must be to their neighbours before crushing can occur. We have also included a factor of  $s_j$  on the right hand side of the inequality to make small particles harder to crush, recognising that smaller particles have a higher crushing stress than larger ones [17]. This crushing event has some frequency which is proportional to the shear strain rate, allowing us to define the breakage rate as

$$b_{i,j} = k_b |\dot{\gamma}_i| \mathcal{H}(\beta s_{i,j} - |s_{i,j} - \bar{s}_{i,j}|), \quad (10)$$

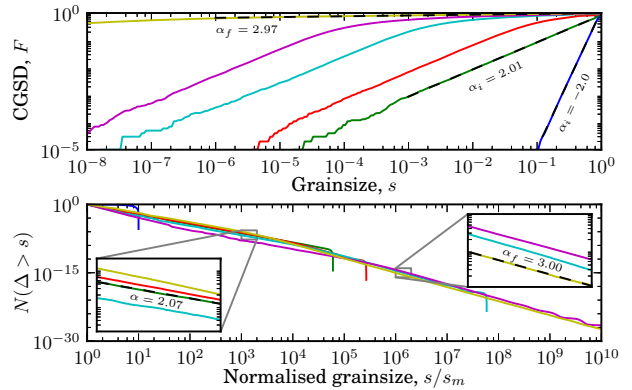


**Fig. 4** Cycles of breakage towards an attractor. *Top*: Cumulative grain size distributions at different numbers of cycles of loading. Each line represents the grading after a certain number of crushing-remixing cycles. From bottom right to top left, they are 0, 1, 10, 50, 100 and 500 cycles. The system approaches  $\alpha = 3$ , or a horizontal line in this plot. *Bottom*: The same data as in the top plot, now shown as number of particles  $\Delta$  greater than a certain size  $s$ . Insets show zoomed areas of original plot.

where  $k_b$  is a non-dimensional fitting parameter and  $\mathcal{H}$  is the Heaviside function. In (9) we have also defined the fragment size distribution as

$$P(s_a | s_{i,j}) = \Delta s / s_{i,j}, \quad (11)$$

where  $\Delta s$  is the size of the grain size bin in the  $s$  direction containing fragment size  $s_a$ . The simulation occurs over  $N_x$  cells, spaced  $\Delta x$  apart. Initial conditions are generated by sampling  $N_x$  times from  $F = \Delta x$  to  $F = 1$  linearly along the inverse power law distributions defined by

$$s = F^{1/(3-\alpha_i)}. \quad (12)$$

where  $F(s) = \int_{s_m}^s \phi(s') ds'$  is the cumulative grain size distribution function and  $3 - \alpha_i$  is the power law gradient. By time marching with a sufficiently small time step, such that  $b_i \Delta t \leq 1$ , we implement the frequency of breakage in a probabilistic manner.

Figure 3 shows three different initial conditions, and their progression to a steady state grain size distribution. Each initial condition is considered for three values of  $\beta$ . For each case, a new distribution is reached after a single timestep of  $\Delta t = 0.05$ . As time progresses,  $\beta$  controls most of the behaviour of the process. For small values of  $\beta$ , a steady state is reached where the grain size distribution does not change appreciably after time  $t = 5$ , resulting in a power law dimension of  $\alpha = 1.99 \pm 0.01$ . For large  $\beta$ , all of the largest particles are continually crushed, eventually resulting in a system where  $\alpha$  approaches 3.

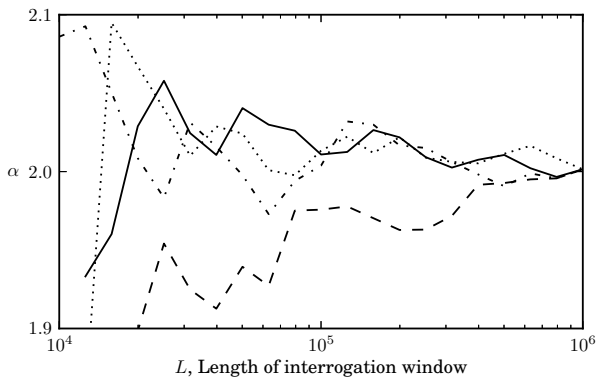


**Fig. 5** Fractal dimension  $\alpha$  against interrogation window length  $L$ .  $\alpha$  value is measured as a best fit of the cumulative grainsize distribution from  $s = 10^{-4}$  to  $10^{-1}$ , restricted to the cells between  $j = a \pm L/2$ . Each line represents a different value of  $a = 0, N_x/4, N_x/2$  and  $3N_x/4$ . For this simulation  $N_x = 10^6$ ,  $\beta = 0.2$ ,  $k_b = 1$  and  $\alpha_i = -2$ .

The cellular automata predicts the same final grain-size distribution largely independent of the initial grading, with some minor effects due to the initial concentration of very large particles. Such a power law grading of the grainsize distribution has been measured in other cellular automata [6,7], discrete element simulations [18] and experiment [2].

Generally fractal dimensions are measured in fault gauges, confined comminution tests and rock avalanches in the range of  $\alpha = 2 - 3$  [19–21]. The limiting value of  $\alpha = 2$  for most cases of our model can be explained using the cellular automaton developed in [20], where every particle in the systems has the same probability of crushing, given some additional geometric constraints. If this probability is exactly 0.5, the system develops a fractal dimension of  $\alpha = 2$ . If the probability is 1, the system reaches  $\alpha = 3$ , which represents a system with large strain, where nearest neighbours change over the crushing period [22]. This distribution in fact corresponds to a random appollonian packing, as in [23].

In Figure 5  $\alpha$  is measured many times in a single simulation. A number of cells,  $L$ , centred at  $a$ , are chosen, and a best fit of  $\alpha$  is measured for the cumulative grainsize distribution. With increasing zoom into the system, the measured power law does not change slope significantly. This is an indication of a fractal distribution [6].

The idea of such final power law grainsize distributions has been applied in [24] to develop a thermodynamically consistent theory for comminution processes in granular materials in closed systems. Extension of this or other theories to open systems where particles can advect has not yet been achieved.

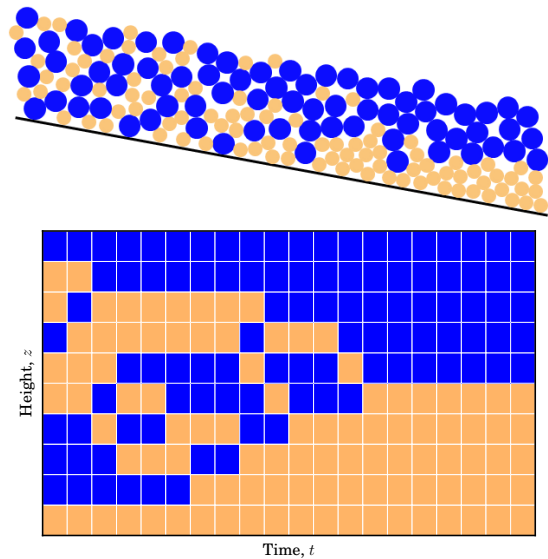


**Fig. 6** Bidisperse cellular automaton. *Top*: Schematic representing bidisperse segregation in 2D flow down an inclined plane. *Bottom*: The complimentary 1D cellular automaton, where large particles and small particles swap over time.

### 3.2 Comparison with continua

To compare the cellular automata rules with a continuum, we consider the evolution of a large number of cells simultaneously, and find averaged properties that represent the continuum scale. We express the breakage rate,  $b_i$ , of a single grainsize fraction  $s_a$  covering sizes over a range of  $\Delta s$  as

$$b_i = \frac{k_b |\dot{\gamma}_i|}{N_x} \sum_{j=1}^{N_x} \mathcal{H}(\beta s_{i,j} - |s_{i,j} - \bar{s}_{i,j}|). \quad (13)$$

To solve this system globally, we need to sum over  $j$ , which represents local information about the nearest neighbours. If we were to represent this in a continuum sense, this local information is smaller than the continuum scale, and so a new length scale,  $\zeta$ , must be introduced. In the cellular automaton, the length scale which controls this behaviour is that of the nearest neighbour zone (here set arbitrarily to  $\Delta x$ ). By increasing the size of the neighbourhood over which we find the local average grainsize, the system would converge towards a different state, where physical proximity of neighbours is not considered.

How to introduce such a length scale in a continuum theory is an open question. In the cellular automaton, we can consider changing this length scale by doing cycles of crushing, as will be shown below.



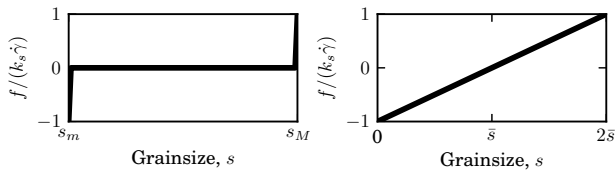


**Fig. 7** The segregation mechanism as a function of grainsize  $s$ . *Left*: Bidisperse rule used previously in [5] *Right*: Polydisperse rule used here, where segregation frequency is a function of distance to the local mean size.

### 3.3 Cycles of crushing: Towards open systems

We can extend this simulation to a quasi-open system by considering a rearrangement of particles within the cellular automaton, but without true advection.

After the system has reached steady state, and no further significant crushing will occur, we shuffle the system, relocating all of the nearest neighbours, and resume crushing until a new steady state is reached. We can continue this cycle until an *ultimate* steady state is reached.

We begin with the simulation shown in the centre of Figure 3, which has an initial grading defined by  $\alpha_i = -2$ , and after one full crushing iteration process has reached  $\alpha = 2$ . As progressively more iterations occur, a region of higher slope develops at larger grainsizes, and this propagates to lower grainsizes with increasing iterations, as shown at the top of Figure 4. This trend is towards  $\alpha = 3$ , however this coincides with a horizontal line in this plot, and cannot be seen clearly. To visualise this more clearly, the bottom plot in Figure 4 shows the same data, but plotted as the number of particles  $\Delta$  greater than a certain size  $s$ , such that the slope of the graph is  $\alpha$ . We define the number of particles per cell as being inversely proportional to the size cubed. The final state has been shuffled and crushed 500 times, tending towards an ultimate grading with this new power law gradient of  $\alpha_f = 3$ .

This effect of cycles of crushing towards  $\alpha_f = 3$  has been observed experimentally [25], numerically with a crushable discrete element method [26] and predicted analytically as the maximum entropy path towards the least efficient packing of the system [23]. It is remarkable that such a simple, one dimensional system as this can replicate the packing involved in such a complex system.

## 4 Open systems

In order to model open systems, where particles can advect between points in space, we need rules for ad-

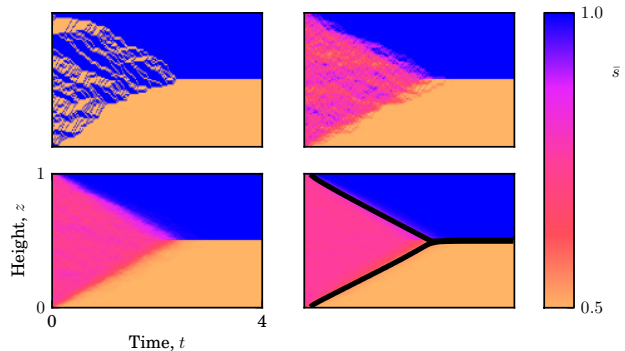


**Fig. 8** The time evolution the average grainsize  $\bar{s}$  of a bidisperse simulation with varying  $N_x$  subject to segregation only. All cases have  $k_s = 1$  and  $N_z = 100$ . *Clockwise from Top Left*:  $N_x = 1, 10, 100$  and  $1000$ . For the case of  $N_x = 1$  we find the local average grainsize in the  $z$  direction. *Bottom right*: Black lines indicate positions of concentration shocks from solution of analogous continuum equation.

vection. To be a truly physical model, we need to satisfy the conservation equation for grainsize  $\phi$  such that

$$\frac{\partial \phi}{\partial t} + \nabla \cdot (\phi \mathbf{u}) = 0. \quad (14)$$

We set up our rules for the cellular automaton such that this conservation law is held for some velocity  $\mathbf{u}$ . The first mechanism we consider is due to segregation. Towards this end, we begin with the simplest case of segregation and describe bimixtures, where we present a model similar to that proposed in [5].

### 4.1 The segregation mechanism

As particles flow they collide, creating new void spaces which are preferentially filled by smaller particles moving, as in Figure 6. The rate of creation of void spaces is governed by the shear strain rate,  $\dot{\gamma}$ .

The simplest description of this system in terms of grainsize is shown on the left of Figure 7 for a bimixture of sizes  $s_m$  and  $s_M$ , where the swapping frequency  $f$  is defined such that small particles always move down, and large particles move up.

We can extend this model to describe polydisperse materials by using the formulation developed in [8], where it was shown through energy considerations that if a particle is larger than the local average, it has some probability of moving up, and conversely if it is smaller than the average it will move down. Increasing distance in the  $s$  direction from the average will increase the likelihood of swapping linearly. This is shown on the right of Figure 7.

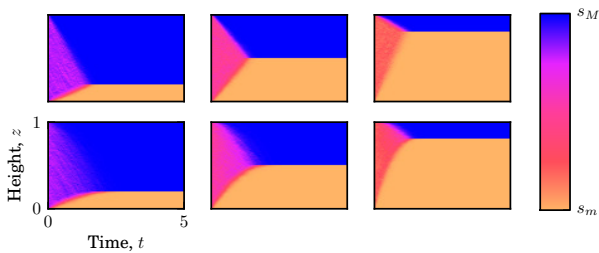


**Fig. 9** Time evolution for bidisperse shear flows subject to segregation. For all cases  $k_s = 1$ . *Left to right*: The system is initially filled with 20%, 50% and 80% small particles respectively. *Top row*: Simple shear, where  $\dot{\gamma} = 1$ . *Bottom row*: Inclined plane flow shear condition, where  $\dot{\gamma} = \sqrt{1-z}$ .

We facilitate this movement by swapping this grain-size with that either above,  $s_{i+1,j}$  or below,  $s_{i-1,j}$  depending on whether it is smaller or larger than the average size  $\bar{s}_{i,j}$ . We define the rate of swapping as  $f = k_s |\dot{\gamma}_i| (s_{i,j}/\bar{s}_{i,j} - 1)$ , with the sign determining the direction:

$$\text{if } \begin{cases} f > 0, & s_{i,j} \leftrightarrow s_{i+1,j} \\ f < 0, & s_{i,j} \leftrightarrow s_{i-1,j}. \end{cases}$$

where  $k_s$  is a non-dimensional parameter controlling the rate of segregation. We iterate in two half time steps, alternately applying this rule firstly to all odd rows, and then all even rows, so that particles are inhibited from moving very large distances in a single time step. Additionally, we only allow swapping upwards if the particle is larger than the one above it, or smaller than the one below it if moving downwards.

#### 4.2 Bidisperse segregation

To model a simple bidisperse material, we take a single column of a bimixture ( $N_x = 1$ ), of equal proportions of sizes  $s_m$  and  $s_M$ , randomly allocated to cells, and allow it to segregate under simple shear with  $\dot{\gamma}(z) = 1$  and  $k_s = 1$ . The result is shown in the top left of Figure 8. We can then run the simulation with  $N_x = 5$  and average over the  $x$ -direction. The result of this is shown in the top right of Figure 8. We can do this repeatedly, to get an increasingly resolved image of the process, as shown in the bottom row of Figure 8 for  $N_x = 50$  and 1000. With increasing resolution, this converges on the analytic solution presented in [8] and [27].

Figure 9 shows the average grainsize at each height over time for two different shear regimes, each for 3 different initial concentrations of small particles,  $s_m$ . The top row depicts simple shear, as in Figure 8, while the bottom row uses a simplified version of the shear strain

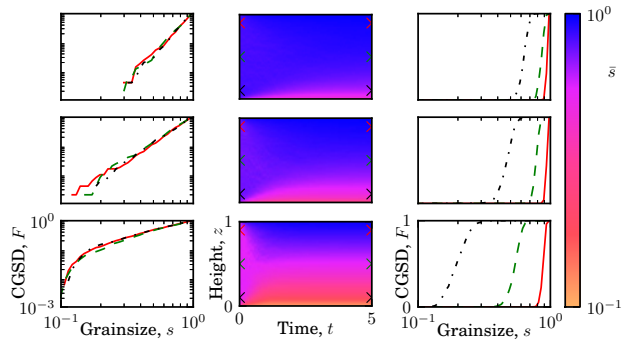


**Fig. 10** Polydisperse segregation under simple shear. For all cases  $k_s = 1$  and  $\dot{\gamma} = 1$ . *Top to Bottom*: Each row represents a single simulation with initial condition defined by  $\alpha_i = -2, 0$  and 2 respectively. *Left*: Initial cumulative grainsize distribution at three different heights. The solid red, dashed green and dash-dotted black lines represents  $z = 0.9, 0.5$  and 0.1 respectively. *Middle*: Plot of the average grainsize  $\bar{s}$  over height and time. *Right*: Final cumulative grainsize distributions, plotted in the same manner as the initial grainsize distributions.

rate profile predicted in [8] for the case of inclined plane flow:  $\dot{\gamma} = \sqrt{(1-z)}/\bar{s}$ . In each case, complete segregation is observed, where every large particle lies above every small particle. The non-uniform shear strain rate in the bottom case causes non-uniform transient behaviour towards a steady grading that is the same as the top case. According to the formulation presented here, the final grading is independent of the loading condition.

As shown in [5], this model represents a very simple analogy of the analytic works done by [28,27] to model bidisperse segregation, with a very simple extension to polydisperse systems, as shown below.

#### 4.3 Polydisperse segregation

We can create a polydisperse sample by generating initial conditions in the same way as previously described for the breakage cellular automaton, using Equation 12. The segregation patterns produced for a range of initial conditions at constant segregation rate  $k_s = 1$  and with  $\dot{\gamma} = 1$  are shown in Figure 10. Since this is now a polydisperse sample, we can calculate the grainsize distribution  $\phi(s)$ . On the left hand side of Figure 10 are the initial cumulative grainsize distributions, which are homogeneous. During the simulation, segregation occurs, creating a non-homogeneous steady state condition after some time. These grainsize distributions, which now vary with height, are shown on the right hand side of the same Figure.

Averaging over all cells at a given height  $i$ , we can express the mean segregative velocity  $u_i$  of a single

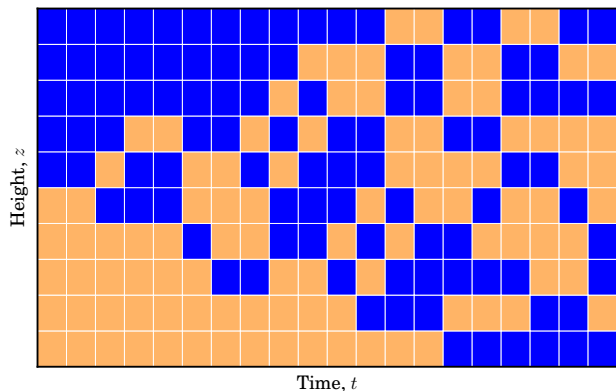


**Fig. 11** The mixing mechanism. Ten cells, initially segregated with all large particles (blue) above small particles (yellow), subjected to the mixing mechanism only. Over time, the system reaches a disordered state.

grainsize fraction centred at  $s_a$  from all cells at height  $i$  in a time  $\Delta t$  as

$$u_i(s_a) = \frac{1}{N_x} \sum_{j=1}^{N_x} f_{i,j}(s_a) = \frac{k_s |\dot{\gamma}_i|}{N_x} \sum_{j=1}^{N_x} \left( \frac{s_a}{\bar{s}_{i,j}} - 1 \right). \quad (15)$$

We have included the local average grainsize  $\bar{s}_{i,j}$  in the formulation so that we know which particles are locally small or large. As particles are being swapped between heights — between representative volume elements at the continuum scale — we only require a single average grainsize per height, and can in this case freely extend the neighbourhood domain over which we find the average grainsize  $\bar{s}$  to include every cell at height  $j$ , labelling it now  $\bar{s}_i = 1/N_x \sum_j s_{i,j}$ . In this case, the mean velocity can be expressed as

$$u_i(s_a) = k_s |\dot{\gamma}_i| \left( \frac{s_a}{\bar{s}_i} - 1 \right). \quad (16)$$

Compare this with the analytic description of the segregation velocity with no diffusion as predicted by [8] for a continuum with internal grainsize coordinate  $s$ ,

$$u(s) = |\dot{\gamma}| \frac{g \cos \theta}{c} \left( \frac{s}{\bar{s}} - 1 \right), \quad (17)$$

where  $c$  is a fitting parameter,  $g$  is the acceleration due to gravity, and  $\theta$  is the angle of the plane down which flow is occurring. As shown in [29], cellular automata can successfully be used as a coarse finite differencing method to model systems such as these without resorting to complicated flux limited finite difference schemes, as would otherwise be necessary.

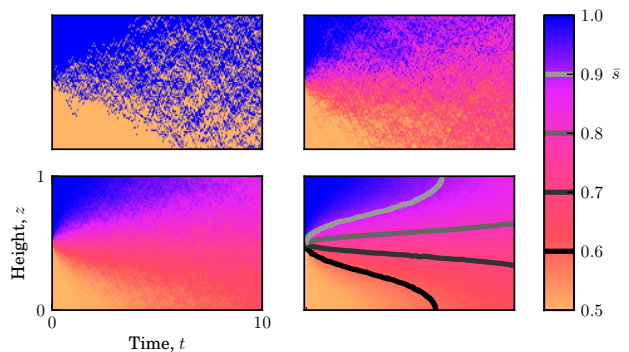


**Fig. 12** The time evolution the average grainsize  $\bar{s}$  of a bidisperse simulation with varying  $N_x$  subject to mixing only. All cases have  $D = 0.01$  and  $N_z = 100$ . *Clockwise from Top Left:*  $N_x = 1, 5, 50$  and  $1000$ . *Bottom right:* Solid lines indicate contours from solution of analogous continuum equation.

This model, together with the rule for remixing, which will be shown next, represents the simplest description of the analytic description presented in [8].

#### 4.4 Remixing

In nature we rarely see such perfect segregation as that pictured above. This is due to the random fluctuation of particles as the flow propagates down slope. As has been done before analytically [30], we can capture this effect by introducing remixing into the flow. For the simplest case, we allow particles to swap randomly either up or down with some frequency, given by a constant  $D/\Delta z^2$ . At this stage we let this probability be independent of the shear strain rate  $\dot{\gamma}$ , although a strong dependency has been observed [31] in experiments. With frequency of swapping controlled by the diffusivity,  $D$ ,

Flip a coin, if heads:  $s_i \leftrightarrow s_{i-1}$   
if tails:  $s_i \leftrightarrow s_{i+1}$

An example of the mixing rule acting on a single column of cells over time is shown in Figure 11. Initially, the system is perfectly segregated, but over time the system becomes randomised due to the presence of remixing. The characteristic time for mixing to occur is the inverse of the diffusivity  $D/H^2$ .

We are describing a system of cells undergoing Brownian motion, whereby particles move by the application of random forces over time scales that are short relative to the motion of the particle. When considered over long time scales and large numbers of particles, this is analogous to Fickian diffusion [31]. Many other cellular automata exist to model pure diffusion [32].

As in the case of segregation, this process can be averaged over the  $x$  direction to describe the evolution

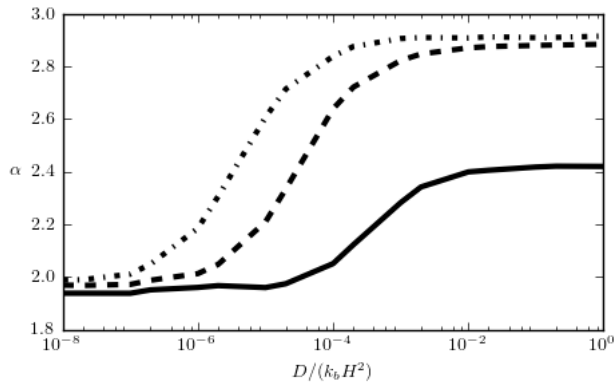


**Fig. 13** Coupled comminution and mixing. Varying values of  $D/(k_b H^2)$ . For all cases,  $N_z = 21$ ,  $N_x = 1000$ . Plot shows final value of best fit to power law part of cumulative grainsize distribution at  $t = 5$ , 50 and 500, corresponding to the solid, dashed and dash-dotted lines respectively.

of the average grainsize at any height over time. By increasing the number of cells in the  $x$  direction, we can increase the smoothness of our solution. Figure 12 shows the same system as Figure 11, initially segregated, that mixes over time to create a homogeneous system, but now for increasing numbers of cells in the  $x$  direction.

This diffusive behaviour can be described at the continuous limit using Fick's first law of diffusion,

$$\frac{\partial \phi}{\partial t} = D \frac{\partial^2 \phi}{\partial t^2}. \quad (18)$$

## 5 Coupled problems

We now have three distinct processes which can be described simultaneously in a single simulation. These have all been shown above with their analogous continuum description, yet not in all cases could a direct link be shown. For the case of comminution, an internal length scale governing the spatial distribution of grain-size over a sub-continuum length scale was required.

As all of the mechanisms previously described have been created in the same framework, we can simply run a cellular automaton which includes multiple phenomena at the same time. As will be shown in this Section, we can investigate the interactions between the mechanisms by varying the parameters which control their effects.

### 5.1 Comminution and mixing

We begin with a cellular automata that includes both comminution and mixing. This system represents an ex-

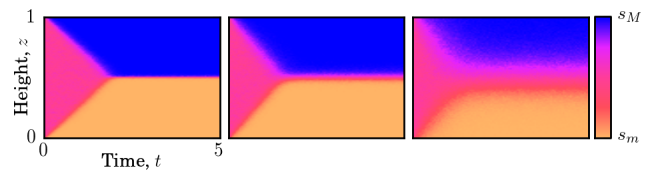


**Fig. 14** Bidisperse segregation under simple shear with diffusion. *Left to Right*: Increasing diffusivity  $D = 0.002$ , 0.01 and 0.05 with constant segregation coefficient  $k_s = 1$ . Increasing the mixing coefficient smooths out concentration shocks in the spatial direction, giving more physically representative solutions.

tension of the cycles of crushing pictured in Figure 4, but now with true advection. In this case, as in Figure 4, we expect that after a short time relative to the diffusive time, the system will reach  $\alpha_f = 2$ , as significant mixing has not yet occurred. At longer times, the system will approach  $\alpha_f = 3$ , and its final grading. This effect is captured in Figure 13, where the diffusive time is controlled by the ratio  $D/(k_b H^2)$ , and the system is constrained at  $\alpha_f = 2.91$ .

For vanishingly small diffusivities, the system will still approach  $\alpha_f = 3$ , but only after very long periods of comminution. Conversely, at very large diffusivities, the system passes  $\alpha_f = 2$  very rapidly, and approaches  $\alpha_f = 3$  in a relatively short time.

### 5.2 Segregation and mixing

In flows of polydisperse granular materials where comminution does not occur, we can model the evolution of the grainsize distribution as being comprised of segregative and diffusive remixing components. This occurs in many industrial mixing processes, and may be sufficient to model levee formation and runout characteristics in landslides. At higher speeds remixing increases, suppressing segregation, while at low speeds segregation can play a dominant role in the flow behaviour.

The effect of coupling mixing and segregation in a bimixture can be seen in Figure 14, where increasing diffusivity  $D$  smooths out the concentration shock between the two phases of large and small particles. This can be treated in an identical manner for polydisperse mixtures.

This has been shown analytically for bidisperse systems in [30] and validated experimentally in [33].

Generally, suppressing spurious numerical diffusion is a non-trivial task, requiring sophisticated finite differencing schemes [34] to maintain hyperbolicity. This type of stability, which generally controls the accuracy of the numerical results, is not an issue for solutions obtained using cellular automata [5].



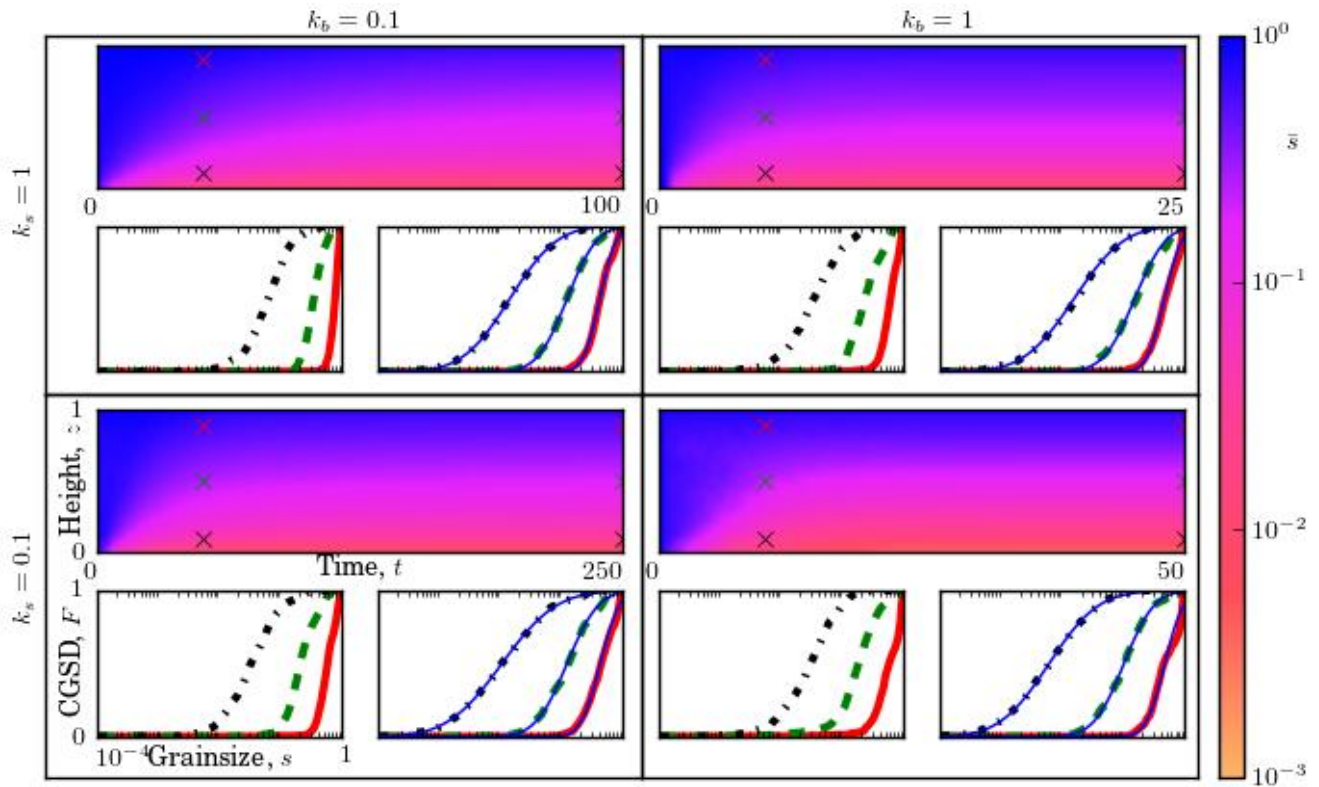


**Fig. 15** A crushable flow with two mechanisms: segregation and comminution. Initially, the system is homogeneous, being a polydisperse sample with initial grainsize distribution defined by  $\alpha_i = -2$ . Four cases are considered with varying  $k_b$  and  $k_s$ . For each case, three plots are shown. *Top*: Evolution of the average grainsize at every height over time. *Bottom left*: Cumulative grainsize distribution at three points in the flow, corresponding to the crosses in the above plot. Top is red solid line, middle is green dashed line and bottom is black dash-dotted line. *Bottom right*: Cumulative grainsize distributions at steady state at same heights as previously. Solid blue lines represent best fit cumulative log-normal distributions.

### 5.3 Segregation and comminution

In many situations, segregation and comminution occur simultaneously in a flow situation, such as in the grain milling depicted in Figure 1. In other cases, it is not even clear if segregation has occurred, yet particles are advecting in space and strong comminution is observed, such as in earthquake faulting and snow avalanches. In many of these cases, we observe log-normal grainsize distributions, rather than power law distributions, which exist at all depths of flow. The existence of these curves represents the competition between the two mechanisms, where the comminution attempts to form a power law distribution, and the segregation attempts to create a locally monodisperse distribution. A log-normal distribution is one that obeys the following scaling for the cumulative grainsize distribution  $F_{LN}$ ,

$$F_{LN} = \frac{1}{2} \operatorname{erfc} \left( -\frac{\ln s - \mu}{\sigma \sqrt{2}} \right), \quad (19)$$

where  $\mu$  and  $\sigma$  are the location and scale parameters, and  $\operatorname{erfc}$  is the complimentary error function.

In Figure 15, simulations are shown in which both segregation and comminution are present. For all cases, log-normal cumulative grainsize distributions are observed over all depths, with p-values in the bottom half generally less than 0.001.

As expected, increasing  $k_s$  or  $k_b$  decreases the time to reach a steady state in terms of the average grainsize  $\bar{s}$ . It is evident that significant changes in the grainsize distribution will not occur indefinitely, even though segregation brings together particles of similar size, and comminution is accelerated by the segregation.

### 5.4 Segregation, mixing and crushing

We can now couple all three mechanisms and observe the evolution of the grainsize distribution as all of the constituent mechanisms interact. Each time step, we first check each cell and if the breakage rule is met, we change the cell's grainsize. Secondly, we iterate over

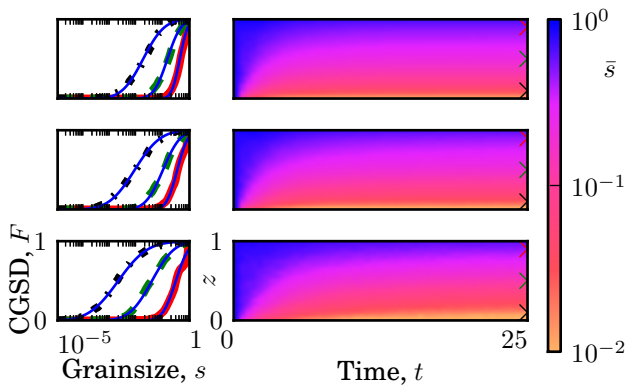


**Fig. 16** A crushable flow with all three mechanisms. For all cases  $k_s = k_b = 1$  and  $H = 1$  is the height of the system. Initially, the system is homogeneous, being a polydisperse sample with initial grainsize distribution defined by  $\alpha_i = -2$ . Each row represents the same initial condition but with varying amounts of mixing. From top to bottom,  $D = 0, 0.005$  and  $0.05$  respectively. *Left*: Cumulative grainsize distribution averaged at three heights  $z = 0.1, 0.5$  and  $0.9$  at steady state (black, green and red respectively). *Right*: The average grain-size at every height evolving over time.

all of the cells and swap them with a neighbour if the segregation rule is met. Finally, we again iterate over all cells and if the diffusion rule is met, we swap randomly with a neighbour.

We now have a system that models avalanche and landslide flow, where particles at the base are sheared and crush, creating a lubrication layer, such as in Figure 15. The inclusion of mixing in the system, as shown in Figure 16, enhances the spread of sizes produced by comminution, and reduces the size of particles in the bottom-most layer of flow, enhancing the lubrication effect. Again, log-normal cumulative grainsize distributions are measured, which represent those found in many geophysical processes, such as in snow avalanches [35].

### 5.5 An equivalent continuum model

Considering conservation of mass alone, we can express all three mechanisms in a continuum form as

$$\frac{\partial \phi}{\partial t} + k_s \frac{\partial}{\partial z} \left( \phi |\dot{\gamma}| \left( \frac{s}{\bar{s}} - 1 \right) \right) = D \frac{\partial^2 \phi}{\partial t^2} + b\phi - \int_s^{s_M} P(s|s') b(s') \phi(s') ds'. \quad (20)$$

This model differs from the cellular automata in the sense that the internal coordinate  $s$  does not retain information about local neighbours. Because of this, cycles of crushing cannot be produced. This omission gives an important insight into the use of continuum

theories to represent internally (i.e. within the representative volume element) spatially correlated material.

For the mechanisms of segregation and mixing, the length scale representing the local neighbourhood is not an important consideration. However for comminution, it must be included as part of the model to enable us to predict the correct final distribution.

## 6 Conclusions

We have shown that cellular automata can successfully capture the most important physical foundations behind evolving phenomena in crushable granular flows. To do this, we have used three distinct cellular automata to explain the dominant mechanisms during such flows: comminution, segregation and mixing.

By assembling all three cellular automata together we were able to explore the interactions between these phenomena. One surprising outcome is that in closed systems, crushable granular material are limited by power laws, however during flow the interaction with segregation and remixing the system is limited by log-normal distributions.

This paper highlights the power of the cellular automata as a means to inspire continuum models. We have demonstrated that it is often possible to recover an analogous continuum description from the limit of the cellular automata rules. An interesting result of this tactic is the result that comminution does not follow this rule. For comminution, the ability to model cycles of crushing using a conventional continuum model with a grainsize coordinate is currently impossible, as some local rules are inherent to the system that must be included to describe the local configuration of grains.

The success of this cellular automata is that it enables us to study the evolution and limits of the grain-size distribution in different scenarios. Current continuum models require a priori knowledge the grainsize distribution, and cannot educate us on the physical mechanisms involved in reaching this final state.

IE acknowledges grant DP0986876 from the ARC.

## References

1. F. Legros, *Engineering Geology* **63**, 301 (2002)
2. B. Imre, J. Laue, S. Springman, *Granular Matter* **12**(3), 267 (2010)
3. R. Iverson, in *Debris flow Mechanics and Mitigation Conference, Mills Press, Davos* (2003), pp. 303–314
4. S. Wolfram, *Advanced Series on Complex Systems*, Singapore: World Scientific Publication (1986)
5. B. Marks, I. Einav, *Granular Matter* **13**, 211 (2011)
6. S. Steacy, C. Sammis, *Nature* **353**(6341), 250 (1991)

7. G. McDowell, M. Bolton, D. Robertson, *Journal of the Mechanics and Physics of Solids* **44**(12), 2079 (1996)
8. B. Marks, P. Rognon, I. Einav, *Journal of Fluid Mechanics* **690**, 499 (2012)
9. S. Redner, *Statistical models for the fracture of disordered media*, New York: North-Holland **321**, 348 (1990)
10. D. Ramkrishna, *Population balances: Theory and applications to particulate systems in engineering* (Academic Press San Diego, 2000)
11. T. Toffoli, *Physica D: Nonlinear Phenomena* **10**(1-2), 117 (1984)
12. S. Raffler, ArXiv e-prints (2011)
13. A. Randolph, R. Ranjan, *International Journal of Mineral Processing* **4**(2), 99 (1977)
14. T. Peterson, M. Scotto, A. Sarofim, *Powder technology* **45**(1), 87 (1985)
15. E.D. McGrady, R.M. Ziff, *Phys. Rev. Lett.* **58**, 892 (1987)
16. M. Williams, *Aerosol Science and Technology* **12**(3), 538 (1990)
17. W. Weibull, et al., *Journal of applied mechanics* **18**(3), 293 (1951)
18. O. Ben-Nun, I. Einav, A. Tordesillas, *Phys. Rev. Lett.* **104**(10), 108001 (2010). DOI 10.1103/PhysRevLett.104.108001
19. Y. Ben-Zion, C.G. Sammis, *Pure and Applied Geophysics* **160**, 677 (2003)
20. D. Turcotte, *Journal of Geophysical Research* **91**(B2), 1921 (1986)
21. G.B. Crosta, P. Frattini, N. Fusi, *Journal of Geophysical Research: Earth Surface* **112**(F1) (2007)
22. C. Sammis, G. King, *Geophysical Research Letters* **34**(4), L04312 (2007)
23. G. Delaney, S. Hutzler, T. Aste, *Physical review letters* **101**(12), 120602 (2008)
24. I. Einav, *Journal of the Mechanics and Physics of Solids* **55**(6), 1274 (2007)
25. J. Lőrincz, E. Imre, M. Gálos, Q. Trang, K. Rajkai, S. Fityus, G. Telekes, *International Journal of Geomechanics* **5**(4), 311 (2005)
26. B. Oded, *Confined comminution of granular materials: Self-organisation, attractors and patterns*. Ph.D. thesis, University of Sydney (2010)
27. J. Gray, A. Thornton, *Proc. Roy. Soc. A* **461**(2057), 1447 (2005)
28. S. Savage, C. Lun, *Journal of Fluid Mechanics* **189**, 311 (1988)
29. B. Marks, I. Einav, P. Rognon, in *Advances in Bifurcation and Degradation in Geomaterials, Springer Series in Geomechanics and Geoengineering*, vol. 11, ed. by S. Bonelli, C. Dascalu, F. Nicot (Springer Netherlands, 2011), pp. 145–151
30. J. Gray, V.A. Chugunov, *Journal of Fluid Mechanics* **569**, 365 (2006)
31. B. Utter, R.P. Behringer, *Phys. Rev. E* **69**(3), 031308 (2004). DOI 10.1103/PhysRevE.69.031308
32. B. Chopard, M. Droz, *Journal of statistical physics* **64**(3-4), 859 (1991)
33. S. Wiederseiner, N. Andreini, G. Épely-Chauvin, G. Moser, M. Monnereau, J.M.N.T. Gray, C. Ancey, *Physics of Fluids* **23**(1), 013301 (2011)
34. A. Kurganov, E. Tadmor, *Journal of Computational Physics* **160**(1), 241 (2000)
35. P. Bartelt, B.W. McArdell, *Journal of Glaciology* **55**(193), 829 (2009)

## CHAPTER 9

### **Conclusion**

---

This work has introduced the concept of the grainsize distribution into the modelling of granular flows. By including this additional internal coordinate, I have explained the mechanism of segregation in the simplest possible way: a stress gradient in the grainsize direction. Also, crushing during flow can be expressed in this framework in a simple manner, where both fractal and power-law grainsize distributions evolve naturally.

In Chapter 3, beginning with the simple idea that segregation in one dimension can be described as the swapping of particles, I have devised a cellular automata which is a representation of the basic physics required to describe kinetic sieving for steady flows.

In this model, I have shown that the previous analytic work on kinetic sieving can be consolidated into a cohesive, concise theory which contains the essence of both works. This simplistic model of segregation can reproduce the behaviour observed in both continuum mechanics and statistical mechanics representations of the same phenomenon. The cellular automaton, however, gives no insight as to what is causing the segregation during granular flows. Finally, this paper shows how cellular automata can be used as an alternative means to solve hyperbolic partial differential equations with concentration shocks, as they suffer from fewer numerical instabilities.

In Chapter 4, I have derived the first polydisperse theory for granular segregation by introducing the grainsize coordinate. The resulting five dimensional continuum theory explains the mechanism of kinetic sieving as a stress gradient in the grainsize direction, and captures the interplay between segregation and remixing.



By including a simple constitutive model that scales with the mean local grainsize, the kinematics can be directly related to the grainsize dynamics, allowing us to measure a lubrication effect that is caused by segregation, which accelerates the flow. This model predicts not only the grainsize distribution at every point in space and time within the flow, but also the kinematics. I have successfully compared this theory with discrete element simulations, and have shown that the theory can be used to model systems with arbitrary grainsize distributions.

When the theory was used to represent a bimixture, comparison with previous theories was possible. For this system, the role of size contrast between the two constituents was made clear for the first time. For multi-component systems, it was shown that the only previous theory was sensitive to how the sizes were binned, and as a result needed a large number of fitting parameters that varied with time.

For one dimensional steady flows, such as many industrial flows, and geophysical flows on smooth terrain, it is now possible to predict the time for segregation. Using this knowledge, we can tailor conditions to either reduce or increase the extent of segregation as necessary. The theory also predicted that small particles aggregating at the base of the flow can create a lubrication effect.

A fluctuation decomposition of the continuum theory was shown in Chapter 5 that decouples the bulk and grainsize dynamics. This validates the current theories of segregation, where the segregation kinematics are dissociated from the bulk flow. Additionally, the explicit description of the two systems using a grainsize-enhanced continuum theory allows for implementation into existing numerical methods for large deformation flow problems.

The potential uses for such a tool are innumerable. This type of analysis could be used for modelling in a large number of diverse fields of interest, such as tumbling mills, chute flows, hopper discharge and filling, landslides, river sedimentation, off-world mining and planetary ring dynamics.

In Chapter 6, a steady state solution of the continuum theory was developed. In many situations, the time for segregation is much shorter than the time of flow, and so the time

dependent behaviour of the segregation is unimportant. In these cases, there is no reason to solve the temporal problem, and a simpler set of ordinary differential equations was presented that can be solved once the stress gradients and diffusivity of the system are known.

This solution highlights the fact that for systems with stable, steady state flows and arbitrary grainsize distributions, segregation can be predicted. This is the first predictive model for segregation patterns.

I have shown in an inclined chute experiment that the peak forces measured on impact with a rigid obstacle depend strongly on the grainsize distribution of the incoming flow. At approximately 5% fine particles a bidisperse avalanche of this sand reaches the largest peak force, at the scale of the experiment 20% larger than if modelling with a monodisperse sand.

For the safe design of protection structures, this effect must be quantified and considered, as monodisperse tests will give non-conservative estimates of the design loads on a structure. The prediction of this force has not been considered in this work, but can be posed in terms of the spatial variability of the grainsize distribution in a 2D or 3D flow geometry. To do this, the theory described in Chapter 5 needs to capture the changes in the grainsize distribution during flow, and to use constitutive laws that depend on the local grainsize distributions. In this way internal rheology, basal roughness effects, and wall interaction can all be expressed in terms of their dependence on the grainsize distribution. It is only when we have this level of understanding of the kinematics of flowing granular material that will we be able to safely design protection structures to impede the flow of avalanches, debris flows and landslides.

Finally, expanded cellular automata were derived to describe polydisperse segregation, mixing and comminution in Chapter 8. The segregation and mixing automata were shown to represent analytic solutions that have already been validated experimentally and numerically. The comminution automaton was shown to predict power law distributions in no flow conditions, which represent physical solutions as measured in experiment and numerical analysis. By coupling these automata together, I have shown how the interaction between these mechanisms gives rise to stable log-normal grainsize distributions which are depth dependent, as measured

in landslides, debris flows and avalanches. This is the first predictive model of log-normal grainsize distribution evolution.

I have also shown how the cellular automata described in Chapter 8 can be used to inspire continuum models, and how the grainsize coordinate can be used to describe population balance models that do not require a priori knowledge of the final grading curves.

Together, this body of knowledge allows us, for the first time, to see the utility of including a grainsize coordinate in a numerical or analytic description of a granular system. By adding this ingredient, complex phenomena can be described simply and accurately. This is a paradigm shift in the description of granular materials for the fields of research that study granular flows, such as glaciology, snow avalanches, debris flows, landslides, erosion processes, hopper filling and discharge, comminution and draw down mining.

By expanding on the work undertaken during my PhD, we will see significant improvement in the understanding, modelling, efficiency, and safety of these industries.

## **9.1 Future outlook**

Clearly, there is much work to do to be done to push this work further. The first step of this process would be to incorporate the fluctuation decomposition shown in Chapter 5 into a two or three dimensional model, so that investigations of segregation in other geometries can begin systematically. This would allow for an understanding of levee formation during avalanche runout and segregation induced mobility changes. In addition, the fluctuation decomposition should be extended to include crushing.

I believe that a material point method implementation either with or without crushing would allow us to realise these goals. Once crushing is included, we can look at draw down mining, snow avalanches, and the effect of crushing in large mobility avalanches. Also, there would be large applicability to the design of mixers and crushers for the mining and chemical processing industries.

A further refinement to the theory would be the inclusion of a passive fluid phase, as described for a bimixture in Thornton et al. (2006). The role of spatial variability of pore pressures during debris flow could then be studied, as these appear to control the granular fronts and liquid tails observed in nature. Once that is complete, the work would benefit from a full decoupling into a two phase material of separate fluid and granular fluid components so that erosion and deposition could be modelled.

An assumption made in Chapter 4 was that the diffusivity,  $D$  was independent of grainsize. From preliminary discrete element investigation, it appears that this is not the case. It would behove us, then, to find a scaling law to represent the true variability of diffusion with grainsize.

A further assumption in Chapter 4 was that the inertial time scaled with the mean particle size. This has not been validated experimentally. Large deformation shear tests, such as in a ring shear or stadium shear device, would be able find the relationship between viscosity and the grainsize distribution.

Finally, experimental validation of the ideas presented in this dissertation are lacking. To validate these theories, full field measurements of three dimensional flows are required from experimental and numerical analyses. While these tools are being developed I would urge those interested to find an existing experimental apparatus, and re-run previous tests but now varying the grainsize distribution. With a good collection of boundary value measurements for a variety of flow problems, we can expand our understand of the grainsize dynamics in granular flows.

## Bibliography

- ABS-Lawinenairbags, Peter Aschauer GmbH (Apr. 2013). *Operating Principle*. URL: <http://abs-airbag.de/en/abs-system/stay-on-top-to-stay-alive/>.
- Alonso, JJ and HJ Herrmann (1996). ‘Shape of the tail of a two-dimensional sandpile’. In: *Physical Review Letters* 76.26, pp. 4911–4914.
- Alonso-Marroquin, Fernando and Yucang Wang (2009). ‘An efficient algorithm for granular dynamics simulations with complex-shaped objects’. In: *Granular Matter* 11.5, pp. 317–329.
- Andò, Edward et al. (2012). ‘Grain-scale experimental investigation of localised deformation in sand: a discrete particle tracking approach’. In: *Acta Geotechnica* 7.1, pp. 1–13.
- Armanini, Aronne (2013). ‘Granular flows driven by gravity’. In: *Journal of Hydraulic Research* 51.2, pp. 111–120.
- Arya, Lalit M and Jack F Paris (1981). ‘A physicoempirical model to predict the soil moisture characteristic from particle-size distribution and bulk density data’. In: *Soil Science Society of America Journal* 45.6, pp. 1023–1030.
- D2487, ASTM Standard (2011). *Standard Practice for Classification of Soils for Engineering Purposes (Unified Soil Classification System)*. ASTM International, West Conshohocken, PA.
- Bagnold, Ralph A. (1941). *The Physics Of Blown Sand And Desert Dunes*. Dover Earth Science Series. Dover Publications.
- Bagnold, Ralph A (1954). ‘Experiments on a gravity-free dispersion of large solid spheres in a Newtonian fluid under shear’. In: *Proceedings of the Royal Society of London. Series A. Mathematical and Physical Sciences* 225.1160, pp. 49–63.
- Bagnoli, Frank (1941). *Dynamical Modeling In Biotechnology*. World Scientific. Chap. Cellular Automata.

- Bartelt, P and BW McArdell (2009). 'Granulometric investigations of snow avalanches'. In: *Journal of Glaciology* 55.193, pp. 829–833.
- Bear, Jacob (1972). *Dynamics of fluids in porous media*. Courier Dover Publications.
- Ben-Nun, O., I. Einav and A. Tordesillas (Mar. 2010). 'Force Attractor in Confined Comminution of Granular Materials'. In: *Physical Review Letters* 104.10, p. 108001.
- Ben-Zion, Y. and C. G. Sammis (2003). 'Characterization of Fault Zones'. In: *Pure and Applied Geophysics* 160 (3-4), pp. 677–715.
- Bertrand, F., L.-A. Leclaire and G. Levecque (2005). 'DEM-based models for the mixing of granular materials'. In: *Chemical Engineering Science* 60.8–9, pp. 2517–2531.
- Bingham, Eugene Cook (1917). *An investigation of the laws of plastic flow*. Vol. 13. 2. Govt. Print. Off.
- Boer, Gerben BJ de et al. (1987). 'Laser diffraction spectrometry: Fraunhofer diffraction versus Mie scattering'. In: *Particle & Particle Systems Characterization* 4.1-4, pp. 14–19.
- Bolton, Malcolm D (2000). *The role of micro-mechanics in soil mechanics*. Tech. rep. Cambridge University Engineering Department.
- Bond, Fred C (1952). 'The third theory of comminution'. In: *Transactions of the American Institute of Mining, Metallurgical and Petroleum Engineers* 193.2, pp. 484–494.
- Branney, Michael J and Peter Kokelaar (1992). 'A reappraisal of ignimbrite emplacement: progressive aggradation and changes from particulate to non-particulate flow during emplacement of high-grade ignimbrite'. In: *Bulletin of Volcanology* 54.6, pp. 504–520.
- Brugger, Hermann et al. (2007). 'The impact of avalanche rescue devices on survival'. In: *Resuscitation* 75.3, pp. 476–483.
- Buser, Othmar and Perry Bartelt (2009). 'Production and decay of random kinetic energy in granular snow avalanches'. In: *Journal of Glaciology* 55.189, pp. 3–12.
- Campbell, Charles S (1997). 'Self-diffusion in granular shear flows'. In: *Journal of Fluid Mechanics* 348.1, pp. 85–101.
- Carman, PC (1937). 'Fluid flow through granular beds'. In: *Transactions - Institution of Chemical Engineeres* 15, pp. 150–166.
- Cataldo, Robert De (2012). 'The Acoustics of Particle Crushing'. MA thesis. Australia: The University of Sydney.

- Chanut, Benoit, Thierry Faug and Mohamed Naaim (2010). 'Time-varying force from dense granular avalanches on a wall'. In: *Physical Review E* 82.4, p. 041302.
- Cheong, YS et al. (2004). 'Modelling fragment size distribution using two-parameter Weibull equation'. In: *International Journal of Mineral Processing* 74, S227–S237.
- Chopard, Bastien and Michel Droz (1998). *Cellular automata modeling of physical systems*. Vol. 122. Springer.
- Christen, M, J Kowalski and P Bartelt (2010). 'RAMMS: Numerical simulation of dense snow avalanches in three-dimensional terrain'. In: *Cold Regions Science and Technology* 63.1, pp. 1–14.
- Cleary, Paul W, Guy Metcalfe and Kurt Liffman (1998). 'How well do discrete element granular flow models capture the essentials of mixing processes?' In: *Applied Mathematical Modelling* 22.12, pp. 995 –1008.
- Conway, John (1970). 'The game of life'. In: *Scientific American* 223.4, p. 4.
- Cook, Matthew (2004). 'Universality in elementary cellular automata'. In: *Complex Systems* 15.1, pp. 1–40.
- Coulomb, Charles-Augustin de (1773). 'Sur une application des règles, de maximis et minimis à quelque problèmes de statique, relatifs à l'architecture'. In: *Mémoires de mathématique et de physique, présentés à l'Académie royale des sciences*.
- Crosta, Giovanni B., Paolo Frattini and Nicoletta Fusi (2007). 'Fragmentation in the Val Pola rock avalanche, Italian Alps'. In: *Journal of Geophysical Research: Earth Surface* 112.F1. ISSN: 2156-2202.
- Cundall, Peter A and Otto DL Strack (1979). 'A discrete numerical model for granular assemblies'. In: *Geotechnique* 29.1, pp. 47–65.
- Davies, TR and MJ McSaveney (1999). 'Runout of dry granular avalanches'. In: *Canadian Geotechnical Journal* 36.2, pp. 313–320.
- Deutsch, Andreas, Sabine Dormann and Philip K Maini (2005). *Cellular automaton modeling of biological pattern formation: characterization, applications, and analysis*. Springer.
- Dolgunin, VN and AA Ukolov (1995). 'Segregation modeling of particle rapid gravity flow'. In: *Powder Technology* 83.2, pp. 95–104.

- Donald, MB and B Roseman (1962). 'Mixing and De-mixing of solid particles; Part I'. In: *British Chemical Engineering* 7.10.
- Drahn, J.A. and J Bridgwater (1983). 'The mechanisms of free surface segregation'. In: *Powder Technology* 36.1, p. 39.
- Drescher, A and G De Josselin de Jong (1972). 'Photoelastic verification of a mechanical model for the flow of a granular material'. In: *Journal of the Mechanics and Physics of Solids* 20.5, pp. 337–340.
- Duran, Jacques (2000). *Sands, powders, and grains*. Springer New York.
- E Ewing, Richard and Hong Wang (2001). 'A summary of numerical methods for time-dependent advection-dominated partial differential equations'. In: *Journal of Computational and Applied Mathematics* 128.1, pp. 423–445.
- Einav, I and GD Nguyen (2009). 'Cataclastic and ultra-cataclastic shear using breakage mechanics'. In: *Batsheva De Rothschild Seminar on "Shear Physics at the Meso-scale in Earthquake and Landslide Mechanics"*. Ein Gedi, the Dead Sea Valley, Israel, pp. 26–30.
- Einav, Itai (2007a). 'Breakage mechanics - Part 1: theory'. In: *Journal of the Mechanics and Physics of Solids* 55.6, pp. 1274–1297.
- (2007b). 'Breakage mechanics - Part 2: Modelling granular materials'. In: *Journal of the Mechanics and Physics of Solids* 55.6, pp. 1298–1320.
- Einstein, Albert (1905). 'The theory of the brownian movement'. In: *Annalen der Physik und Chemie* 17, p. 549.
- Ermentrout, G Bard, Leah Edelstein-Keshet et al. (1993). 'Cellular automata approaches to biological modeling'. In: *Journal of theoretical Biology* 160.1, pp. 97–133.
- Faug, Thierry, Rémi Beguin and Benoit Chanut (Aug. 2009). 'Mean steady granular force on a wall overflowed by free-surface gravity-driven dense flows'. In: *Physical Review E* 80 (2), p. 021305.
- Fermi, Enrico, J Pasta and S Ulam (1955). *Studies of nonlinear problems*. Tech. rep. I, Los Alamos Scientific Laboratory Report No. LA-1940.
- Fick, Adolf (1855). 'Ueber Diffusion'. In: *Annalen der Physik und Chemie* 170.1, pp. 59–86.
- Folk, Robert L (1966). 'A review of grain-size parameters'. In: *Sedimentology* 6.2, pp. 73–93.
- Fredkin, Edward (1991). 'Digital mechanics'. In: *Physica D* 45, pp. 254–270.



- Gennes, Pierre-Gilles de (1999). 'Granular matter: a tentative view'. In: *Reviews of Modern Physics* 71.2, S374–S382.
- Ghemmour, Assia, Guillaume Chambon and Mohamed Naaim (2008). 'Gravitary Free Surface Flows Used as a Rheometrical Tool: The Case of Viscoplastic Fluids'. In: *AIP Conference Proceedings*. Vol. 1027, p. 1039.
- Godunov, Sergei Konstantinovich (1959). 'A difference method for numerical calculation of discontinuous solutions of the equations of hydrodynamics'. In: *Matematicheskii Sbornik* 89.3, pp. 271–306.
- Goossens, Dirk (2008). 'Techniques to measure grain-size distributions of loamy sediments: a comparative study of ten instruments for wet analysis'. In: *Sedimentology* 55.1, pp. 65–96.
- Gray, JMNT and Christophe Ancey (2011). 'Multi-component particle-size segregation in shallow granular avalanches'. In: *Journal of Fluid Mechanics* 678, p. 535.
- Gray, JMNT and VA Chugunov (2006). 'Particle-size segregation and diffusive remixing in shallow granular avalanches'. In: *Journal of Fluid Mechanics* 569.1, pp. 365–398.
- Gray, JMNT and BP Kokelaar (2010). 'Large particle segregation, transport and accumulation in granular free-surface flows'. In: *Journal of Fluid Mechanics* 652, pp. 105–137.
- Gray, JMNT and AR Thornton (2005). 'A theory for particle size segregation in shallow granular free-surface flows'. In: *Proceedings of the Royal Society A: Mathematical, Physical and Engineering Sciences* 461.2057, pp. 1447–1473.
- Gruber, Urs and Stefan Margreth (2001). 'Winter 1999: a valuable test of the avalanche-hazard mapping procedure in Switzerland'. In: *Annals of Glaciology* 32.1, pp. 328–332.
- Güttler, Carsten et al. (2013). 'Granular convection and the Brazil nut effect in reduced gravity'. In: *arXiv preprint arXiv:1304.0569*.
- Haldane, John Burdon Sanderson (1926). 'On being the right size'. In: *Newman, JR (Ed.): The world of Mathematics 2*.
- Hampton, Monty A, Homa J Lee and Jacques Locat (1996). 'Submarine landslides'. In: *Reviews of Geophysics* 34.1, pp. 33–59.
- Hardin, Bobby O (1985). 'Crushing of soil particles'. In: *Journal of Geotechnical Engineering* 111.10, pp. 1177–1192.

- Hazen, A (1911). ‘Discussion of Dams on sand foundations’. In: *Transactions of the American Society of Civil Engineers*. Ed. by A. C. Koenig. Vol. 73.
- Herschel, Winslow H and Ronald Bulkley (1926). ‘Konsistenzmessungen von gummi-benzollösungen’. In: *Kolloid-Zeitschrift* 39.4, pp. 291–300.
- Hertz, Heinrich (1882). ‘Über die Berührung fester elastischer Körper’. In: *Journal für die reine und angewandte Mathematik* 92.
- Hill, Kimberly M. et al. (2010). ‘Granular segregation studies for the development of a radar-based three-dimensional sensing system’. In: *Granular Matter* 12.2, pp. 201–207.
- Hill, KM, G Gioia and D Amaravadi (2004). ‘Radial segregation patterns in rotating granular mixtures: Waviness selection’. In: *Physical Review Letters* 93.22, pp. 224–301.
- Hiramatsu, Y and Y Oka (1966). ‘Determination of the tensile strength of rock by a compression test of an irregular test piece’. In: *International Journal of Rock Mechanics and Mining Sciences & Geomechanics Abstracts*. Vol. 3. Elsevier, pp. 89–90.
- Hong, Daniel C, Paul V Quinn and Stefan Luding (2001). ‘Reverse Brazil nut problem: competition between percolation and condensation’. In: *Physical Review Letters* 86.15, pp. 3423–3426.
- Hutter, Kolumban, Yongqi Wang and Shiva P Pudasaini (2005). ‘The Savage–Hutter avalanche model: how far can it be pushed?’ In: *Philosophical Transactions of the Royal Society A: Mathematical, Physical and Engineering Sciences* 363.1832, pp. 1507–1528.
- Ilichinski, Andrew (2001). *Cellular automata: a discrete universe*. World Scientific Publishing Company.
- Imre, Bernd, Jan Laue and Sarah Marcella Springman (2010). ‘Fractal fragmentation of rocks within sturzstroms: insight derived from physical experiments within the ETH geotechnical drum centrifuge’. In: *Granular Matter* 12.3, pp. 267–285.
- Iverson, Richard M (2003). ‘The debris-flow rheology myth’. In: *Debris-flow hazards mitigation: mechanics, prediction, and assessment* 1, pp. 303–314.
- Johanson, JR (1978). ‘Particle segregation... and what to do about it’. In: *Chemical Engineering* 85.11, pp. 183–188.
- Jop, Pierre, Yoël Forterre and Olivier Pouliquen (2006). ‘A constitutive law for dense granular flows’. In: *Nature* 441.7094, pp. 727–730.

- Kelly, Errol G and David J Spottiswood (1982). *Introduction to mineral processing*. Wiley New York.
- Khakhar, DV, JJ McCarthy and JM Ottino (1997). ‘Radial segregation of granular mixtures in rotating cylinders’. In: *Physics of Fluids* 9, p. 3600.
- Khakhar, DV, Ashish V Orpe and SK Hajra (2003). ‘Segregation of granular materials in rotating cylinders’. In: *Physica A: Statistical Mechanics and its Applications* 318.1, pp. 129–136.
- Khakhar, DV et al. (2001). ‘Surface flow of granular materials: model and experiments in heap formation’. In: *Journal of Fluid Mechanics* 441, pp. 255–264.
- Kick, Friedrich (1885). *Das Gesetz der proportionalen Widerstände und seine Anwendungen: Nebst Versuchen über das Verhalten verschiedener Materialien bei gleichen Formänderungen sowohl unter der Presse als dem Schlagwerk*. A. Felix.
- King, RP (1993). ‘Comminution research—a success story that has not yet ended’. In: *Proc. of XVIII Intl. Mineral Processing Congress, Sydney, Australia*.
- Knight, JB, HM Jaeger and SR Nagel (1993). ‘Vibration-induced size separation in granular media: The convection connection’. In: *Physical Review Letters* 70.24, pp. 3728–3731.
- Koeppe, J.P., M. Enz and J. Kakalios (Oct. 1998). ‘Phase diagram for avalanche stratification of granular media’. In: *Physical Review E* 58.4, pp. 4104–4107.
- Kozeny, Josef (1927). ‘Ueber kapillare leitung des wassers im boden’. In: *Sitzungsber. Akad. Wiss. Wien* 136, pp. 271–306.
- Kurganov, A. and E. Tadmor (2000). ‘New High-Resolution Central Schemes for Nonlinear Conservation Laws and Convection-Diffusion Equations’. In: *Journal of Computational Physics* 160.1, pp. 241–282.
- LeVeque, Randall J (2002). *Finite volume methods for hyperbolic problems*. Vol. 31. Cambridge university press.
- Liu, Andrea J and Sidney R Nagel (2001). *Jamming and rheology: constrained dynamics on microscopic and macroscopic scales*. CRC Press I Llc.
- Lo, CY, MD Bolton and YP Cheng (2010). ‘Velocity fields of granular flows down a rough incline: a DEM investigation’. In: *Granular Matter* 12.5, pp. 477–482.

- Lowrison, George Charles (1974). *Crushing and grinding: the size reduction of solid materials*. Butterworths London.
- Luding, Stefan (2004). ‘Molecular dynamics simulations of granular materials’. In: *The physics of granular media*, pp. 297–324.
- Majmudar, T. S. et al. (Jan. 2007). ‘Jamming Transition in Granular Systems’. In: *Physical Review Letters* 98 (5), p. 058001.
- Makse, H.A. (1997). ‘Stratification instability in granular flows’. In: *Physical Review E* 56.6, pp. 7008–7016.
- Margolus, Norman, Tommaso Toffoli and Gerard Vichniac (1986). ‘Cellular-automata supercomputers for fluid-dynamics modeling’. In: *Physical Review Letters* 56.16, pp. 1694–1696.
- Marks, Benjy, Pierre Rognon and Itai Einav (2012). ‘Grainsize dynamics of polydisperse granular segregation down inclined planes’. In: *Journal of Fluid Mechanics* 690, pp. 499–511.
- Masch, Frank D and Kleber J Denny (1966). ‘Grain size distribution and its effect on the permeability of unconsolidated sands’. In: *Water Resources Research* 2.4, pp. 665–677.
- May, Lindsay BH, Michael Shearer and Karen E Daniels (2010). ‘Scalar conservation laws with nonconstant coefficients with application to particle size segregation in granular flow’. In: *Journal of nonlinear science* 20.6, pp. 689–707.
- McArdell, Brian W, Perry Bartelt and Julia Kowalski (2007). ‘Field observations of basal forces and fluid pore pressure in a debris flow’. In: *Geophysical Research Letters* 34.7.
- McCarthy, JJ (2009). ‘Turning the corner in segregation’. In: *Powder Technology* 192.2, pp. 137–142.
- McDowell, GR, MD Bolton and D. Robertson (1996). ‘The fractal crushing of granular materials’. In: *Journal of the Mechanics and Physics of Solids* 44.12, pp. 2079–2101.
- McGrady, E. D. and Robert M. Ziff (Mar. 1987). ‘“Shattering” transition in fragmentation’. In: *Physical Review Letters* 58 (9), pp. 892–895.
- Menon, Narayanan and Douglas J Durian (1997). ‘Particle motions in a gas-fluidized bed of sand’. In: *Physical Review Letters* 79.18, pp. 3407–3410.

- MiDi, GDR (2004). 'On dense granular flows'. In: *The European Physical Journal E: Soft Matter and Biological Physics* 14.4, pp. 341–365.
- Mobius, M.E. et al. (2001). 'Brazil-nut effect: Size separation of granular particles'. In: *Nature* 414.6861, p. 270.
- Moriguchi, Shuji et al. (2009). 'Estimating the impact force generated by granular flow on a rigid obstruction'. In: *Acta Geotechnica* 4 (1), pp. 57–71.
- Moro, F et al. (2010). 'Large mobility of dry snow avalanches: Insights from small-scale laboratory tests on granular avalanches of bidisperse materials'. In: *Cold Regions Science and Technology* 62.1, pp. 55–66.
- Muzzio, Fernando J, Troy Shinbrot and Benjamin J Glasser (2002). 'Powder technology in the pharmaceutical industry: the need to catch up fast'. In: *Powder Technology* 124.1–2, pp. 1–7.
- Nakagawa, M. et al. (1993). 'Non-invasive measurements of granular flows by magnetic resonance imaging'. In: *Experiments in Fluids* 16.1, pp. 54–60.
- Naylor, M.A. (1980). 'The origin of inverse grading in muddy debris flow deposits; a review'. In: *Journal of Sedimentary Research* 50.4, pp. 1111–1116.
- Norem, Harald, Fridtjov Irgens and Bonsak Schieldrop (1988). *Simulation of snow avalanche flow in run-out zones*. Norges Geotekniske Institutt.
- Perfect, E. (1997). 'Fractal models for the fragmentation of rocks and soils: a review'. In: *Engineering Geology* 48.3–4, pp. 185–198.
- Peterson, TW, MV Scotto and AF Sarofim (1985). 'Comparison of comminution data with analytical solutions of the fragmentation equation'. In: *Powder technology* 45.1, pp. 87–93.
- Petley, David (2012). 'Global patterns of loss of life from landslides'. In: *Geology*.
- Pouliquen, Olivier (1999). 'Scaling laws in granular flows down rough inclined planes'. In: *Physics of Fluids* 11, p. 542.
- Pouliquen, Olivier and Yoel Forterre (2002). 'Friction law for dense granular flows: application to the motion of a mass down a rough inclined plane'. In: *Journal of Fluid Mechanics* 453, pp. 133–151.

- Powell, MS and RD Morrison (2007). 'The future of comminution modelling'. In: *International Journal of Mineral Processing* 84.1, pp. 228–239.
- Prigozhin, Leonid and Haim Kalman (1998). 'Radial mixing and segregation of a binary mixture in a rotating drum: model and experiment'. In: *Physical Review E* 57.2, pp. 2073–2080.
- Ramkrishna, Doraiswami (2000). *Population balances: Theory and applications to particulate systems in engineering*. Academic Press San Diego.
- Ramkrishna, Doraiswami and Alan W Mahoney (2002). 'Population balance modeling. Promise for the future'. In: *Chemical Engineering Science* 57.4, pp. 595–606.
- Randolph, A.D. and R. Ranjan (1977). 'Effect of a material-flow model in prediction of particle-size distributions in open-and closed-circuit mills'. In: *International Journal of Mineral Processing* 4.2, pp. 99–110.
- Rastello, Marie et al. (2011). 'Size of snow particles in a powder-snow avalanche'. In: *Journal of Glaciology* 57.201, pp. 151–156.
- Reynolds, Osborne (1885). 'On the dilatancy of media composed of rigid particles in contact'. In: *Philos. Mag. Ser. 5* 50.
- (1895). 'On the dynamical theory of incompressible viscous fluids and the determination of the criterion'. In: *Philosophical Transactions of the Royal Society of London. A* 186, pp. 123–164.
- Ristow, Gerald H (1994). 'Particle mass segregation in a two-dimensional rotating drum'. In: *EPL (Europhysics Letters)* 28.2, p. 97.
- Rittinger, Peter Ritter von (1867). *Lehrbuch der aufbereitungskunde in ihrer neuesten entwicklung und ausbildung systematisch dargestellt*. Ernst & Korn (Gropius' sche buch-und kunsthandlung).
- Rognon, P. and C. Gay (2008). 'Soft Dynamics simulation. 1. Normal approach of two deformable particles in a viscous fluid and optimal-approach strategy'. In: *The European Physical Journal E* 27 (3), pp. 253–260.
- Rognon, Pierre G. et al. (2007). 'Dense flows of bidisperse assemblies of disks down an inclined plane'. In: *Physics of Fluids* 19.

- Rosato, Anthony et al. (Mar. 1987). 'Why the Brazil nuts are on top: Size segregation of particulate matter by shaking'. In: *Physical Review Letters* 58 (10), pp. 1038–1040.
- Russell, Adrian R and Itai Einav (2013). 'Energy dissipation from particulate systems undergoing a single particle crushing event'. In: *Granular Matter*, pp. 1–16.
- Ryu, Hojin J and Fumio Saito (1991). 'Single particle crushing of nonmetallic inorganic brittle materials'. In: *Solid state ionics* 47.1, pp. 35–50.
- Salm, B (1993). 'Flow, flow transition and runout distances of flowing avalanches'. In: *Annals of Glaciology* 18, pp. 221–221.
- Sanvitale, Nicoletta and Elisabeth T Bowman (2012). 'Internal imaging of saturated granular free-surface flows'. In: *International Journal of Physical Modelling in Geotechnics* 12.4, pp. 129–142.
- Savage, SB and K Hutter (1989). 'The motion of a finite mass of granular material down a rough incline'. In: *Journal of Fluid Mechanics* 199.1, pp. 177–215.
- Savage, SB and CKK Lun (1988). 'Particle size segregation in inclined chute flow of dry cohesionless granular solids'. In: *Journal of Fluid Mechanics* 189, pp. 311–335.
- Schoenert, K (1986). 'On the limitation of energy saving in milling. 1'. In: *World Congress Particle Technology, Part II, Comminution, Nurnberg, April*, pp. 16–19.
- Schweitzer, Frank and Jörg Zimmermann (2001). 'Communication and self-organization in complex systems: A basic approach'. In: *Knowledge, Complexity and Innovation Systems*, pp. 275–296.
- Shearer, M., J.M.N.T. Gray and A. R. Thornton (Jan. 2008). 'Stable solutions of a scalar conservation law for particle-size segregation in dense granular avalanches'. In: *European Journal of Applied Mathematics* 19 (01), pp. 61–86.
- Shinohara, Kunio, Kazunori Shoji and T Tanaka (1972). 'Mechanism of size segregation of particles in filling a hopper'. In: *Industrial & Engineering Chemistry Process Design and Development* 11.3, pp. 369–376.
- Silbert, L. E. et al. (Oct. 2001). 'Granular flow down an inclined plane: Bagnold scaling and rheology'. In: *Physical Review E* 64.5.
- Smith, WO, Paul D Foote and PF Busang (1929). 'Packing of homogeneous spheres'. In: *Physical Review* 34.9, p. 1271.

- Steady, S.J. and C.G. Sammis (1991). 'An automaton for fractal patterns of fragmentation'. In: *Nature* 353.6341, pp. 250–252.
- Sulsky, Deborah, Shi-Jian Zhou and Howard L. Schreyer (1995). 'Application of a particle-in-cell method to solid mechanics'. In: *Computer Physics Communications* 87.12, pp. 236–252. ISSN: 0010-4655.
- Syvitski, James PM (2007). *Principles, methods and application of particle size analysis*. Cambridge University Press.
- Thornton, AR and JMNT Gray (2008). 'Breaking size segregation waves and particle recirculation in granular avalanches'. In: *Journal of Fluid Mechanics* 596, pp. 261–284.
- Thornton, AR, JMNT Gray and AJ Hogg (2006). 'A three-phase mixture theory for particle size segregation in shallow granular free-surface flows'. In: *Journal of Fluid Mechanics* 550, pp. 1–26.
- Thornton, A. R. et al. (Aug. 2012). 'Modeling of particle size segregation: Calibration using the discrete particle method'. In: *International Journal of Modern Physics C* 23.8, p. 1240014.
- Turcotte, DL (1986). 'Fractals and fragmentation'. In: *Journal of Geophysical Research* 91.B2, pp. 1921–1926.
- Turnbull, B (2011). 'Scaling Laws for Melting Ice Avalanches'. In: *Physical Review Letters* 107.25, p. 258001.
- Udden, Johan August (1898). *The mechanical composition of wind deposits*. 1. Lutheran Augustana book concern, printers.
- Ulam, Stanislaw (1952). 'Random processes and transformations'. In: *Proceedings of the International Congress on Mathematics*. Vol. 2. Public School Publishing, pp. 264–275.
- Utter, Brian and Robert P Behringer (2004). 'Self-diffusion in dense granular shear flows'. In: *Physical Review E* 69.3, p. 031308.
- Valaula, Aurelio (2012). 'Design of protection structures: The influence of grain size'. Masters Thesis. Switzerland: ETH Zürich.
- Van Leer, Bram (1979). 'Towards the ultimate conservative difference scheme. V. A second-order sequel to Godunov's method'. In: *Journal of computational Physics* 32.1, pp. 101–136.



- Weibull, W. et al. (1951). 'A statistical distribution function of wide applicability'. In: *Journal of applied mechanics* 18.3, pp. 293–297.
- Weinhart, Thomas et al. (2012a). 'From discrete particles to continuum fields near a boundary'. In: *Granular Matter* 14.2, pp. 289–294.
- Weinhart, T. et al. (July 2012b). 'Closure relations for shallow granular flows from particle simulations'. In: *Granular matter* 14.4, pp. 531–552.
- Wiederseiner, Sébastien et al. (2011a). 'Experimental investigation into segregating granular flows down chutes'. In: *Physics of Fluids* 23, p. 013301.
- Wiederseiner, Sébastien et al. (2011b). 'Refractive-index and density matching in concentrated particle suspensions: a review'. In: *Experiments in fluids* 50.5, pp. 1183–1206.
- Wilkinson, R Allen et al. (2005). 'Granular materials and the risks they pose for success on the moon and mars'. In: *AIP Conference Proceedings*. Vol. 746, p. 1216.
- Williams, JC (1968). 'The mixing of dry powders'. In: *Powder Technology* 2.1, pp. 13–20.
- Williams, MMR (1990). 'An exact solution of the fragmentation equation'. In: *Aerosol Science and Technology* 12.3, pp. 538–546.
- Wolfram, Stephen (1986). 'Theory and applications of cellular automata'. In: *Advanced Series on Complex Systems, Singapore: World Scientific Publication*.
- (2002). *A new kind of science*. Vol. 5. Wolfram media Champaign.
- Yanagita, T. (1999). 'Three-dimensional cellular automaton model of segregation of granular materials in a rotating cylinder'. In: *Physical Review Letters* 82.17, pp. 3488–3491.
- Yashima, S., Y. Kanda and S. Sano (1987). 'Relationships between particle size and fracture energy or impact velocity required to fracture as estimated from single particle crushing'. In: *Powder Technology* 51.3, pp. 277–282.
- Zhao, HF and LM Zhang (2013). 'Effect of coarse content on the shear behavior of unsaturated coarse granular soils'. In: *Canadian Geotechnical Journal* ja.
- Zhao, HF, LM Zhang and DS Chang (2012). 'Behavior of coarse widely graded soils under low confining pressures'. In: *Journal of Geotechnical and Geoenvironmental Engineering*.

## APPENDIX A

### Post processing

---

The discrete element simulations shown in Chapter 4 required extensive post processing in order to recover continuum properties from the discrete data. This Appendix goes in detail through each of the steps required to post process this data.

#### A1 Volumetric analysis

Because of the geometry of the discrete element simulation shown in Chapter 4, the solution can be discretised into slices that run parallel to the base of the inclined plane. For each slice, the volume of each sphere that lies within the slice,  $V_{sec}$ , has to be found.

The next step is to place the volumetric data in bins of height and size at each time step. It is necessary to store the volume  $V$  of each particle in that slice as

$$V(z, s, t) = \sum_{i=1}^{N_p} V_{sec}(i, z, s, t),$$

where  $N_p$  is the number of particles and  $V_{sec}$  is the volume of particle  $p$  in the slice at height  $z$ , with grainsize  $s$  at time  $t$ .  $V_{sec}$  is found by taking the integral from  $z_s - \frac{\Delta z}{2}$  to  $z_s + \frac{\Delta z}{2}$  of the area of the sphere at that position as

$$V_{sec} = \pi \int_{z_s - \frac{\Delta z}{2}}^{z_s + \frac{\Delta z}{2}} (r^2 - (Z - z)^2) dz,$$

where  $z_s$  is the middle of the slice,  $\Delta z$  the thickness of the slice,  $Z$  the centre of the sphere and  $r$  its radius. Solving the previous equation,

$$V_{sec} = \pi \Delta z \left( r^2 - \frac{\Delta z^2}{12} - (Z - z)^2 \right).$$

This is valid when the sphere continues beyond both boundaries of the slice. When the sphere ends at some point inside the slice, a different formula is necessary. Calling this volume  $V_{cap}$ , with the cap of height  $h$ , the volume is

$$V_{cap} = \frac{\pi h^2 (3r - h)}{3}.$$

## A2 Homogenisation

Now that there is a description of the volume of each particle at each discrete height  $z$ , a particular variable of interest  $X$ , which could represent any particle-based variable such as the velocity or kinetic energy, can be homogenised. The volumetric average quantity  $X(z, s, t)$  is found by:

$$X(z, s, t) = \frac{\sum_{i=1}^{N_p} V_{sec}(i, z, s, t) X(i, z, s, t)}{\sum_{i=1}^{N_p} V_{sec}(i, z, s, t)}.$$

The average quantity at each height,  $\bar{X}(z)$  can then be found by averaging over time and grainsize as

$$\bar{X}(z, t) = \frac{\sum_{i=1}^{N_s} X(z, i, t) V(z, i, t)}{\sum_{i=1}^{N_s} V(z, i, t)},$$

$$\bar{X}(z) = \sum_{i=1}^{N_t} \frac{X(z, i)}{N_t},$$

where  $N_t$  is the number of time steps over which to average. The same quantity, but now as a function of size is found by

$$\hat{X}(z, s, t) = \frac{X(z, s, t)}{\bar{X}(z, t)},$$

$$\bar{X}(s) = \sum_{j=1}^{N_t} \sum_{i=1}^{N_z} \frac{\hat{X}(i, s, j)}{N_t N_z}.$$

Here an assumption is made that the functional dependence of the variable of interest on the grainsize is relative to the mean value at a given height, and does not vary with height. This appears to be the case for the stresses measured in the discrete element model shown in the previous Chapter, but is in no way guaranteed for other geometries or variables.

## A2.1 Solid fraction

The solid fraction can  $\Phi$  can refer to two separate physical entities.  $\Phi(z, t)$  is the volume of solids divided by the total volume, which measures the proportion of space taken up by the solid component of a system.  $\Phi(z, s, t)$ , however, is the proportion of the solid phase occupied by a given size bin. These are calculated as

$$V(z, t) = \sum_{i=1}^{N_s} V(z, i, t)$$

$$\Phi(z, t) = \frac{V(z, t)}{\Delta x \Delta y \Delta z}$$

$$\Phi(z, s, t) = \frac{V(z, s, t)}{V(z, t)},$$

where  $\Delta x$  and  $\Delta y$  are the size of the simulation in the  $x$  and  $y$  directions and  $V$  is the total volume.

## A2.2 Average size

The average size is computed as an approximation to

$$\bar{s} = \int \phi s ds = \frac{V(s)}{V},$$

$$\bar{s}(z, t) = \frac{\sum_{i=1}^{N_s} V(z, i, t) s(i)}{\sum_{j=1}^{N_s} V(z, j, t)},$$

where  $N_s$  is the number of size bins, and  $s(i)$  is the  $i^{th}$  size.

## A2.3 Standard deviation of size

To get a measure of the spread of sizes at a height, the standard deviation of the grainsize,  $\sigma$  is defined as

$$\sigma(z, t)^2 = \frac{\sum_{i=1}^{N_s} (s(i) - \bar{s}(z, t))^2 V(z, i, t)}{\sum_{j=1}^{N_s} V(z, j, t)}$$

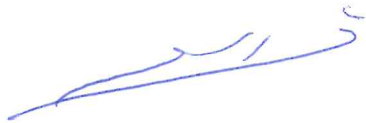
29/05/2013

To whom it may concern,

I can confirm that Benjamin Marks was the author of the journal paper "A cellular automaton for segregation during granular avalanches", published in the journal Granular Matter in 2011, as part of his PhD. For this work, Benjamin lead the research effort and wrote the paper himself.

Benjamin Marks was also the author of the journal paper "Grainsize dynamics of polydisperse granular segregation down inclined planes", published in the Journal of Fluid Mechanics in 2012, as part of his PhD. For this work, Benjamin lead the research effort and wrote the paper himself.

I also agree that Benjamin Marks was the author of the manuscript "Design of protection structures: the role of the grainsize distribution", to be published in the proceedings of the Powders and Grains Conference in 2013. For this work, Benjamin designed the experiment, and supervised Aurelio Valaulta, who performed the experiments. For this paper, Benjamin assisted Aurelio with performing the analysis, and wrote the paper himself.



Professor Itai Einav

School of civil Engineering, J05  
The University of Sydney, NSW  
AUSTRALIA

**Prof. Dr. Alexander M. Puzrin**

Phone +41-44 633 21 80

Phone +41-44-633 25 00 (Secretary)

Fax +41-44-633 14 29

alexander.puzrin@igt.baug.ethz.ch

www.igt.ethz.ch

To whom it may concern,

29 May 2013

**Benjamin Marks**

I confirm that Benjamin Marks was the author of the manuscript "Design of protection structures: the role of the grain size distribution", to be published in the proceedings of the Powders and Grains Conference in 2013. For this work, Benjamin designed the experiment, and supervised Aurelio Valaulta, who performed the experiments. For this paper, Benjamin assisted Aurelio with performing the analysis, and wrote the paper himself.

Sincerely yours,



Prof. Dr. Alexander M. Puzrin

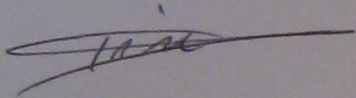


To whom it may concern,

I confirm that Benjamin Marks was the author of the journal paper "Grainsize dynamics of polydisperse granular segregation down inclined planes", published in the Journal of Fluid Mechanics in 2012, as part of his PhD. For this work, Benjamin lead the research effort and wrote the paper himself.

Dr Pierre Rognon

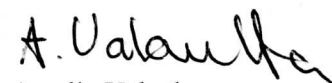
Paris the 28/05/2013

A handwritten signature in black ink, appearing to be "Pierre Rognon", written over a horizontal line.



To whom it may concern,

I confirm that Benjamin Marks was the author of the manuscript "Design of protection structures: the role of the grainsize distribution", to be published in the proceedings of the Powders and Grains Conference in 2013. For this work, Benjamin designed the experiment and supervised me while I performed the tests. For this paper, Benjamin assisted me with performing the analysis, and wrote the paper himself.

A handwritten signature in black ink, appearing to read "A. Valaula". The signature is written in a cursive, somewhat stylized font.

Aurelio Valaula